INVESTIGATING PREMATURE AGEING OF BLAST FURNACE TAPHOLE CLAY CONTAINING A RESOLE RESIN AND LIQUID PITCH BINDER

THESIS REPORT

Submitted by

I.J. CAMERON

in partial fulfilment of the award of the degree

MASTER OF ENGINEERING (METALLURGY)

UNIVERSITEIT VAN PRETORIA
UNIVERSITY OF PRETORIA
YUNIBESITHI YA PRETORIA

DEPARTMENT OF MATERIAL SCIENCE AND METALLURGICAL ENGINEERING

2021-02-08

ABSTRACT

This report investigates the cause of the reduction in workability and increased ageing of a blast furnace taphole clay. The taphole clay contains 60 mass% alumina, with a phenol-formaldehyde resole resin (PFR) and liquid pitch as a binder system. The clay aggregates as well as powder matrix raw materials were analysed using XRF, XRD and SEM-EDS for characterisation and impurity detection such as sulphur and free lime. The presence of free lime can cause premature cross-linking of the resin in the binder while the presence of sulphur can reduce the curing time of the resin. The wettability as well as particle size distribution (PSD) of all the raw materials were investigated to confirm a uniform particle size distribution of the dry aggregate of the taphole clay and wettability compatibility between the dry raw material and both resin and liquid pitch. The resin and liquid pitch characterisation, as well as interaction between resole resin and liquid pitch, were evaluated using viscosity measurements, Fourier-transform infrared spectroscopy (FTIR), thermogravimetric analysis (TGA) and differential scanning calorimetry (DSC). The analyses confirmed a chemical interaction between the resole resin and liquid pitch, where the chemical structure of the resole resin was broken down when the two liquids were mixed. This prevented curing of the resin to occur. After ageing of the resin and liquid pitch mixtures, premature cross-linking of the resin occurred, causing the curing process to move to lower temperatures, i.e. earlier onset of curing. This reduction in curing temperature, after ageing, was confirmed by an increase in binder viscosity at lower temperatures (starting at 60°C) than the curing temperature (121-126°C) of the virgin resole resin in the binder. This increase in viscosity of the binder mixture is the primary cause of the reduced workability, increased ageing and increasing Marshall extrusion pressure (MEP) of the taphole clay.

KEYWORDS: [tap hole; phenol-formaldehyde; pitch; workability; ageing]

TABLE OF CONTENT

TABLE OF FIGURES

ACKNOWLEDGEMENT

Non est ad astra mollis e terries via

My gratitude goes to my research supervisor Professor Andrie Garbers-Craig who has not only supported me through this journey in a technical capacity but also greatly through encouragement and empathy. Her unconditional love for the field of pyrometallurgy is infectious and my success would not have been possible without her support and input. To the laboratory staff in the Department of Metallurgical Engineering, I would like to extend a gratitude.

My second acknowledgement is to Doctor Shatish Ramjee for his continued support and guidance through my laboratory experimentation and interpretation. He is an expert in polymer science and pitch related materials which contributed greatly to the success of this project. To the laboratory staff in the Department of Chemical Engineering at University of Pretoria, I would also like to extend a gratitude.

Familia ante omnia

The greatest gift I have is my family and the sincerest appreciation goes to my parents, Amanda Cameron and Izak A.J. Cameron for their love and outright support in my academics. The perseverance and strength I attained and emotional support I received during this journey is owing to F.S.J van Huyssteen and C.G. Hartman.

Above all I give thanks to our God almighty for the guidance, energy, perseverance, strength and good mind and physical health to be able to finish this project and thesis.

“We must have perseverance and above all confidence in ourselves”- Marie Curie

Chapter I – Problem statement and background

1. Introduction

Blast furnace taphole clay has been used for decades with little change from the primitive raw materials and binders the product utilises. Recent developments have looked at using cheaper alternative raw materials as aggregates to reduce the price of the clay as well as tar-alternative binders that are less harmful to the environment and operators manufacturing or using the material. The move towards creating a more environmentally friendly "green" taphole clay was a key objective of the development that led to this investigation. The change in the binder that was introduced for this product development was a synthetic liquid pitch with a resole resin instead of the conventional high volatile tar and resole resin combination. The reduction in toxicity by replacing the coal tar pitch with the liquid pitch, reduced by 95%.

The problem that arose with this change was that the clay started ageing prematurely, which presented as a crumbling effect of the clay as well as a reduction in workability. The objective of this study was to determine if the change in binder combination was the cause of this premature ageing of the clay and if this change in binder combination results in a polymerisation/cross-linking effect of the resole resin that would explain the premature ageing.

As part of this investigation, both the raw material aggregates and binders were characterised and the probable cause(s) of premature ageing determined. The mineralogy of the aggregate and matrix raw materials of the clay as well as impurities present in the aggregates were examined using X-Ray Diffraction (XRD), X-Ray Fluorescence (XRF) and Scanning Electron Microscopy (SEM-EDS). These testing methods were used to confirm the composition of the aggregates as well as identify any impurities that may contribute to possible polymerisation/cross-linking of the resin in the binder. To characterise and investigate the interaction between the resole resin and the liquid pitch binder, viscosity, Fourier-transformed infrared spectroscopy (FTIR), thermogravimetric analysis (TGA) and differential scanning calorimetry (DSC) were used. The investigation also examined different mixtures of the resole resin and liquid pitch to determine if polymerisation or cross-linking behaviour occurs, and if so, what the effect on the viscosity, workability and ageing of the taphole clay is.

Chapter II – Review of related literature and studies

2. Literature (Theory)

2.1. Blast furnace tap hole – Design and Operation

The blast furnace is the most familiar furnace type that is used for iron production. The design and operation of these furnaces differ between manufacturers and each design is unique from another. Some iron manufacturers have two to three different blast furnaces. The main function of the blast furnace is to produce pig iron (high carbon iron) from iron ore, pellets and sinter, which are fed as a feed raw material. Figure 1 is a schematic diagram of a simplistic design of a blast furnace (Tec-Science, 2018/12/06).

The throat section of the furnace is where raw materials such as lump ore, sinter, pellets, coke, and flux are charged into the furnace. This section also consists of a gas extraction hood. The stack/shaft part of the furnace is where a bed is constructed that consists of alternating layers of coke and charge raw materials. These beds are extremely important as it assists with gas movement in the bed and gives some structural integrity in the furnace for reduced liquid iron to move through. The direct reduction of iron ore takes place in this part of the furnace (Yang, et al., 2014). The belly part of the furnace is the carburising zone. In this section of the furnace reduced iron reacts with carbon in the coke to produce cementite (Fe_3C). This phase has a lower melting point as that of pure iron to assist in melting which takes place in the bosh part of the furnace. This part of the furnace reaches temperatures of around 2000°C where oxygen is blown into the furnace through the tuyéres (Yang, et al., 2014). The melted pig iron, as well as the slag, collects in the hearth of the furnace. Once the liquid pig iron reaches the hearth of the furnace, it needs to be tapped. Tapping takes place through holes in the furnace called tap holes. Some furnace designs have two tap holes, one for the pig iron and one for the slag, where others only have a single tap hole that taps both pig iron and slag (Tec-Science, 2018/12/06).

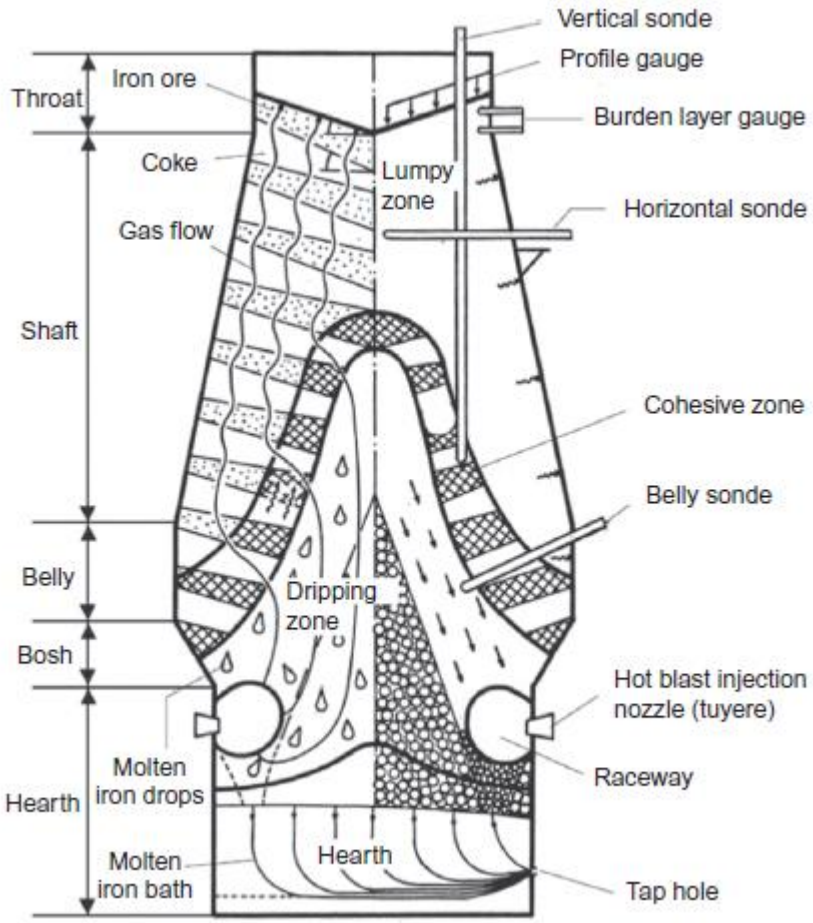

Figure 1: Ironmaking blast furnace (Yang, et al., 2014)

The schematic diagram in Figure 2 is an example of a blast furnace taphole that taps both pig iron and slag simultaneously.

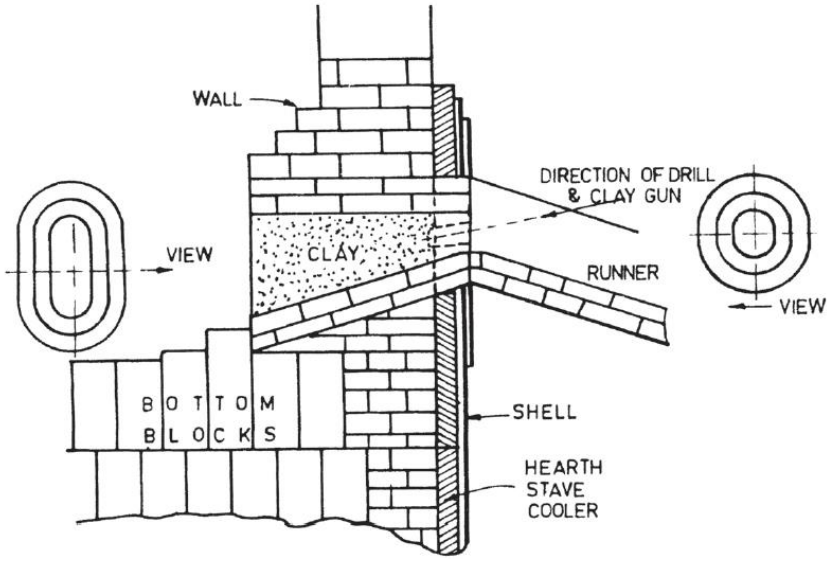

Figure 2: Blast furnace tap hole (Tupkary, 2018)

The design of the tap hole is more intricate than the remainder of the hearth of the furnace. The tap hole needs to withstand extremely harsh conditions. Other than being refractory at high operating temperatures, the tap hole design needs to withstand high liquid and gas velocities that exit the tap hole (Geyers & Halifa, 2014), have a high mechanical strength to be able to resist the pressure of molten liquid against the tap hole as well have sufficient strength to have some structural integrity since the tap hole does not have external support as the rest of the hearth (Geyers & Halifa, 2014). The tap hole also needs to be impermeable during taps to prevent metal or slag penetration which will reduce the integrity of the tap hole (Geyers & Halifa, 2014). The design in Figure 2 is a simplistic design of a tap hole but may change from manufacturer to manufacturer. The tap hole usually consists of a notch in the hearth of the furnace that is branched with water-cooled cast steel frame onto a runner (Tupkary, 2018). The runner is the raceway in which the pig iron taps, along which the liquid pig iron is transported away from the furnace to a location where it is tapped into torpedo ladles. The runner is lined with fireclay or 60 mass% alumina bricks as well as a cast working lining onto the bricks (Tupkary, 2018).

The inside of the hearth is lined with graphite blocks that are placed against the shell of the furnace. These bricks are used to line the bottom and top part where the notch is made in the hearth for the tap hole (Tupkary, 2018). The use of graphite blocks, as opposed to earlier fireclay brick designs, is due to the good thermal conductive properties as well as the ease of forming a freeze lining on these bricks (Geyers & Halifa, 2014). These bricks are keyed into place to prevent expulsion of the bricks during tapping due to high furnace pressures (Geyers & Halifa, 2014). The inside opening of the tap hole is larger than the notch in the furnace so that it can be closed properly with a plugging clay, i.e. taphole clay after tapping (Tupkary, 2018). The use of graphite blocks is also for chemical compatibility between the liquid pig iron and graphite blocks. The tapped pig iron is high in carbon, which still needs to be removed during the refining process, this ensures there is limited interaction between the liquid pig iron and the graphite blocks in the hearth (Geyers & Halifa, 2014).

Some more intricate tap hole designs include a pig iron tap hole on the one side of the furnace and a slag tap hole on the opposite side of the furnace. The slag tap hole is generally placed higher than that of the pig iron tap hole as to tap both at different stages. For small throughputs, i.e. ~1500-4500t/day, the single tap hole (tapping both pig iron and slag) is feasible. As production rates increase, the use of two different tap holes becomes more important as to reduce the tapping time and increase throughput (Tupkary, 2018).

2.1.1. Tapping practice

The melting process starts by charging the blast furnace with raw material and introducing enriched oxygen through the tuyéres to assist with the reduction and melting process. Once the liquid pig iron has accumulated in the hearth of the furnace and the hearth capacity is reached, the furnace needs to be tapped. Tapping is done by using one of the multiple processes. The preferred method is by using a hydraulic drill (Figure 3). The drill has the function of drilling with a hammer action if the tap hole struggles to open. This hammer action is used as last resort to open the tap hole as the vibration from the hammer action damages the graphite blocks of the tap hole as well as the clay mushroom that build up behind the tap hole on the inside of the furnace (Geyers & Halifa, 2014).

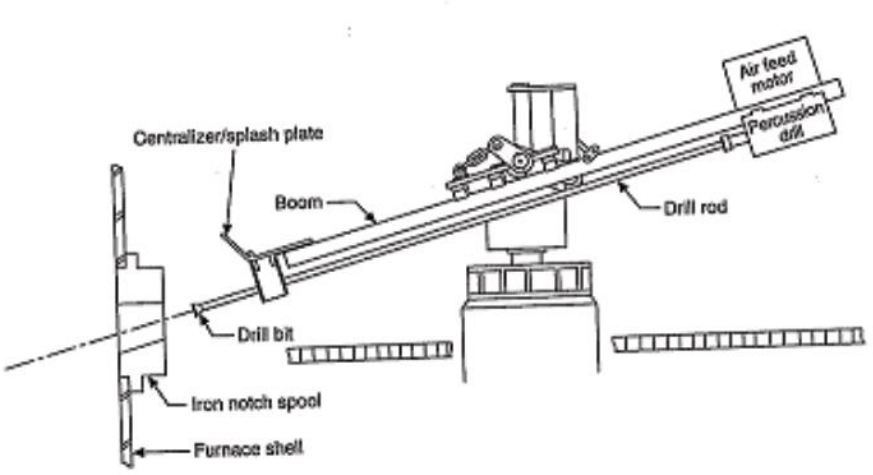

Figure 3: Hydraulic drill used to open the tap hole of the blast furnace (Tupkary, 2018)

The tapping process starts by making an incision in the taphole clay with the hydraulic drill using a 3m long rod. The hydraulic drill is swung from the side of the furnace and lowered so the drill tip is in line with the tap hole. The hydraulic drill is placed at an angle and the incision into the tap hole is made at an angle. The rod has a tungsten carbide tip that is used to drill a tap line through the taphole clay. The drill tip sizes depend on the flow rate that is required when tapping (Geyers & Halifa, 2014). Once the incision is made, the remainder of the rod is drilled into the tap hole until it opens. The drill is swung back to its starting position after which the furnace can be tapped. Tapping operations that utilise a single tap hole tap both pig iron and slag simultaneously. The separation of the pig iron and the slag is done by using a skimmer block. Due to the differences in density between pig iron (SG = 7.9) and slag (SG = 2.0), separate streams are created where the pig iron runs underneath the skimmer through the trough system to torpedo ladles where the slag is kept behind, as the skimmer prevents the slag on top of the pig iron to flow past to the torpedo ladles (Geyers & Halifa, 2014). The slag is then granulated and placed on slag heaps.

The end of the tap is signified by the splashing of the pig iron and slag from the tap hole as the gas from the tuyéres exits the furnace at the tap hole and creates the splashing effect (Geyers & Halifa, 2014). Once the end of the tap is reached the tap hole needs to be plugged.

2.1.2. Plugging practice

Once the furnace is at the end of the tap, the mud gun/clay gun is swung from the side of the tap hole until it lines up with the tap hole similarly to when drilling of the tap hole takes place. The mud gun tip is placed against the tap hole and the clay loaded in the gun is pushed into the tap hole. The mud gun is loaded with clods of taphole clay before plugging and the clay is heated in the gun to assist with moving the clay through the mud gun into the tap hole. The temperature in the mud gun should not exceed 40°C, as this influences the performance of resin bonded taphole clays (Satyendra, 2015). Mud gun (Figure 4) temperatures are generally between 20 - 30°C (Satyendra, 2015).

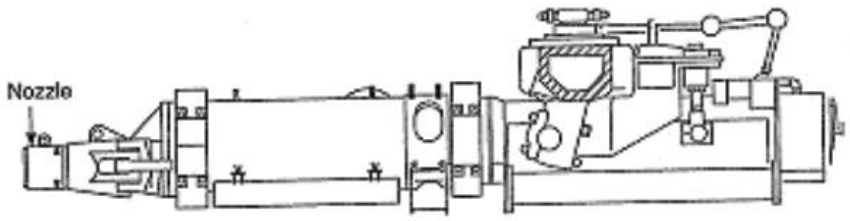

Figure 4: Mud gun/clay gun used to plug of tap hole - elevation view (Geyers & Halifa, 2014)

During plugging, special care must be taken to ensure that the tap hole is plugged and that it closes properly. The objective is to fill the taphole with clay of which the porosity needs to be reduced as it is heated through expansion of the clay. This is usually monitored by the quantity of taphole clay that is pushed into the tap hole. Modern mud guns have mass indicators on the outside of the gun to show the quantity of clay that is left in the gun which will give the mud gun operator an indication of the clay mass that is present in the tap hole. If the tap hole is not closed properly, the clay mass might spill out of the tap hole which is dangerous and costly (Geyers & Halifa, 2014). Spillage of taphole clay into the trough will result in sparks which, together with the hot gas and liquid being expelled from the tap hole, is dangerous (Tupkary, 2018). The mud gun will have to be loaded with clay again to be able to plug the furnace again.

When the blast furnace tap hole is plugged, two main objectives need to be met. These objectives include to achieve the desired tap hole length and a sufficient clay mushroom build-up on the inside of the furnace. During plugging the operator must ensure that the tap hole length is above a certain specification as short tap hole lengths will result in tap hole glowing and possibilities of self-opening of the tap hole. The self-opening of the tap hole will result in hot liquid pig iron and slag to be expelled from the tap hole, which creates a dangerous and volatile environment if tapping is not pre-planned. During the plugging, carburising, and carbonising occurs in the taphole clay. As the taphole clay is inserted into the tap hole, volatiles, and residual moisture in the clay volatilises from the taphole clay (carburising). As the temperature increases, the organic matter that is present in the taphole clay, converts to carbon through carbonising. The carburising ensures rapid evolution of gas that is formed in the clay as it is heated whilst carbonising converts the organic matter in the clay to carbon which assists with the strength development of the clay. The mushroom build-up in Figure 5 is the desired example of build-up inside the furnace.

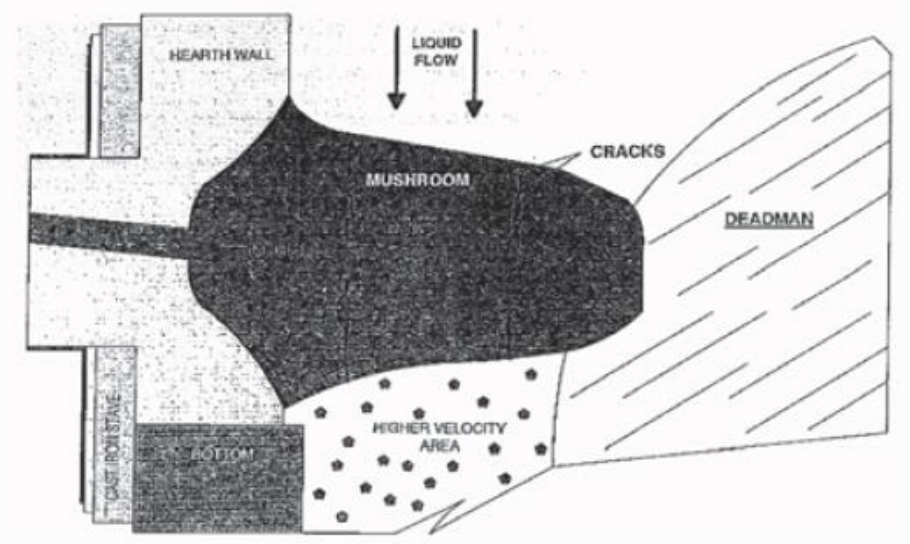

Figure 5: Schematic diagram of a tap hole mushroom mass which connects the deadman and tap hole (R, et al., 2003)

As the plugging of the tap hole takes place, the objective is to ensure a properly formed bulbous mass, called the mushroom, inside the tap hole. This mushroom is important to ensure the protection of the tap hole during smelting and tapping (Kongoli, 2006). As the taphole clay is pushed into the tap hole, the desired result is for the mushroom to form a union between the tap hole (hearth wall) and the deadman in the furnace (Kongoli, 2006). The deadman, into which the mushroom needs to grow into, is a porous coke bed in the lower part of the furnace that functions as a structure to maintain the integrity of the charge that is fed into the furnace (Brannbacka, et al., 2000). The deadman plays a crucial role in that it ensures gas movement towards the charge of raw materials and flowing of hot reduced iron to the lower part of the furnace towards the tap hole (Brannbacka, et al., 2000). As the reduced iron moves through the deadman, it picks up carbon to form pig iron, after which it exits the tap hole. The mushroom shape and size are important as it determines the extent of tap hole protection. The size effect, in Figures 6 and 7, where thermal scans of the tap hole during tapping at different mushroom radii illustrate the effect of temperature and erosion of the hearth as well as the tap hole at different mushroom sizes.

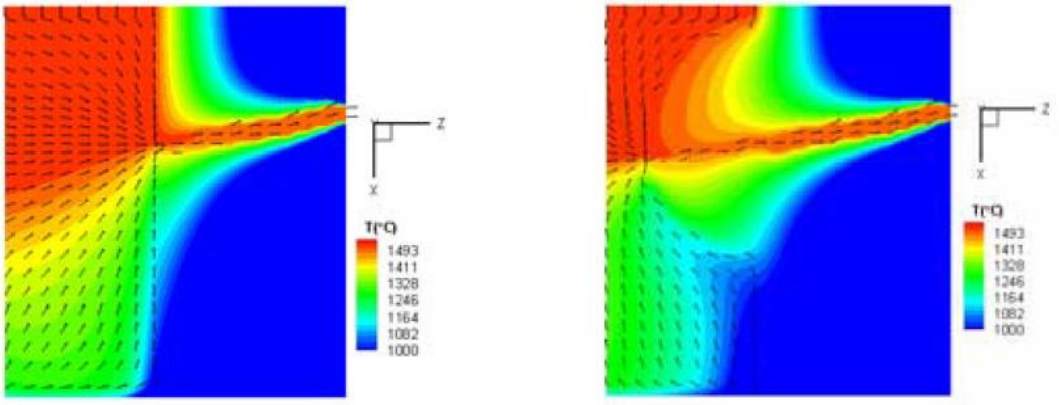

Figure 6: Thermal scans of the blast furnace taphole during tapping - left: No mushroom, right: 1.5m radius mushroom (Kongoli, 2006)

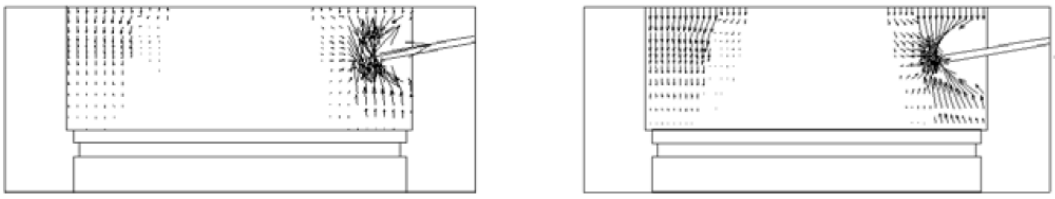

Figure 7: Vector field showing liquid velocities during tapping at different mushroom radii - left: 1.0m radius mushroom, right: 1.5m radius mushroom (Kongoli, 2006)

In Figure 6, the effect of tap hole temperatures on the mushroom size is shown. If no mushroom formed on the inner part of the tap hole, the sidewall temperature as well as the graphite blocks in the tap hole are at extremely high temperatures. Generally, the tap hole temperature needs to be as low as possible to prevent excessive heating of the tap hole (glowing) as well as increasing the life of the tap hole graphite blocks. To reduce the temperature, a big enough mushroom needs to be formed to help dissipate some of the heat away from the tap hole as well as the hearth (Kongoli, 2006). In Figure 7, the schematic diagram shows the degree of erosion due to liquid velocities at different mushroom sizes. As the mushroom diameter increases less liquid turbulence is created at the tap hole during tapping. This reduction in turbulence near the tap hole will reduce the erosion, i.e. elephant footing, caused by the liquid pig iron and slag as it exits the tap hole (Kongoli, 2006). The reduction in erosion will increase the life of the tap hole blocks and tap hole integrity.

As mentioned, wear of the tap hole is due to erosion, but the exact mechanism has not been discussed in detail. The wear of the tap hole is described in a sequence of three steps: penetration, corrosion, and erosion. During penetration, the liquid pig iron infiltrates the pores of the refractory surrounding the tap hole. Once the refractory has been penetrated, corrosion of the refractory takes place and increases as the liquid pig iron penetrate the refractory. The corrosion is temperature-dependent investigated by Campbell & Pericleous (Campbell & Pericleous, 2002) due to the temperature increases the extent of the refractory corrosion also increases. After the refractory has been penetrated and weakened by corrosion, erosion will increase the wear of the tap hole if the shear stress of the liquid is enough to remove small sections of the refractory (Campbell & Pericleous, 2002). The

erosion starts on the inner side of the tap hole graphite blocks and moves towards the hearth surface towards the tap hole (Figure 8).

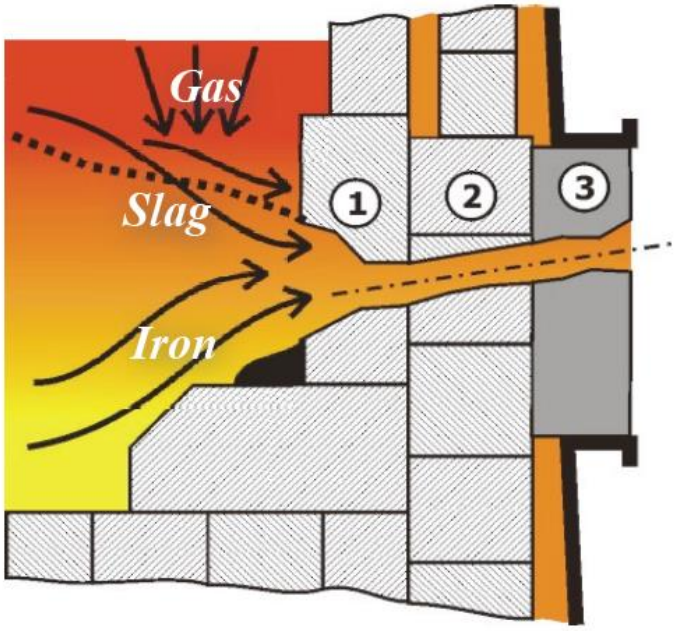

Figure 8: Schematic diagram showing the wear of the tap hole blocks by liquid pig iron, slag and gas movement around the tap hole (Geyers & Halifa, 2014)

2.2. Blast furnace taphole clay – Development and Operation

The design of a taphole clay is considered very intricate as the raw material selection process is dependent on the industrial process that is used. For blast furnace operations, the factors that determine the correct selection of taphole clay include ensuring the clay plasticity, mechanical strength and refractoriness (Parnahaj, et al., 2012). The clay needs to be refractory at high temperatures as well as have sufficient plasticity to be able to work the clay in the mud gun, to be able to plug the tap hole and ensure a proper seal of the tap hole to prevent the liquid pig iron and slag in the furnace to run out of the tap hole or penetrating the clay (Parnahaj, et al., 2012). The taphole clay strength development is also extremely important. To ensure the clay develops sufficient strength, the resin present in the clay needs to be cured long enough for it to release volatiles gradually and create sufficient strength through polymerisation of the resin as well as carburisation, to be able to withstand the internal pressure inside the furnace exerted on the tap hole (Geyers & Halifa, 2014).

Every furnace taphole clay is different even if the same raw materials are used, as furnaces are unique and accordingly taphole clay needs to be developed uniquely for a specific furnace. An example of two types of taphole clays is summarised in Table 1. Both clays are resin bonded, i.e. do not contain tar as part of the binder, and one is a 36 mass% alumina clay and the other a 66 mass% alumina clay. The alumina content of the clays is dependent on the raw material that is used in the development of the clay.

Table 1: Properties of taphole clay development examples – medium alumina amount and high-alumina amount clays (Routschka, et al., 2012)

Product	A – 66 mass% alumina	B – 36 mass% alumina
Raw material base	Corundum (Al_2O_3) + Silicon carbide (SiC)	Bauxite (Al_2O_3) + Silicon carbide (SiC)
Maximum service temperature	1600°C	1550°C
Type of bond	Organic chemical (Resin)	Organic chemical (Resin)
Chemical		
Al_2O_3	66.00	36.00
SiO_2	15.50	45.00
Fe_2O_3	0.40	0.90
CaO	-	-
SiC	18.00	18.00
C	6.00	11.00
MgO	-	-
ZrO_2	-	-
Physical Properties		
Pre-firing [°C]	1400	1400
Bulk density [g/cm^3]	2.20	2.08
Apparent porosity [%]	19.80	19.00
Cold crushing strength [MPa]	9.50	11.00
Linear change (irregular) [%] – on heating; expansion (+); contraction (-)	+0.30	+0.20

The properties in Table 1 are generally the characteristics for consideration when designing a taphole clay. Other properties such as hot modulus of rupture (HMoR) of the clay, loss on ignition (LOI) (clay mass difference after heating from 25°C to a desired temperature), volatile loss, Marshall extrusion pressure (MEP) can also be used to supplement the development of the clay. The 66 mass% alumina clay in Table 1 is considered a high alumina clay and 36 mass% alumina clay a medium alumina taphole clay. The maximum service temperatures are dependent on the chemical composition or the additives in the clay that cause fluxing. The fluxing assist with sintering of the taphole clay (Routschka, et al., 2012). The other components in the chemical analysis like iron oxide are impurities associated with the aggregate that is used in the clay. The taphole clay generally contains silicon carbide (SiC) to assist with abrasion resistance usually in the order of ~20% (of 97-99% SiC purity in the raw material). The organic carbon quantity of the clay is dependent on the level of carbonising required. This is related to the strength of the clay together with the resin binder used. The higher the organic carbon content, the higher the degree of carbonising and higher the strength (cold crushing strength) of the clay (Routschka, et al., 2012).

The pre-firing temperature specified in Table 1 refers to the temperature at which the clay is fired before the physical tests are conducted. All the tests are conducted under reducing conditions to get an accurate representation of the results. The apparent porosity of the clay refers to the percentage of open pores in the clay matrix. This is extremely important for both volatile releases from the resin in the clay to give proper strength development, as well as minimise the pig iron and slag penetration in the clay during operation (Routschka, et al., 2012). The cold crushing strength of the clay relates to the strength needed to keep the tap hole from opening due

to liquid metal mass and internal furnace pressure. This is extremely important as the strength of the clay will be the determining factor for self-opening instances of the tap hole because of the brittle nature of the clay. The last property in Table 1 is the permanent linear change (thermal expansion) which refers to the percentage of expansion the clay experiences at a certain temperature. This indicates how well the clay seals the tap hole once it is placed and whether the tap hole will properly close without any leakage. The thermal expansion ensures a proper seal with the tap hole but to the expense of the taphole clay porosity. With the increase in thermal expansion, the clay porosity increases which can become problematic when slag or hot metal starts to penetrate the structure of the clay. The balance between thermal expansion and increase in porosity of the clay needs to be well designed to ensure a good tap hole seal but also minimal delay with drilling out hard taphole clay. The organic carbon added to the clay, which is converted to carbon through carbonising, functions also as a means of non-wetting agent due to its surface properties that do not interact well with the slag viscosity and surface tension as well as an increased thermal conductivity due to the carbon (Nelson, 2014). The non-wetting ability of the carbon structure ensures that slag or hot metal does not penetrate the pores of the clay that might cause problems when the clay needs to be drilled out of the tap hole. The increased thermal conductivity due to higher aggregate additions of organic carbon, assists with the transfer of heat through the clay as well as conducting it efficiently. A lower thermal conductivity would not ensure proper sintering and longer holding times (Nelson, 2014).

The development of a taphole clay for a specific application depends on multiple factors that need to be considered. These include (Nelson, 2014):

- The clay needs to be soft and plastic enough to be pushed through the mud gun into the tap hole with ease and be able to be drilled open straight through the centre of the tap hole in a certain time frame. The clay also needs to be hard enough to withstand the pressure from inside the furnace due to gas and liquid pig iron mass that exert pressure on the tap hole. The clay also needs to be hard enough to ensure reduced wear by liquid pig iron and slag during tapping and serve as a protective layer between the liquid pig iron and graphite blocks of the tap hole.
- After curing and carbonisation of clay, the clay needs to have enough strength to ensure a proper seal without shrinkage that may cause tap hole leakages. The clay strength development needs to take place within a required holding time and after the tap hole is closed, the dwell time required for proper melting in the furnace needs to be adhered to. The dwell time commences once a successful and safe tap hole close has been achieved without subsequent damage to the tap hole due to gas evolution through the tap hole or liquid pig iron turbulence inside the furnace. The extent of damage on the tap hole due to turbulent liquid pig iron inside the furnace is a function of the mushroom integrity and size.
- After drilling open the tap hole, a controlled tapping stream with minimal surging or splashing must be maintained.

The design and development of a taphole clay is a continuous process because the formulation usually requires small changes until it operates satisfactorily according to a certain blast furnace process. Some guidelines assist

in moving closer to the desired product. The taphole clay usually consists of three major parts, i.e. aggregate, matrix and binder (Siva Kumar, et al., 2017). The function of each of these is important and they work together to achieve a successful clay design. The aggregate is used as filler in the clay as well as a measure of increasing the sinterability and abrasion resistance of the clay. The second part of the clay, the matrix, controls the reactivity of the clay, the packing density (particle size distribution) and non-wetting abilities by using non-wetting additives (Siva Kumar, et al., 2017). Finally, the binder controls the workability of the clay as well as acts as a temporary binder to hold the matrix and aggregate together until it is pushed into the tap hole (Siva Kumar, et al., 2017). The binder also ensures that sufficient clay strength is achieved as it is heated in the tap hole to maintain a secure and successful seal (Siva Kumar, et al., 2017).

2.2.1. Aggregate

The aggregate of the taphole clay refers to particle size ranges from 5mm down to 45um. Depending on the sinterability the clay needs to achieve, either a 5mm top fraction or 3mm top fraction is required (Geyers & Halifa, 2014). If the clay needs to sinter very well or relatively quick, a 3mm top fraction is used and if the sinterability needs to be reduced a 5mm top fraction is incorporated. The sinterability is an important aspect to consider when short tapping times are required. If the sinterability is too intensive, the tap hole drilling will take considerably longer and can also lead to reduced taphole clay lengths in the tap hole and increased production times. The sinterability relates to the strength of the clay after firing (cold crushing strength) and with what ease the tap hole can be opened after melting. The reduction in taphole clay lengths will reduce the mushroom build-up and result in tap hole blocks being worn and tap hole temperatures increasing.

The aggregates generally used for taphole clay development include graphite, fused or tabular alumina, bauxite, andalusite (Mulcoa 60), calcined clay and silica sand. The alumina (Al_2O_3) contents of these raw materials, except for graphite, differ and depending on the high-temperature properties required for the clay, the selection is made accordingly. Alumina has a high corrosion resistance (Siva Kumar, et al., 2017) and increases the temperature at which the clay can operate as the alumina content increases. Graphite can also be used as an aggregate if the clay requires a very good non-wetting ability (Geyers & Halifa, 2014). Some of the raw materials also contain impurity components such as hematite (Fe_2O_3) and lime (CaO) that can influence the performance of the clay. The use of either fused or tabular alumina is done only on occasion or if furnace temperatures are extremely high or slag is very aggressively corrosive. These raw materials are extremely expensive and since a taphole clay is a consumable, the cost of it needs to be as low possible.

Another raw material that is also readily used in taphole clay is silicon carbide. The use of this raw material will increase the abrasion resistance and reduce the slag corrosion when up to 10% of this material is added (Siva Kumar, et al., 2017). The selection of the particle size of the silicon carbide depends on where the highest degree of corrosion exists. Adding silicon carbide up to 10% in either the 1-3mm (Siva Kumar, et al., 2017) or 0-0.3mm size fraction, will improve the corrosion resistance significantly, resulting in clay that performs better and lasts longer. Increasing the abrasion resistance will also help to reduce the wear the tap hole blocks will experience as

the taphole clay protects the tap hole blocks for longer. Silicon carbide adds a small degree of thermal conductivity of the clay that is required for proper sintering and effective heating of the clay.

The properties of the taphole clay can be controlled by varying the ratios of 3-5mm, 1-3mm and 0-1mm (+45µm-1mm) aggregate size fractions. The following guidelines are used (Nelson, 2014) (Siva Kumar, et al., 2017):

- The 3-5mm size fraction: This fraction usually contains 20-25 mass% of either of the aggregates mentioned, i.e. bauxite, andalusite, sintered or fused alumina and fireclay or chamotte. Selecting which aggregate(s), depends on your sintering properties and slag corrosion requirements as well as maximum operating temperature.
- The 1-3mm size fraction: 20-30 mass% of the aggregates mentioned. Selecting between the 3-5mm and 1-3mm percentage distribution in the clay depends on the required sinterability of the clay. If the clay top fraction required is 3mm, then 20-40 mass% of the clay will consist of 1-3mm.
- The +45µm-1mm size fraction: 20-30 mass% depending on the 3-5mm and 1-3mm percentage distribution and whether the clay requires better sinterability and improved slag corrosion resistance. There are some developments where extremely reactive clays are required and these can have up to 40-60% of the +45µm-1mm size fraction depending on the slag permeability.
- The -45µm size fraction: The remainder of the clay is made up of this size fraction. The matrix filler material, as well as additives, contribute towards this size range and this matrix fine material controls your gas flow as well as strength and bulk density (compacting) of your material. Some specialised additives such as zircon or tabular alumina are added which controls your clay thermal cycling and dimensional stability as well as chemical resistance. The non-wetting ability of the taphole clay also resides within this fraction and special additions to the clay are made to facilitate this.

2.2.1.1. Andalusite

The mineral andalusite is a natural occurring aluminium-silicate and forms part of the family of polymorphic forms with Al_2SiO_5 stoichiometry, which also includes kyanite and sillimanite (Kogel, et al., 2006). The crystal of andalusite has a translucent white appearance with a reddish-brown cross in the centre of the cubic particle. The reddish-brown cross, called the chiastolite cross, refers to the Fe_2O_3 as an impurity in the mineral (Klein & Dutrow, 2008). The colour of the mineral changes to a sharp white particle once it has gone through the mullitisation above 1400°C (Klein & Dutrow, 2008). The composition of the mineral differs depending on where the ore body was mined. Certain andalusite is mined in South-Africa, France, and Spain, with these countries being the largest producers of andalusite. Figure 9 is a map of the mining operations of andalusite and its neighbour minerals.

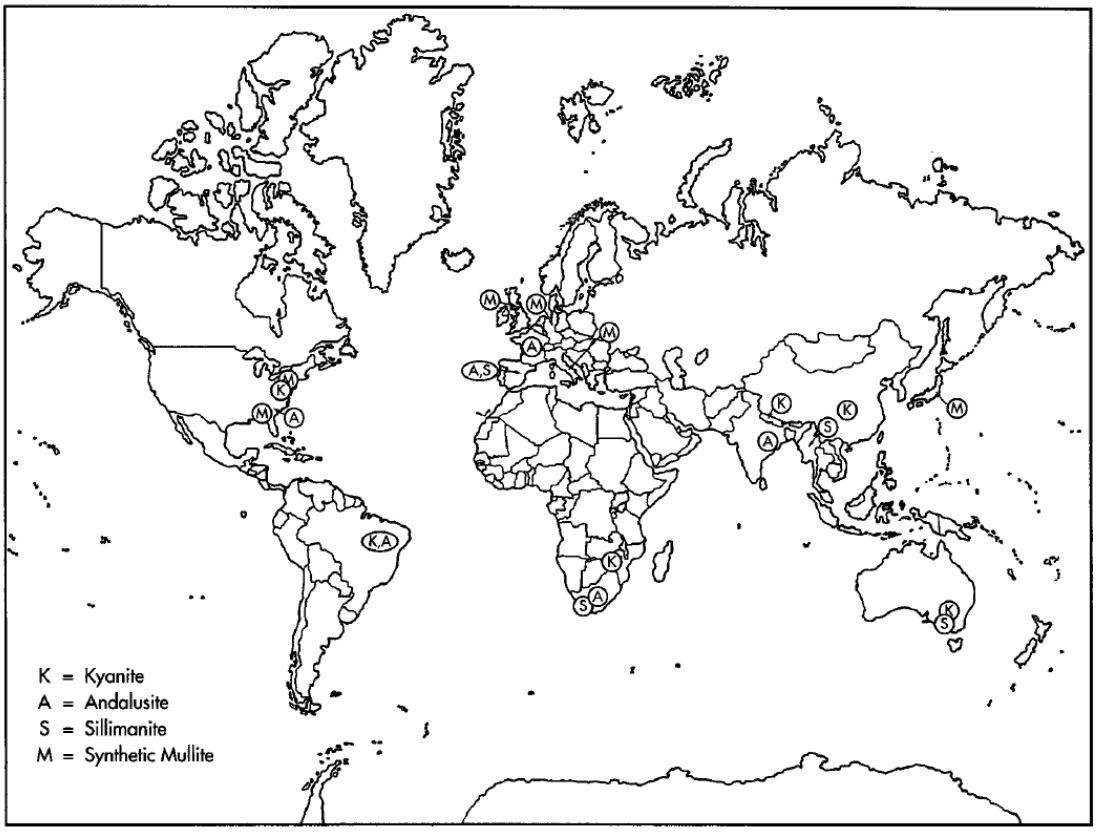

Figure 9: Map of global mining and production sites for andalusite, sillimanite and kyanite (Kogel, et al., 2006)

Depending on where the ore body is mined it will have different chemical compositions. The andalusite mined in South-Africa has a composition range that is summarised in Table 2 together with some typical physical properties (Kogel, et al., 2006). Some andalusite that is mined in France have higher Al_2O_3 contents up to 64% (Kogel, et al., 2006) and that is higher grade than the andalusite mined in South-Africa and Spain (Klein & Dutrow, 2008). The exact composition of stoichiometric andalusite (Al_2SiO_5) is Al_2O_3: 63.2%, SiO_2: 36.8%, but the composition of the mineral range, according to Table 2. The stoichiometry of alumina to silica present in the andalusite will determine the percentage of mullitisation that will occur on heating, i.e. percentage Al_2SiO_5 as mullite above 1400°C.

Table 2: Composition and physical properties of andalusite (South-Africa) (Kogel, et al., 2006)

Composition (%)	Al_2O_3: 52.00 – 57.00 SiO_2: 35.00 – 44.00 Fe_2O_3: 1.00 – 4.50 TiO_2: 0.04 – 4.00
Specific gravity (g/cm^3)	3.16 – 3.20
Hardness (Mohs)	7.50
Volume change	Very slight increase
Density after mullitisation (g/cm^3)	3.04

The crystallography of andalusite is orthorhombic that occurs in a square prism crystal (Klein & Dutrow, 2008). The mineral andalusite (Al_2SiO_5) consists of either kyanite or sillimanite with impurity phases cordierite, garnet, micas and leucite (Klein & Dutrow, 2008). The extent of the impurities contained in the mineral is a function of the ore body and where it was mined. The impurities also give the mineral andalusite a distinctive colour that is different from other sources of andalusite.

2.2.1.2. Calcined Clay

The mineral kaolinite is a natural clay type which consists of kaolin or clay (Ciullo, 1996). This mineral is naturally soft and is constituted of surface hydroxyl groups that need to be removed during calcining to produce calcined clay (Ciullo, 1996). The calcined clay product is harder, more absorbent, brighter in colour and more dimensionally stable. The occurrence of kaolinite is very diverse which includes sedimentary rocks formed at low temperatures and pressures, weathered aluminium-silicate like feldspar, the soil where it has been transported through water flow like in lakes where clay sediments form with quartz and other minerals (Klein & Dutrow, 2008). Kaolinite is commonly used in China for pottery and other types of ceramic applications (Klein & Dutrow, 2008). The clays are also used in refractory operations due to its sticking ability attributed to the micas in the clay.

The mineralogy of kaolinite is a triclinic crystal structure where alumina octahedral and silica tetrahedral sites fill the triclinic crystal (Klein & Dutrow, 2008). This mineral is an earth whitish colour and is sometimes coloured due to the presence of impurities (Klein & Dutrow, 2008). The theoretical formula is $Al_2SiO_5(OH)_4$ with a composition of Al_2O_3: 39.5%, SiO_2: 46.54% and H_2O (moisture): 13.96% (Kennedy, 1990). The impurities presented in kaolinite will depend on how the clay layer was formed and where its exact geographical location was. The summarised information in Table 3 is of the different geographical locations of clay as well as their associated impurities. The majority of any kaolinite mineral contains the phase kaolin with the sum being made up of moisture (hydroxyl groups) and other impurities (Kennedy, 1990).

Table 3: Composition and impurities in kaolinite from three different geological locations (Kennedy, 1990)

Geographical Location	Impurities/Phases	Quantity (%)
United States – Georgia	Major phase: Kaolinite Impurities: Quartz, Muscovite, Biotite, Smectite, Ilmenite, Anatase, Rutile, Leucoxene, Goethite, Zircon, Tourmaline, Kyanite, Graphite	85.00 – 95.00 Remainder
United States – North Carolina	Major phase: Kaolinite Impurities: Quartz, Muscovite, Microcline, Plagioclase	10.00-40.00 Remainder
England	Major phase: Kaolinite Impurities: Quartz, Mica, Potash Feldspar, Tourmaline	10.00-40.00 Remainder

The results in Table 3 are only from the major mining entities that produce kaolinite. The United States of America is the largest producer of kaolinite, followed by the United Kingdom and Russia (Kennedy, 1990). Other minor producers are based in Europe, Africa and South America.

The use of kaolinite in refractories is for its filler properties as well as plastic behaviour and sintering abilities. Some kaolinite has high mica percentages that assist with a sticky effect in the clay whereas some have higher potash feldspar percentages that assist with fluxing at high temperatures, i.e. sinterability.

2.2.1.3. Bauxite

Bauxite is mined and used in primarily the production of alumina. A total of 90% of the global mining of bauxite goes towards making alumina via the Hall-Héroult process (Authier-Martin, et al., 2001). The remainder of the stock is used for refractory production, abrasion resistance, and in the chemical industry. The mineral bauxite consists of three major phases, i.e. diaspore, gibbsite and boehmite. Two main types of bauxite can be grouped, i.e. karstic and latertic (Xuefei, et al., 2011). The latertic bauxite consists mainly of gibbsite whereas karstic bauxite consists of boehmite and diaspore (Xuefei, et al., 2011). The grains of the bauxite appear round-, with a dull earthy, white, grey-, and yellowish colour.

Although bauxite is constituted out of three major phases, there are also significant levels of impurities depending on the geological location at which the bauxite was mined. Table 4 summarises compositional- as well as physical information regarding bauxite that is mined in Guangxi, China.

Table 4: Compositional and physical properties of bauxite from Guangxi, China (Xuefei, et al., 2011)

Composition (%) – XRF	Al_2O_3: 49.85 – 75.09 Fe_2O_3: 2.08 – 27.29 SiO_2: 0.81 – 8.11 FeO: 0.19 – 7.00 TiO_2: 2.60 – 4.82
Composition (%) - XRD	Diaspore: 52.00 – 83.00 Hematite: 0.00 – 18.00 Kaolinite: 0.00 – 21.00 Gibbsite: 0.00 – 14.00 Anatase: 4.00 – 10.00 Chamosite: Remainder
Specific gravity (g/cm^3)	3.02 – 3.40
Hardness (Mohs)	2.00 – 2.50
Volume change	Shrinks significantly

Although the impurities mentioned in Table 4 are characteristic to bauxite, some other trace impurities can also be found in different geological ores. The major and minor phases that can be present in bauxite given all the possible geological locations where mining is possible are summarised in Table 5 (Authier-Martin, et al., 2001).

Table 5 : Phases present in bauxite (Xuefei, et al., 2011)

Element	Mineral
Major	
Aluminium	Gibbsite Boehmite
Silicon	Quartz Kaolinite/Halloysite
Iron	Hematite Aluminium Goethite
Minor	
Carbon	Organic Carbon
Phosphorus	Wavellite Crandallite-H
Calcium	Calcite Crandallite-H
Potassium	Illite
Manganese	Lithiophorite
Magnesium	Magnesite Dolomite
Sodium	Dawsonite
Strontium	Celestite
Sulphur	Woodhouseite Pyrite

The mineral location and microstructural features of bauxite are shown in Figure 10. The scanning electron microscopy image shows how the diaspore is surrounded by chamosite with goethite running as long stringers or round nodules. The goethite and diaspore can also co-exist together as shown in Figure 10e where the goethite nodules are enclosed by the diaspore. Some small hematite nodules are also observed in Figure 10f enclosed by kaolinite.

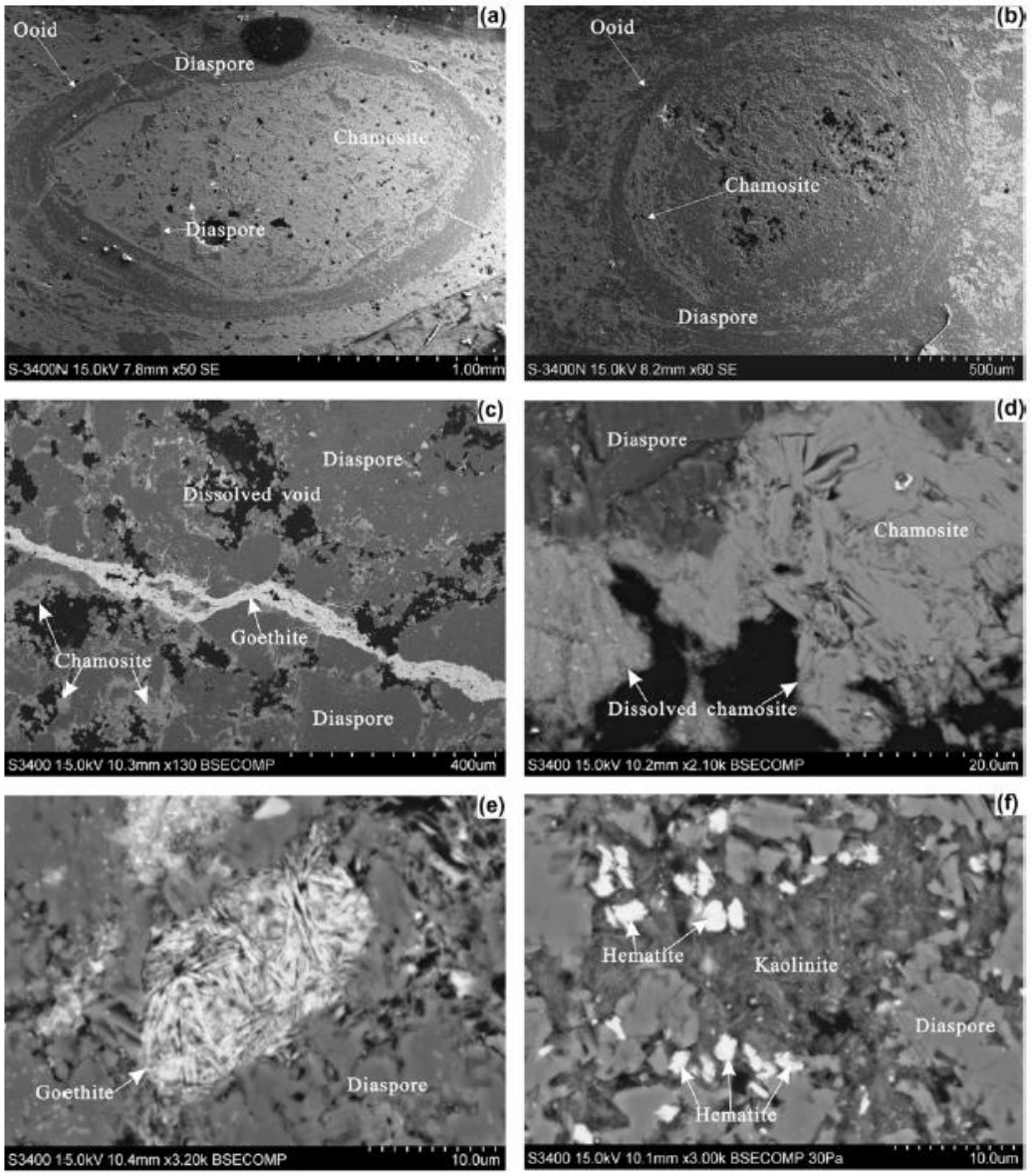

Figure 10: Backscatter electron images of bauxite from Guangxi, China (Xuefei, et al., 2011)

2.2.2. Matrix

The second important part in designing a taphole clay is the matrix of the clay. There are subdivisions of the matrix that is referred to by a certain size range. The matrix of the clay usually contains both the -1mm+45µm size fraction and -45µm. The -45µm particle size fraction is called the fine matrix and constitutes 50 mass% of the total clay mass (Nelson, 2014). The matrix usually consists of a few components and each has a certain function. The matrix consists of the matrix material, fillers, special additives (Siva Kumar, et al., 2017). The use of these combinations of components, assist with compacting the clay to avoid liquid/slag penetration during operation, strength development of the clay, pig iron or slag erosion and corrosion as well as abrasion resistance of the clay during tapping and smelting (Nelson, 2014). The use of pure alumina or silica matrix material assists with linear expansion

of the clay that will ensure a proper seal is maintained during smelting as temperatures fluctuate and may cause related shrinkage or excessive expansion with super-heating or cooling during tapping (Nelson, 2014).

The following matrix raw materials have a specific function and all of them work together to achieve a clay that is malleable, strong and resistant enough for the harsh tapping environment it experiences (Siva Kumar, et al., 2017):

- Alumina, Silica, alumina-silicates or coke fillers (matrix material),
- Graphite, Coal
- Silicon Carbide,
- Special Additives (Sulphur, Ferro-silicon Nitride, Zircon, Aluminium, Silicon)

The use of the filler materials is to increase the compactability and bulk density of the clay. Depending on the operating temperatures and environment in which the clay operates, the use of pure alumina or pure silica filler material will assist with high-temperature refractoriness (Geyers & Halifa, 2014). The graphite or coal assists with the non-wetting which reduces the erosion of the clay (Siva Kumar, et al., 2017). The shape of the graphite used in the clay also increases the gas permeability which assists with the quick release of volatiles from the clay (Siva Kumar, et al., 2017). The volatiles is from either the binder or resin used in the clay and significantly influences the strength development of the clay. Silicon carbide is used in the matrix of the clay to increase the abrasion resistance of the clay and give a degree of oxidation resistance during smelting (Siva Kumar, et al., 2017).

The special additives are used in the taphole clay design where there is a need for certain properties to be elevated than what is already present in the clay. Sulphur is normally added if the clay contains a form of resin. The sulphur assists with vulcanisation of the resin by forming cross-linkages to give strength to the clay (Mark, et al., 2013). The amount of sulphur added will influence the rate of vulcanisation and how quick the resin in the taphole clay cross-links and develops strength (Mark, et al., 2013). The type of resin used in the clay will also influence the curing time if used in synergism with sulphur. The use of ferrosilicon nitride assists with sinterability of the clay as well as slag corrosion (Siva Kumar, et al., 2017). Increasing the nitride content in the clay will result in the clay becoming harder which will assist with slag erosion resistance but will result in longer tapping times as longer drilling times will be required to open the tap hole. Nitrides should be added in correct and applicable quantities as increasing the sinterability of the clay too significantly will result in less tap hole wear during tapping which will result in reduced tap hole lengths and insufficient mushroom build up in the inside of the furnace. During tapping, the tap hole is required to wear a certain amount, but the wear needs to be just enough to clear out the previously used clay so that new clay can be plugged into the tap hole. If the tap hole does not wear enough during tapping, the new taphole clay cannot be pushed properly into the tap hole, which will result in shorter tap hole lengths and not enough material being pushed into the tap hole for the mushroom to build up properly.

The use of aluminium or silicon metal powder acts as increased antioxidants in the clay which reduced slag corrosion and increases the hot modulus of rupture (Siva Kumar, et al., 2017). The silicon powder causes some permanent dimensional changes after firing that is favourable for taphole clay use where aluminium powder does not cause dimensional changes (Siva Kumar, et al., 2017).

2.2.2.1. Calcined Alumina

The calcined alumina produced for ceramic applications is a pure source of alumina, which is used in the matrix of the clay. Calcined alumina is created from alumina produced from bauxite in the Bayer process (Authier-Martin, et al., 2001). There are three categories of calcined alumina that can be manufactured, and the type depends on the quantity of soda-ash (Na_2O) it contains (Authier-Martin, et al., 2001). The normal- and low-soda alumina are manufactured during the Bayer process. The third type is ultra-pure calcined alumina of 99.99% Al_2O_3. The purity of the normal grade calcined alumina consists of 99.0 – 99.5% Al_2O_3 with 0.1 – 0.3% Na_2O, while the low-soda calcined alumina contains 99.7% Al_2O_3 and <0.1% Na_2O. The range of specific densities for this calcined alumina range from 3.1 – 3.4%. The conversion of bauxite to calcined alumina occurs when high-grade bauxite is calcined in rotary kilns between 1100 - 1450°C. During the calcining, the bauxite converts to alpha-alumina, i.e. corundum, through the transformation from gamma-alumina, to beta alumina and then lastly alpha-alumina (Authier-Martin, et al., 2001). The largest manufacturers of calcined alumina are Germany and France although some are produced in Brazil and China as well. The production costs for this process is high and only large plant capacity utilisation and low-cost resources will make this viable.

The main phase in calcined alumina is corundum as this is the last transformation phase that exists after calcining. Corundum has a hexagonal crystal structure but can also occur in the prismatic, bipyramidal, tabular, rhombohedral and acicular crystal structure (Deer, 1992). The colour of the mineral depends on the purity of the material. Colours range from translucent to white, brown, pink, yellow, orange, blue, green and violet depending on the impurities present (Deer, 1992). The calcined alumina has a purity of 99% and higher which presents as a pure white crystal of corundum. Other uses for this material are in polishing media and refractory material uses other than taphole clay, e.g. gunning and castable materials. The use of corundum in taphole clay allows for the clays to be used at high operating temperatures (>1400°C), gives the clays good corrosion resistance to aggressive slag and also gives it erosion resistance.

2.2.2.2. Silicon Carbide

Silicon carbide occurs naturally with some different forms present in an orebody. The crystalline mineral is referred to as moissanite and depending on the type of dimers it has in its hexagonal crystal structure, different polymorphs of this mineral can occur (Mehl, et al., 2017). The most commonly known forms of moissanite are the Type I (15R) and Type II (6H) as well as the 4H polymorphs (Baunn, et al., 1963). The crystallography of this mineral is remarkably diverse due to the multiple polymorphs it can exist as. Generally, the crystals are irregularly rounded with a thin lamina of lime material that is penetrated with metallic iron (Baunn, et al., 1963). The crystals are dark, orange-yellow, and not transparent with a smooth and polished surface. The specific gravity of these crystals is in the order of 3.23 – 3.24 with higher density material lower down into the mining layer (Baunn, et al., 1963).

Since the natural occurrence of moissanite is very rare (Baunn, et al., 1963), silicon carbide for refractory applications is synthetically prepared. The manufacturing is done by Acheson process which is a sintering process

that involves mixing silica sand (quartz) with carbon in a carbon resistance furnace to product this sintered mass referred to as carborundum, which is crushed down to size (INSACO, 2006).

The analysis shown in Table 6, is of a naturally occurring moissanite crystal that was analysed with XRF, XRD and SEM-EDS. The silica content (SiO_2) in Table 6 is the total silica content which comes from moissanite, silicon, silica and Fe-silicide.

Table 6: Chemical composition (XRF) and phase analysis of naturally occurring moissanite (Pierro, et al., 2003).

X-Ray Fluorescence	Percentage
SiO_2	55.84
TiO_2	0.02
Al_2O_3	0.41
FeO	0.09
MnO	0.01
MgO	28.49
CaO	1.43
Na_2O	0.02
K_2O	0.03
P_2O_5	0.01
LOI	18.31
X-Ray Diffraction	Percentage
Moissanite	69.68
Silica	25.30
Impurities (MgFe-Silicides, Magnesiochromite, Fe-, Al-, Cl-rich phases, silicon	4.00

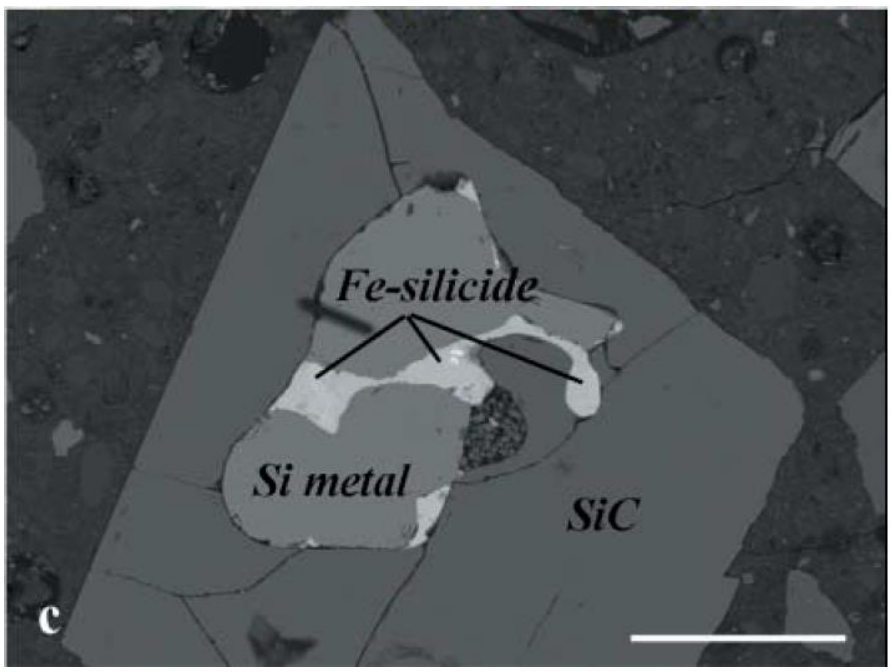

Figure 11: SEM backscattered electron image of moissanite crystal (scale bar is 200µm) (Pierro, et al., 2003)

A backscatter electron image of the crystal that was used for analysis is shown in Figure 11. The image shows the shape of the crystal as an irregular square with silicon carbide enclosing Fe-rich silicides as well as small Si-metal

particles. These Si-metal particles will only occur in moissanite that is mined naturally, synthetically produced carborundum will not contain Si in metallic form but rather silica as unreacted. The high silica content of the raw material is due to free silica associated with the same ore body. The crystal shown in Figure 11 is that of a moissanite crystal.

2.2.2.3. Coal

The description of coal is truly diverse as the constituents of coal vary and in different seams of coal in the same mining operation, coal composition differs. A description given by (Miller & Bruce, 2005) is that coal is a heterogenous combustible sedimentary rock that comprises of organic and inorganic matter. The organic parts of coal are primarily hydrogen, oxygen and carbon with trace amounts of sulphur and nitrogen (Miller & Bruce, 2005). The inorganic part is constituents that contribute towards ash formation (Miller & Bruce, 2005). Coal is a mineral that is present all over the world and it differs in deposits (type), the coalification degree (rank) and the impurities present in the coal (grade) (Miller & Bruce, 2005).

The process of coalification is that which describes the process in which initial peat/moss need to undergo to transform into coal. The coalification process is described as follows (Miller & Bruce, 2005):

$$peat \rightarrow lignite \rightarrow subbituminous\ coal \rightarrow bituminous\ coal \rightarrow anthracite$$

The distribution of deposits of coal globally, and how it has formed through the ages, are shown in Figure 12.

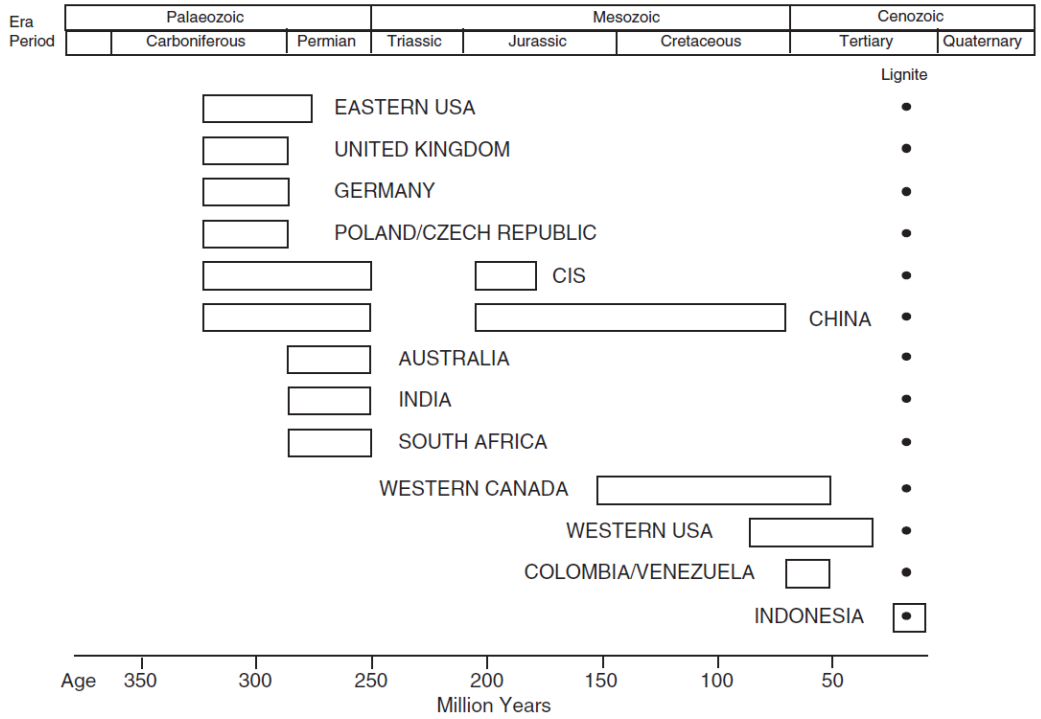

Figure 12: Coalification and deposits as formed through time globally (Miller & Bruce, 2005)

The classification of coal is dependent on how the coal is analysed and how the coal is ranked according to combustion and moisture. The basic coal analysis that is available or that can be reported is summarised in Figure 13.

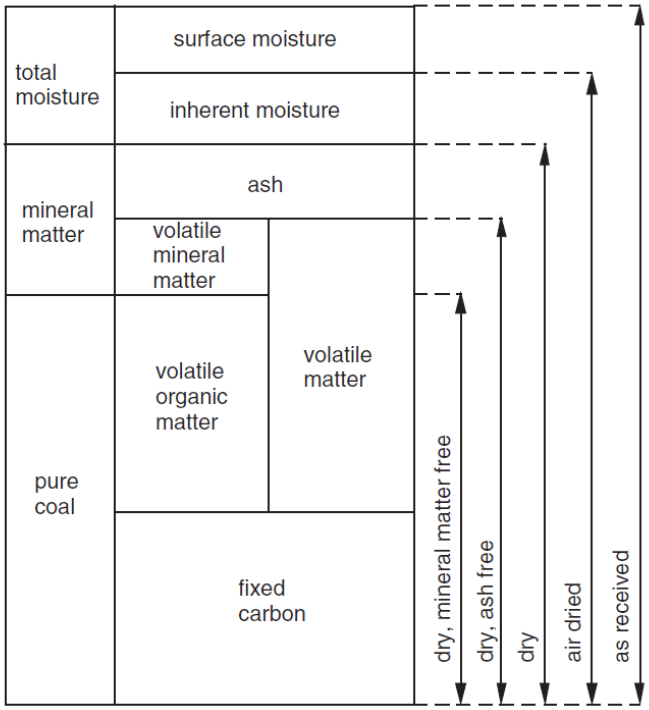

Figure 13: Analytical base vs. the components present in coal (Miller & Bruce, 2005)

There are three possible analyses of coal, dependent on what is required. The analyses include two which are component analyses and the third being a calorific analysis (Miller & Bruce, 2005). The chemical analysis can either be proximate or ultimate where proximate only gives relative values of moisture, volatiles, ash and carbon content. The ultimate gives amounts of hydrogen, oxygen, carbon, sulphur and nitrogen (Miller & Bruce, 2005). The third and last type of analysis gives the coal calorific value which is the amount of energy a given amount of coal will provide if it is combusted (Miller & Bruce, 2005). An example of the ranking of the coal, based on calorific value, moisture and volatiles is shown in Figure 14.

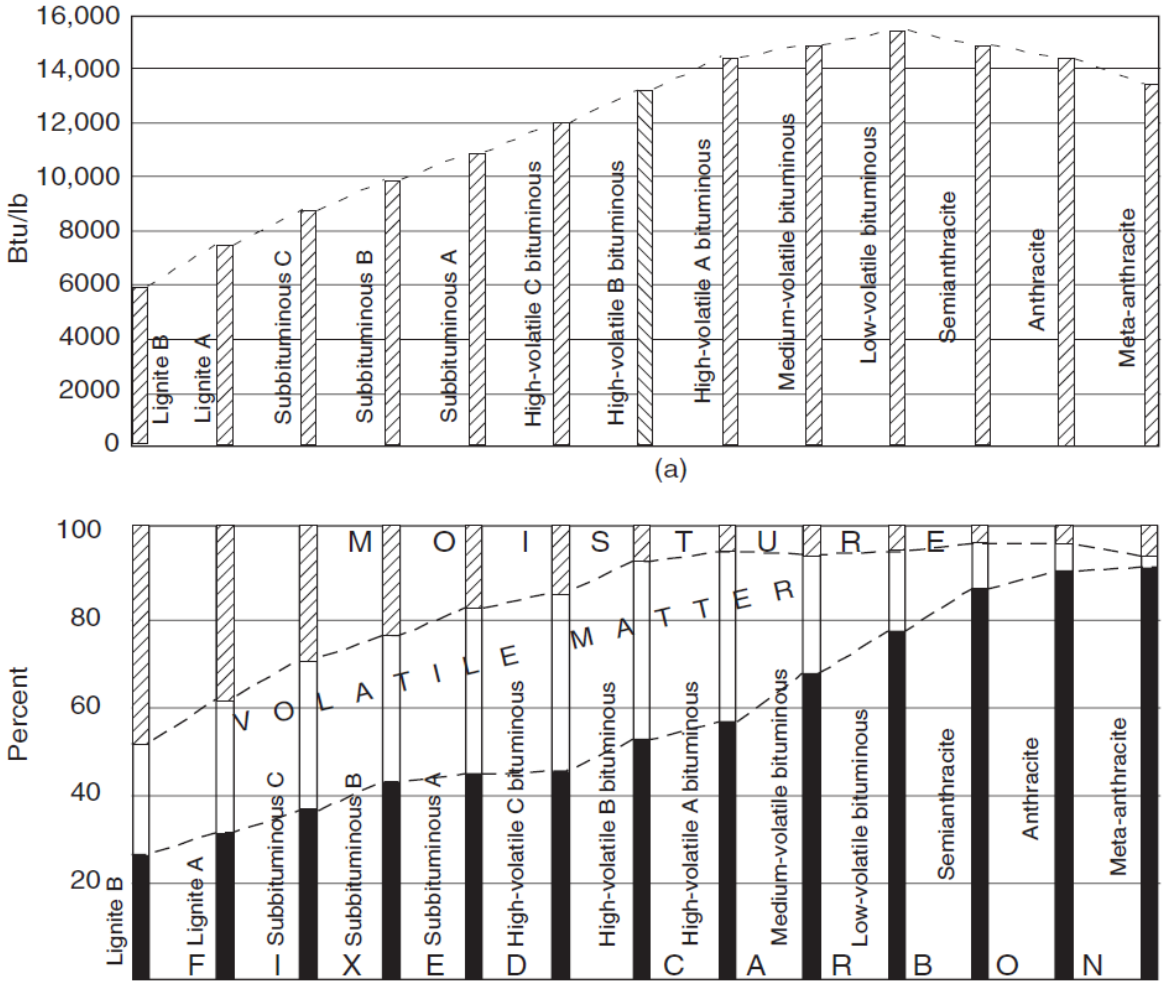

Figure 14: Ranking of coal, based on calorific value (a), moisture and volatiles (b) (Miller & Bruce, 2005)

Although there has not been a process developed for classifying coal, there are some approximations that can be used to determine the classification of coal. The American standard as summarised in Table 7, makes use of the fixed carbon, volatiles, and heating/calorific values to group types of coals accordingly. This is used as a guideline as to what a certain rank of coal analysis should be.

Table 7: The ASTM classification of coal by rank (Miller & Bruce, 2005)

Class/Group	Fixed Carbon (%)	Volatiles (%)	Heating Value (Btu/lb)
Anthracitic			
Meta-anthracitic	>98.00	<2.00	-
Anthracitic	92.00 – 98.00	2.00 – 8.00	
Semi-anthracitic	86.00 – 92.00	8.00 – 14.00	
Bituminous			
Low-Volatile	78.00 – 86.00	14.00 – 22.00	
Medium-Volatile	69.00 – 78.00	22.00 – 31.00	
High-volatile A	<69.00	>31.00	>14000.00
High-volatile B	-	-	13000.00 – 14000.00
High-volatile C	-	-	10500.00 – 13000.00
Subbituminous			
Subbituminous A	-	-	10500.00 – 11500.00

Subbituminous B	-	-	9500.00 – 10500.00
Subbituminous C	-	-	8300.00 – 9500.00
Lignitic			
Lignitic A	-	-	6300.00 – 8300.00
Lignitic B	-	-	<6300.00

The standard of classifying coal according to rank (Table 7), only present the carbon and volatile analysis of the coal. Given that there are ash forming compounds also present in coal, the coal is comprised of oxide minerals of different types depending on the geological location. The minerals that have been recorded in coal are given in Table 8. These are all the possible minerals that can be present or have been recorded in coal all over the world.

Table 8: Possible minerals that can be found in coal (Glikson & Mastalerz, 2000)

Type	Minerals
Clay minerals	Kaolinite, Smectite, Illite, Sericite, Muscovite, Halloysite, Chlorite
Sulphide minerals	Pyrite, Marcasite, Greigite, Sphalerite, Galena, Chalcopyrite, Pyrrhotite, Arsenopyrite, Millerite
Oxide minerals	Quartz, Hematite, Magnetite, Rutile, Anatase, Brookite, Limonite, Goethite, Lepidocrocite, Diaspore
Phosphate minerals	Apatite, Goyazite, Gorceixite, Crandallite, Monazite, Xenotime
Carbonate minerals	Calcite, Dolomite, Siderite, Ankerite, Witherite, Dawsonite, Strontionite, Argonite, Magnesite
Sulphate minerals	Barite, Gypsum, Anhydrite, Bassanite, Jarosite, Szomolnokite, Rozenite

The mining of coal is a continuous process of which requirements for this fossil fuel remains steady. Because of the environmental liabilities coal combustion is associated with, as well as the problematic ash formation, fossil fuels are becoming less used compared to other natural resources for combustion. Coal reserves and where in the world they can be mined as well as the contribution of each of these on a global scale are summarised in Figure 15 and Figure 16. The geological location of coal has a significant effect on its classification and analysis. The information used to construct the graphs was from a world survey conducted and updated as of 29 December 2019 (British Petroleum, 2019). The type of coal that is generally used in taphole clay designs are a low-volatile, low ash (<15 mass%), low moisture (<10 mass%) raw material with a 70-80 mass% carbon content. The use of coal is a lower grade source of carbon than other more expensive sources such as synthetic carbon or graphite.

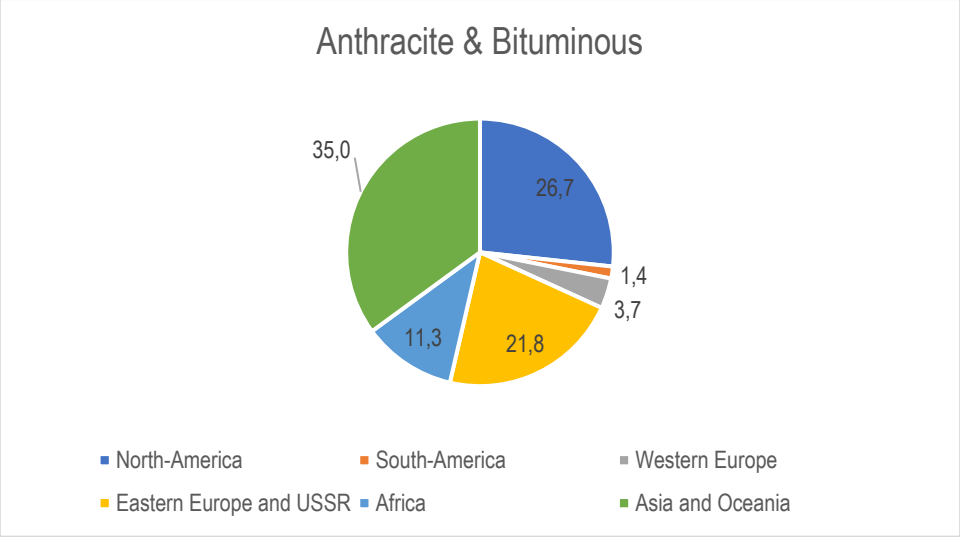

Figure 15: Chart showing the world resource of Anthracite and Bituminous coal and the contribution of each country it can be mined in (British Petroleum, 2019)

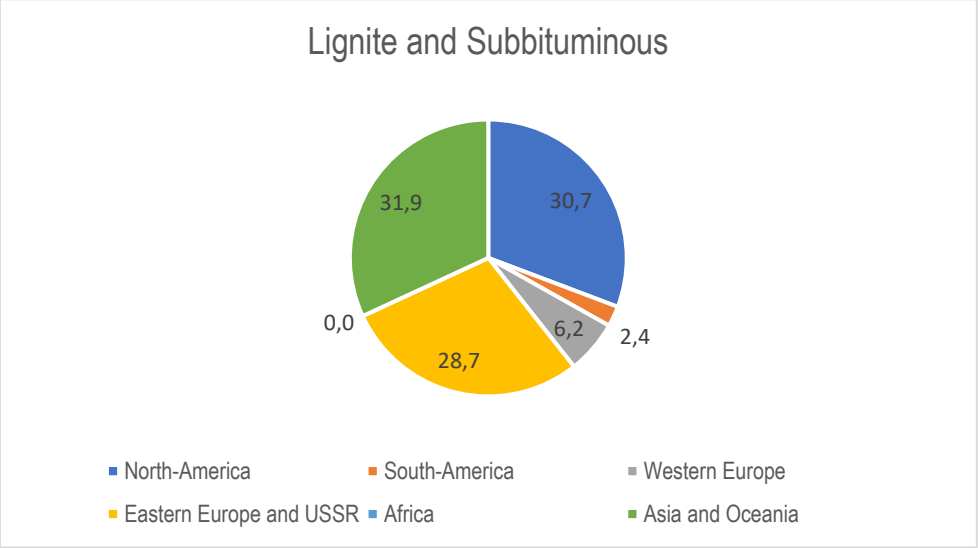

Figure 16: Chart showing the world resource of Lignite and Subbituminous coal and the contribution of each country it can be mined in (British Petroleum, 2019)

2.2.3. Binders

The binder used in a taphole clay has a great influence on the successful performance of the clay. The binder is a liquid, 20% by mass usually, that is used to bind the aggregate and matrix material of the clay in a temporary form whereby it can be plugged or handled (Siva Kumar, et al., 2017). The binder has a significant effect on the extrusion and strength development of the clay (Siva Kumar, et al., 2017). The advances that have been made in improving the binder of the clay started when taphole clays were designed with water as plasticizer (Siva Kumar, et al., 2017). The water was adequate as the taphole clay contained clay and other plasticizers. After it was found that the water-based taphole clays potentially could oxidise the tap hole carbon blocks, the decision was made to move to coal tar pitch (Siva Kumar, et al., 2017). The coal-tar pitch was later replaced with tar which started the period of tar-based taphole clays. The use of low-moisture tar in taphole clays increased the workability of the clay significantly

which meant that the clay needed to be heated to become malleable (Nelson, 2014). With the use of tar-based taphole clays, the corrosion resistance of the clay increased dramatically as compared to water-based taphole clays (Siva Kumar, et al., 2017).

As tar became the preferred binder for taphole clays in the early 2000s, phenolic resins got introduced to taphole clay developments. The use of the resin as a binder or in combination with tar gave a better strength development and control on the curing speed of the clay (Nelson, 2014). The use of tar did not give sufficient strength to the clay and curing speeds for these clays were also slow. The slow curing speeds of these clays generally caused longer plugging times during blast furnace tapping because the mud gun needed to stay in place longer for the clay to properly sinter and build enough strength to be able to close the tap hole. There are some countries like India and South-Africa that still make use of tar-based taphole clays. As advancements have been made in taphole clay designs, the majority of manufacturers have moved to resin bonded taphole clays. The reason being that resin bonded clays are generally softer and more malleable, they are less harmful to the environment and humans and also because resin bonded taphole clays can easily be altered to better control the curing times required (Nelson, 2014).

The advantages mentioned of using resin bonded taphole clay in preference to tar bonded clay are founded as it reduced mud gun dwell times during plugging and increased production rates with quicker tap hole turnaround times (Nelson, 2014). With this said, the use of resin as a binder should be considered carefully and specifically the type of resin. As resin bonded clays are notoriously quick curing this can cause problems in some instances where too quick curing occurs. The temperature of the tap hole then increases as the tap hole is not properly plugged. During plugging the clay will start to cure either in the mud gun or while it is being pushed into the tap hole (Nelson, 2014). This will cause the taphole clay not to move to the inside of the tap hole and will result in short tap hole lengths. Some of these quick curing taphole clays also result in very hard curing which increases the drilling time of the clay and reduces the production rate and longer tap hole turnaround times (Nelson, 2014).

To assist with the concerns around resin bonded clays, the use of oils has been implemented which is used together with the resin to improve the binder properties. The advantage of using oils is that the viscosity of the binder can be adjusted according to the desired range. It also reduces the quantity of the resin used as a binder whereby the curing speed is adjusted to be slower in cases where it is severely short (Nelson, 2014). Along with these changes, more resin type binders have been developed to be used in taphole clays.

2.2.3.1. Phenol-formaldehyde resin

The most recent binder utilisation in taphole clay development has been the resin and resin-oil combinations. Since taphole clay depends on a resin that needs to cure and at different curing speeds the most primitive use of a curing type resin for taphole clay would be phenol-formaldehyde resin. Both types, i.e. Resole and Novolac, are used in taphole clay. Understanding the fundamentals of the resin will help explain its behaviour when utilising this resin type in a taphole clay.

2.2.3.2. Phenol

The synthesis of phenol is done through a process called the Hock process (Fink, 2017). The synthesis process includes oxidation, concentration and decomposition of cumene. Firstly, the cumene is oxidised to cumene hydroperoxide (CHP), thereafter it is concentrated and then decomposed to phenol and acetone (Fink, 2017). The molecular structure of phenol is shown in Figure 17.

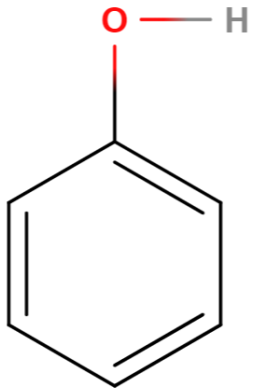

Figure 17: Molecular structure of phenol (Fink, 2017)

2.2.3.3. Formaldehyde

The synthesis of formaldehyde is done using the Formox process which utilises a catalyst which is in general silver or a mixture of molybdenum and iron, where oxidation of methanol in the presence of the catalyst produces formaldehyde and water when done at 250-400°C (Fink, 2017). The molecular structure of formaldehyde is shown in Figure 18.

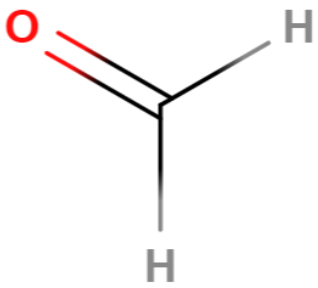

Figure 18: Molecular structure of formaldehyde (Fink, 2017)

Phenol-formaldehyde resins are of the most commonly used resins as it can be utilised in one of three ways, i.e. tackifier, reinforcers or curing agents (Dick & John, 2009). Phenol-formaldehyde resins comprise of a combination of phenol and formaldehyde which are reacted under basic conditions and a catalyst (Fink, 2017). The two main

types of phenol-formaldehyde resin are Novolac and Resole resin. The process of creating phenol-formaldehyde resin is using a basic catalyst in solution, i.e. sodium hydroxide, and then reacting phenol and formaldehyde in a specific ratio. During polycondensation between 30-100°C and over a time of 1-20 hours, phenol-formaldehyde will condense when using mole ratios of formaldehyde to phenol ranging between one to six (Fink, 2017). The reaction mechanism of phenol-formaldehyde formation in the presence of a basic hydroxide catalyst is shown in Figure 19 where the change in molecular structure is shown as the reaction takes place.

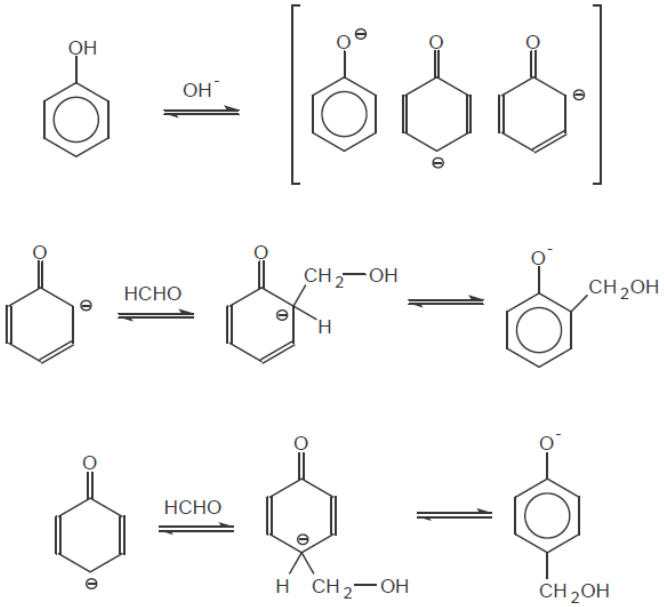

Figure 19: Molecular structure change during the reaction of phenol with formaldehyde (Fink, 2017)

2.2.3.4. Novolac resin

The novolac resin is a thermoplastic resin which means that when exposed to elevated temperatures the resin will soften unless cross-linked (polymerised) with a methylene donor (Dick & John, 2009). The novolac type resin is formed by reacting phenol with formaldehyde in the presence of a catalyst under acidic conditions (Dick & John, 2009). Its structure has one phenol/derivative with at least one aldehyde. The novolac type resins are tackifying and reinforcing resins which makes it suitable for use in rubber manufacturing for tires and belts for vehicles (Dick & John, 2009). Generally, the formaldehyde/phenol ratio for novolac resins is less than one. The synthesis of novolac resin is shown in Figure 20.

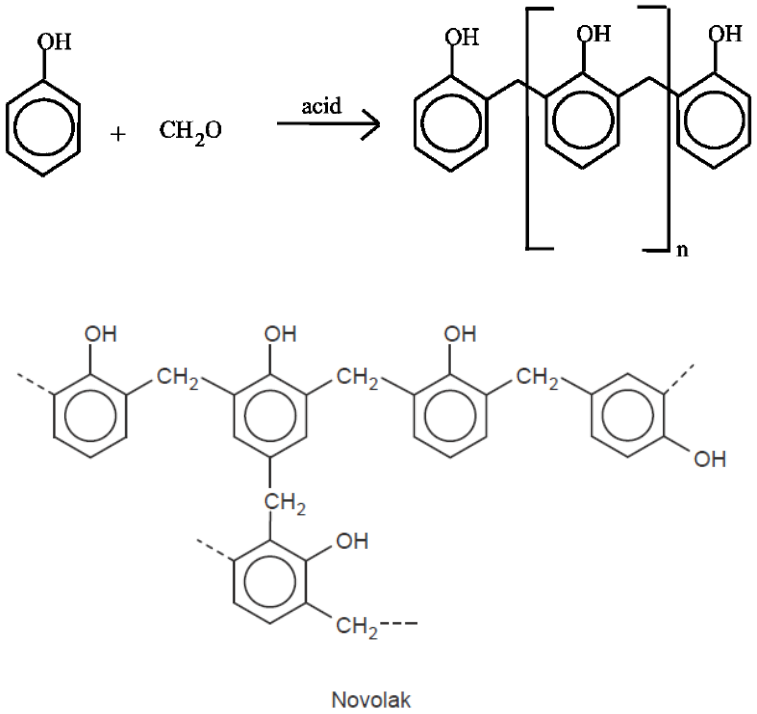

Figure 20: Molecular structure changes during the synthesis of novolac resin (Dick & John, 2009) (Fink, 2017)

2.2.3.5. Resole resin

The resole resin is produced by reacting phenol with formaldehyde in the presence of a basic catalyst between 40-100°C (Dick & John, 2009) (Fink, 2017). The ratio of formaldehyde/phenol is greater than one for resole type resins. These resins can easily be cured by simply heating them past the gel point temperature (Fink, 2017). These resins are generally considered curing type resins which are different from novolacs. If the synthesis of a resole resin would take place under acidic conditions (catalyst), one would have a resin that cures during the prepolymer stage (Fink, 2017). Acidification is another way in which resole type resins can be cured. The change in the molecular structure during the synthesis of resole resins is shown in Figure 21.

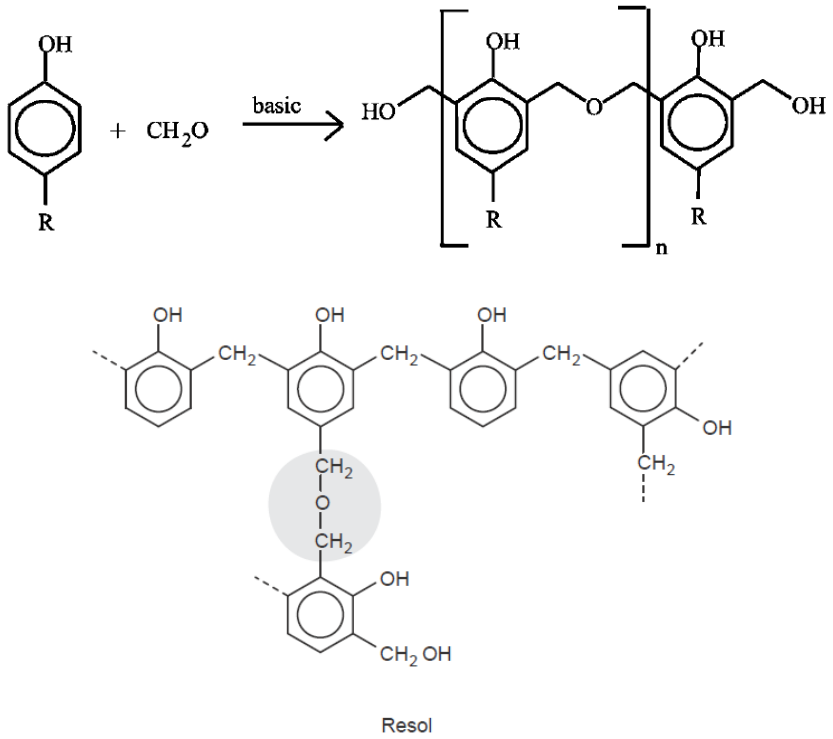

Figure 21: Molecular structure change during the synthesis of resole resin (Dick & John, 2009) (Fink, 2017)

2.2.4. Polymerisation

The polymerisation of phenolic resin is not described simply with a single reaction. The polymerisation is when there is a reaction between a trifunctional phenol and difunctional formaldehyde past the gel point which results in the formation of a three-dimensional structure (Goodman & Ibeh, 1998). The time to gel point will reduce if the temperature is increased with a thermoset resin. The effect of gel point formation as a function of temperature, time, and viscosity on a benzoxazine resin is shown in Figure 22. After the gel point has been reached and as time progresses, curing will occur and will result in a final thermoset (Goodman & Ibeh, 1998). The resins supplied for ready use is generally processed so that it is just below the gel point which during further polymerisation will result in curing to occur past the gel point (Goodman & Ibeh, 1998).

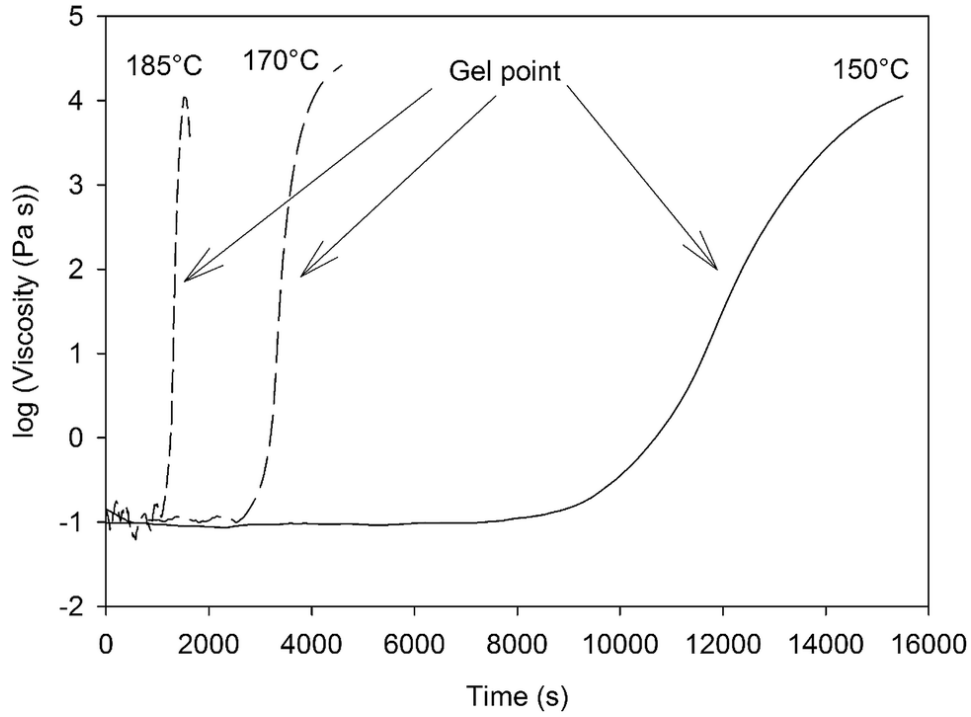

Figure 22: Graph highlighting the change in the rate of gel point formation as a function of temperature for Benzoxazine (Renaud, et al., 2019)

Because polymerisation occurs inevitably quick and frequently, it's classified only into two main groups, i.e. step-growth and chain-growth (Young & Lovell, 1991). The step-growth is described as a polymerisation where the polymer structure growth occurs in a stepwise fashion between any two molecules. The chain-growth is when there is a reaction between a monomer and a reactive chain end-group which will result in a chain polymer growth during polymerisation (Young & Lovell, 1991). For the chain-growth to take place a reaction between the monomer and an initiator needs to start before growth can begin. The step- and chain-growth polymerisations are further classified into more detail as to the reaction and the molecular structures. The possible polymerisation reactions of the two main classifications, as well as the possible products or behaviours of the resin, are summarised in Table 9.

Table 9: Summary of polymerisation mechanisms categorised between step- or chain-growth (Young & Lovell, 1991)

Classification	**Reaction**	**Result/Comment**
Step polymerisation		
Linear step polymerisation	The reaction between pairs of mutually reactive groups provided by difunctional monomers. Trifunctionality and higher will result in non-linear polymers.	Polycondensation – formation of linear polyesters, i.e. monomer reaction where small molecules are eliminated. Polyaddition – formation of polyurethanes, i.e. reaction with monomer reaction where small molecules are not eliminated. Products: Polyamide, polydextrose, polyester, polyurethane.

Non-linear step polymerisation	The reaction between monomers with functionality larger than two which forms a branched structure.	The molecular mass of polymer structure increases significantly. Gel-point – the point at which the first network molecule is formed. Gelation occurs which increases liquid viscosity. Products: Novolacs, Epoxy, Polyurethane Networks.
Chain Polymerisation		
Free radical polymerisation *Free radical – independent species with unpaired electrons	The monomers attach to free-radical sites in polymer structure known as an active centre. The polymer structure grows as every active centre after monomer addition, is moved to a new chain end. Bulk polymerisation – reaction between a monomer and monomer initiator solution. Solution polymerisation – reaction between a monomer and solvent (solvent lowers reaction medium viscosity). Suspension polymerisation – reaction mixture suspended as droplets in an inert medium. The monomer (initiator) and polymer should be insoluble in the suspense medium (Water). Emulsion Polymerisation – similar to suspension polymerisation except initiator must be insoluble in monomer but soluble in the dispersion solution.	Most common polymerisation Bulk polymerisation – Viscosity of reaction medium increases, solution heat generation. Produce polymer product with high molecular mass and high purity. Solution polymerisation – Better rate control, less heat generation. Suspension polymerisation – Solve the bulk polymerisation problem on an industrial scale. Droplets assist with heat dissipation generated, i.e. bulk polymerisation. Products: polystyrene, poly (methyl methacrylate), poly (vinyl acetate), branched polyethylene.
Ionic polymerisation a) Cationic Polymerisation b) Anionic Polymerisation	Olefinic monomer polymerisation via active centres, i.e. positively charged (cationic) and negatively charged (anionic). Cationic – reaction of monomer at a sub-zero temperature in presence of initiator and solvent. Anionic - reaction of monomer at a sub-zero temperature in presence of initiator and solvent.	Cationic – product is high molecular mass polymers Anionic – product is very pure and high molecular mass. Anionic polymerisation is carried out under vacuum and with the use of purified solvents. Products: Monodispersed polymers, Styrene.

There is a section of polymerisation that concerns wettability and polarity of the raw materials and resin binders, that is also important in taphole clay application. The surface chemistry of a powder or aggregate raw material is important with regards to whether it is wettable by the liquid binder or resin. If there is a hydrophobic nature of the powder or aggregate raw materials, it will influence the resin and may cause lowered strength and volatile loss during operation of the clay (Pilarska, et al., 2013). Since wettability and polarity are both considered important

properties, polarity mismatch between the powdered raw materials and the resin binder can cause co-polymerisation to occur (Pilarska, et al., 2013). Because of this, raw material polarity needs to be closely related to that of the binder. The wettability of a particle is determined by its surface contact angle, θ. An illustration of wettability angles and how a liquid is considered wettable on a particle surface is shown in Figure 23.

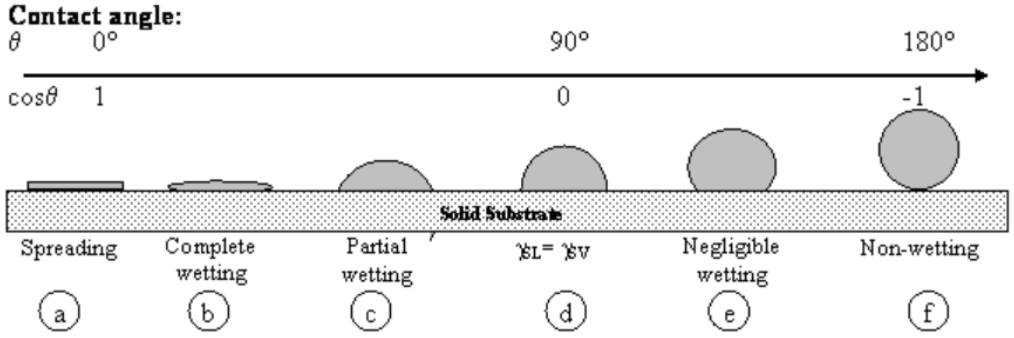

Figure 23: Illustrative figure showing criteria for wettability by liquid medium (Njobuenwu, et al., 2013)

2.2.5. Cross-linking

Whereas during polymerisation a polymeric structure is formed in the presence of a catalyst where multiple monomers are connected, during cross-linking of phenolic resins the polymeric chains are joined to form a large single molecule (Polymer Properties Database, 2020). The cross-linking of the phenolic resins depends on the type of phenolic resin. Novolac resins are formed under acidic catalytic conditions whereas resoles are formed under basic catalytic conditions. The two resins are different in the way that they are cured. The cross-linking of the novolac resins are facilitated by using formaldehyde donors such as hexamethylenetetramine (Kandola & Horrocks, 2001). The cross-linking of resole resins are facilitated using temperature (Kandola & Horrocks, 2001). Resole resins are self-curing because of the reactive functional groups which open the chance of early onset of cross-linking to occur. Although resole resins do not depend on the addition of a curing agent such as novolac resins, it does however have a slower curing rate than novolac resins (Polymer Properties Database, 2020). Some additives have been shown to increase the curing rate which includes sulphur, hydroxide (sodium), magnesium oxides, zinc, barium and salicylic acid (Saeki & Tanaka, 1980). These additives can increase the cross-linking of the resole in the different curing stages.

The curing time and cross-linking associated with curing are dependent on the composition of the resole resin. The functional group changes can be investigated with Fourier-transform infrared spectroscopy (FTIR). The change in functional groups during curing for a solid-state resole resin from Gun EI Chemical Industry CO, Ltd is shown in Figure 24. The functional group changes, during curing, included the reduction in the O-H bond peak at 3100 – 3300 cm^{-1}. The C=C (aromatic) bonds peak intensities also reduced as the sample was cured with the C-O-C stretches at 1100 cm^{-1} and 1060 cm^{-1} increasing (Zhou, et al., 2010).

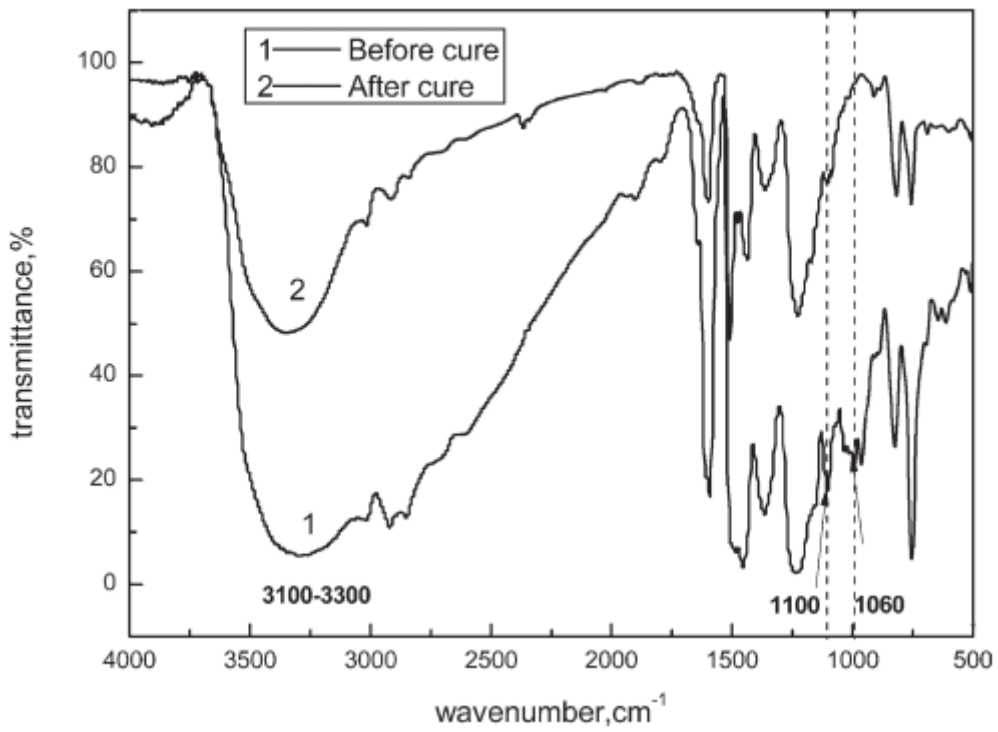

Figure 24: FTIR spectra of solid resole resin, before curing and after curing (Zhou, et al., 2010)

2.3. Marshall extrusion pressure

The Marshall extrusion test indicates the plastic behaviour of a taphole clay at any time after manufacturing or ageing (Nelson, 2014). The test specifies the pressure needed to push the clay through a certain cross-sectional opening, i.e. such as the mud gun opening. The mud gun is a cylindrical barrel that narrows to the point where the clay exits (Tupkary, 2018). If the clay plasticity is not desirable, the mud gun might not be able to push the clay. The extrusion pressure for each taphole clay will differ because of the specific mud gun the clay is pushed with. Certain mud guns can push taphole clays that are extremely hard and then some older mechanical mud guns will not be able to push the same clay into a tap hole. The extrusion test is widely known as the most favourable test to determine the plasticity of a taphole clay. However, industry experts all have different ways in which the test is conducted and will utilise different apparatus, such as orifice designs, to carry out the test. One standard that is popularly used for determining the extrusion pressure is the Australian standard AS 1744.34-2004 (Australian Standard, 2017).

The assembly of the mould used for this test is shown in Figure 25, where it consists of a plunger or piston, cylinder and cone of defined sizes. The standard uses a fixed test temperature of 50°C to conduct the test and constant plunger or piston push rate of 50±5 mm/min with a 0.1kN load. The volume of the taphole clay should be 0.7L within ±2%. The mass required for conducting the extrusion test is calculated using equation 1 which is dependent on the density of the clay, which is predetermined (Australian Standard, 2017).

$$M = \frac{0.7D}{1000} \quad (1)$$

Where, M is the mass of the sample in kg, and D is the density of the clay in kg/m^3.

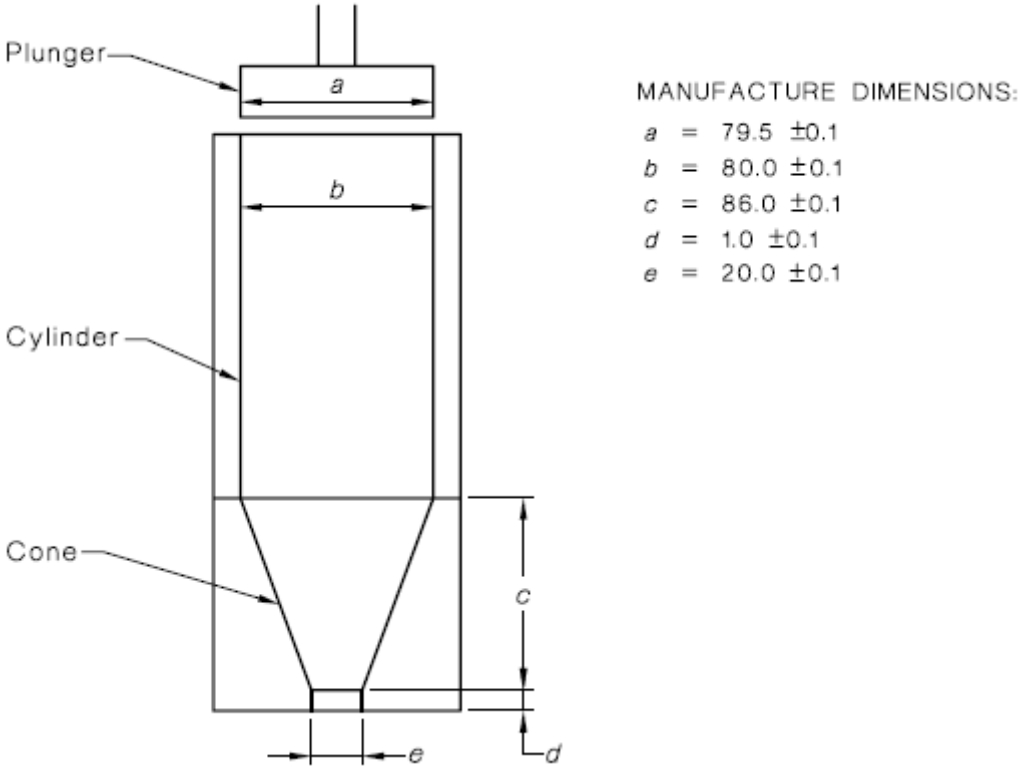

Figure 25: Mould assembly for MEP test. Dimensions are included (Australian Standard, 2017)

After the sample has been weighed, it is heated along with the extrusion mould to the desired temperature, i.e. 50°C. The time at which the clay needs to be kept at the test temperature is dependent on the resin it contains. Certain resins will start to cure if the test temperature is increased. The sample only needs to be kept at 50°C until it reaches the temperature. This needs continual checking and monitoring. The temperature and mould need to be within 1°C of the test temperature. The mould assembly is lubricated, and the sample placed inside of the cylinder. The mould assembly is placed inside the drive unit and the test started. The drive unit is stopped once the plunger or piston is 11±0.5mm above the starting point of the cone. The force readings of the drive unit that extrudes the sample, need to be carefully monitored. The maximum force exerted on the sample needs to be recorded as F_{max} and is done within 0.1kN (Australian Standard, 2017). The extrusion pressure is calculated using equation 2 (Australian Standard, 2017).

$$EP = \frac{10F_{max}}{50.3} \quad (2)$$

Where EP is the extrusion pressure calculated in MPa, F_{max} is the maximum force exerted in the sample in kN, and 50.3 is the cross-sectional area of the extrusion cylinder in mm^2. This is dependent on the design of cylinder and-cone that is being implemented for this test.

The test temperature of the clay has a significant effect on the extrusion pressure and this temperature needs to be as close to the temperature inside of the mud gun as possible. The effect of temperature on the extrusion behaviour of a blast furnace taphole clay is shown in Figure 22 (Wells, 2002). The extrusion pressure reduces significantly as the temperature increases and follows an Arrhenius relationship (Wells, 2002).

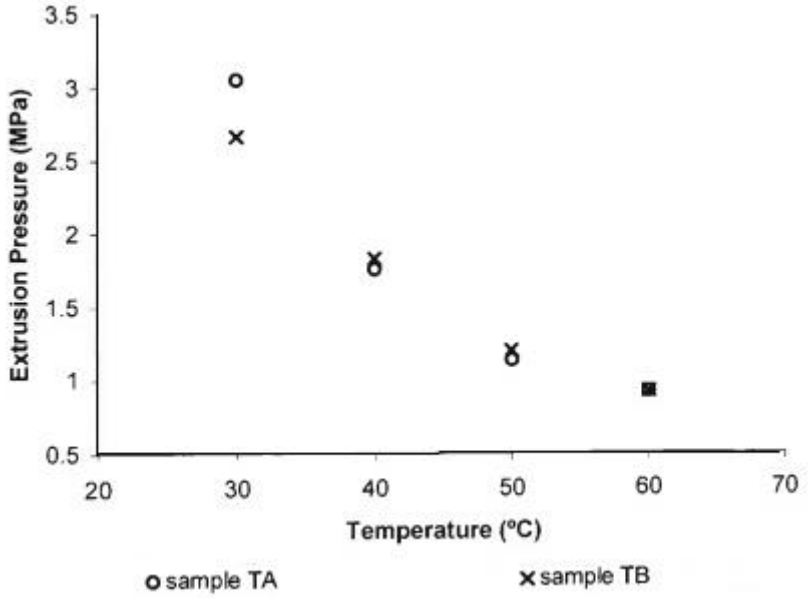

Figure 26: Extrusion pressure vs. temperature graph. Sample TA and TB were taken from the same taphole clay (Wells, 2002)

The effect of ageing on the extrusion pressure is also an important factor to consider when designing a taphole clay. The clay needs to remain plastic for a considerate time to be able to be pushed. The extrusion pressure needs to remain constant as it ages so that the mud gun that is used for plugging the clay does not struggle to push the clay as it ages. This is important that the shelf-life of the clay is long enough that consumers will not have to consume the clay in a short space of time. The desired typical ageing of a taphole clay is shown in Figure 27 (Wells, 2002). The graph shows MEP results of clay that does not contain any hexamethylenetetramine (HMTA) and one that contains 1.65% HMTA. During the 14-day ageing period, the extrusion pressure was tested. The clay that does not contain any HMTA had a small increase in extrusion pressure after day 2. Thereafter, the extrusion pressure remains constant up to day 14. The clay that contains 1.65 HMTA has variable extrusion pressure as the clay ages. This signifies that the plastic behaviour of the clay changes as it ages and does not show consistency. This is an example of an extrusion pressure which will be problematic as the clay ages.

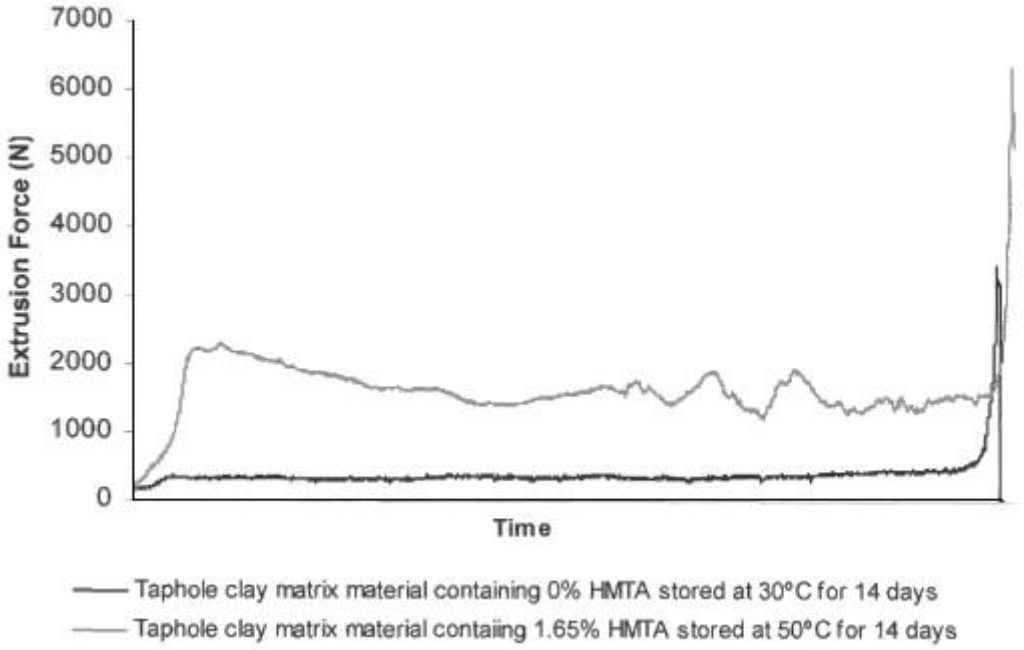

Figure 27: An ageing graph where the changes in taphole clay extrusion pressure with time are shown (Wells, 2002)

2.4. Summary of factors that influence premature ageing

It is worthwhile to reiterate the factors that influence the ageing and workability of taphole clay. These factors originate from either the aggregate and matrix combination or the binder combination and include (Nelson, 2014):

- Particle size distribution (PSD) of the individual raw materials that constitute the taphole clay;
- The solubility of aggregate and matrix raw material in the resin and binder combination (solubility of liquid pitch into resole resin and visa verse is complete);
- Impurities associated with the aggregate and matrix raw material, such as lime and sulphur;
- Temperature;
- The viscosity of the binder, which in turn is influenced by temperature and degree of polymerisation or cross-linking;

The PSD of the aggregates and matrix raw materials used in a taphole clay as well as the PSD of the taphole clay itself plays an important role in its rheological behaviour. The rheology in turn influences the workability of the taphole clay. The rheological effects of the taphole clay are largely a function of volume. The volume is a function of the maximum packing density which is dependent on the PSD (Adeyinka, et al., 2009).Thus having a properly packed clay mass will result in desirable rheological behaviour.

The solubility of the aggregate and matrix raw materials into the binder(s) also influences the workability and ageing of the taphole clay. Polar-polar or non-polar-non-polar interactions between the aggregates, matrix raw materials and binder(s) determine if the clay will form a proper mass or whether the mass will separate after mixing and

ageing (Lin, et al., 1993). The solubility of the resin into another liquid such as tar or liquid pitch is also dependent on the polarity between molecules in each of the solutions (Lin, et al., 1993). The nature of the functional groups of the binders (hydroxyl) and other functional groups may behave more like a surfactant leading to an emulsion like behaviour. Differences in the polarities can also cause separation between the liquids when mixed into the clay mass. This separation after ageing is what will cause the workability of the taphole clay to reduce and the ageing to be increased.

Although the liquid pitch does not have a monomer structure it will be highly unlikely for polymerisation to occur with it, however, this cannot be eliminated completely as the behaviour of this pitch is not well understood. The viscosity of the binder(s) used in taphole clay is influenced by temperature and structural changes of the binder mixture due to polymerisation or cross-linking that occurs. The change in viscosity influences the workability as well as the ageing of the taphole clay (Li, et al., 2018).. During polymerisation, new polymer structures are formed which alters the viscosity of the binder mixture (Moritz, 1989). This change in polymer structure increases the viscosity of the binder mixture which results in reduced workability and increased ageing of the taphole clay after it is manufactured. Premature cross-linking of the resin in the binder mixture will cause the gel-point temperatures of the resin to be altered. This altered gel-point temperature can either be delayed, where a curing reaction will occur at higher temperatures, or where the gel-point temperature is lowered which causes curing of the resin to occur at lower temperatures (Laza, et al., 2001). The premature cross-linking will also alter the viscosity of the binder noticeably. The lowering of the gel-point temperature will cause an increase in binder viscosity at lower temperatures. Certain impurities such as sulphur, lime and halides, which are present in the aggregates and matrix raw materials, will also cause polymerisation or cross-linking of the resin in the binder (Young & Lovell, 1991).

These factors, i.e. PSD of each raw material as well as the taphole clay itself, the wettability of each of the raw materials, the mineralogy and impurities present in each raw material, the viscosity and properties of the binders were investigated to determine the cause of reduced workability and increased ageing of the taphole clay when the resole resin and liquid pitch are used in synergism, as binders.

Chapter III – Experimental setup and test methods

This section examines the possible variables that can influence the workability ageing of taphole clay. These variables include gradings, polarity, impurities, granulometry, temperature and viscosity. Each of the variables was defined as either a dependent variable, independent variable or a constant (Figure 28). The test methods as well as the experimental design were used to evaluate these variables by examining changes in the independent variable and its direct effect on the dependent variable.

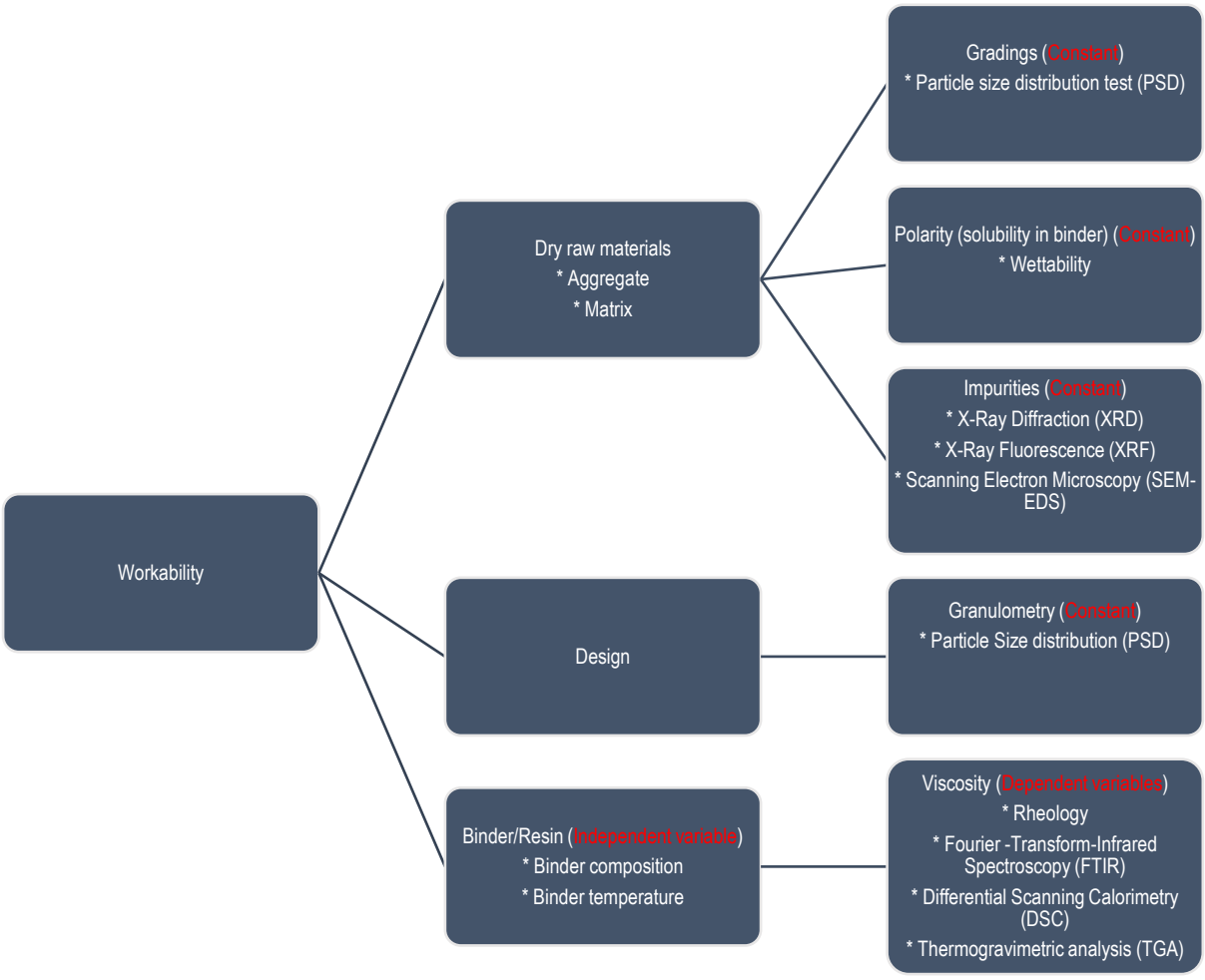

Figure 28: Experimental outline of factors and properties that influence the taphole clay, which was examined in this study

When the possible cause(s) of the premature ageing of the taphole clay was evaluated, certain properties had to be kept constant. The effect of binder viscosity on the workability of the clay was determined when the raw materials, i.e. aggregate, matrix and their PSDs, as well as the design of the clay were kept constant. The raw materials used were from the same source and bag. The taphole clays were constituted according to the detail given in Table 10. The mass percentage of the resin and liquid pitch used were chosen according to a workability specification associated with this clay. The addition of the resole resin and liquid pitch was made in excess of the aggregate and matrix raw materials, i.e. the sum of aggregate and matrix raw materials was 100%, the resole resin and liquid pitch was added in excess of 100% designated by +.

Table 10: Taphole clay design used for evaluation

Raw materials	Size range	Mass percentage	Function
Bauxite	+45µm to -1mm	35	Aggregate
Andalusite	+45µm to -1mm	15	Aggregate
Andalusite (BMF)	-45µm	7.5	Matrix material
Calcined Clay (BMF)	-45µm	7.5	Matrix material
Calcined Alumina	-45µm	5	Matrix material
Clay - kaolinite	-45µm	10	Filler/Sintering
Carbon - Coal	-45µm	5	Gas permeability
Silicon Carbide	+45µm to 0.8mm	15	Abrasion resistance
Phenol-formaldehyde resin (Resole)	-	+1	Strength development
Liquid pitch binder (a combination of high volatile coal tar pitch and heavy oils)	-	+15 – 20	Binder/Filler

The clay design in Table 10 is a simplistic design which was used for the investigation. The clay is a ~60% alumina, resin bonded clay that makes use of a resole resin together with a liquid pitch binder.

As mentioned, the use of the formulation in Table 10 ensures consistency. When evaluating the viscosity effect and possible polymerisation or cross-linking on the workability, all other variables were kept constant. As part of the investigation, one needs to also define the aggregate and binder raw materials along with all the properties in Figure 28 to characterise the clay and the raw materials. Certain properties such as the wettability of raw materials by the binder, the impurities of the raw materials and particle distribution were investigated.

The independent variable that was looked at is the rheology of the liquid combination as well as the extent of reaction (if present). For this, three test methods were utilised of which the experimental design is shown in Figure 29. The samples used for rheology testing were identical to the ones used for FTIR and DSC. The FTIR analysis on the resin, liquid pitch binder and combination as stated in Table 10, investigated if a reaction has or hasn't taken place between the resin and liquid pitch and if there is a change in the molecular structure (a new compound formed) and what this is. DSC was used to determine whether the interaction between the resin and liquid pitch proceed through exo-or endothermic reactions and at which temperature these reactions occur. Additionally, TGA

was used only on the virgin resin and liquid pitch samples to establish the mass loss and determine the maximum temperature at which the DSC can be conducted. The formulation of 1%R + 17%P is the one used in Table 10, which if normalised to 100% yields 5.5%R + 94.5%P (R = resin, P = liquid pitch). The 17% liquid pitch chosen for this specific experiment was done by a percentage that is middle of the range 15-20% pitch (Table 10).

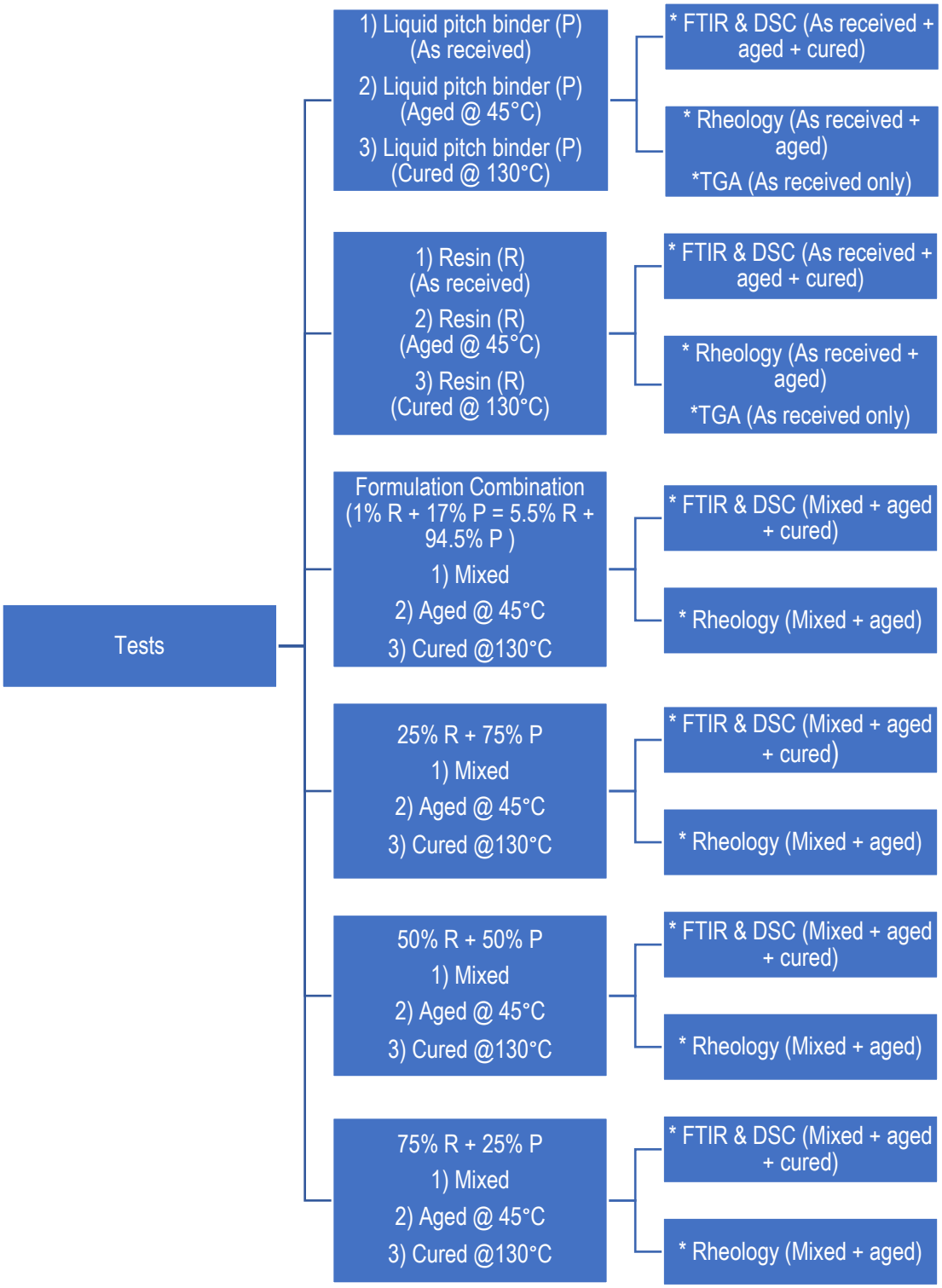

Figure 29: List of binders and binder combinations that were examined with FTIR, DSC, TGA and rheology (R = resole resin, P = Liquid pitch binder)

The as-received samples were from both virgin resin and liquid pitch that were tested within a month of manufacturing. The aged samples of the virgin liquid binders were aged as received at 45°C for two weeks. The weight loss during ageing was also recorded. The mixtures were aged in the same manner, but samples were prepared by weighing out the correct quantities of both liquids sequentially into the same container as to minimise to residue of sample left in the measuring containers. The samples were mixed for 5 minutes at room temperature. The cured samples of the virgin liquid binders were cured as received at 130°C for four hours. The weight loss during ageing was also recorded. The mixtures were cured in the same manner and sample preparation was identical to that of the aged samples. For the virgin liquids as well as each of the mixtures, the same aged and cured samples were used for the different analyses mentioned in Figure 29.

3. Test Methods

The methods and apparatus used for the analysis of properties mentioned in Figure 28 are discussed in this section.

3.1. Workability

The workability of a taphole clay is a measure of the degree of compactability when it is placed under a load. During the application of a load to the sample, the deformation is measured and the change in height is used as the workability index. The procedure for sample preparation of the taphole clay samples was performed in accordance with the ASTM C1054-18 (2018) standard, while the workability was tested according to the ASTM C181-11 (2018) standard (Appendix A).

Apparatus

The apparatuses used during this analysis/test include:

- AFS sand rammer;
- Cylindrical sample holders (H = 120mm, $ø_{inner}$ = 50mm, t = 5mm, open both sides);
- Balance (accurate to 0.1g);
- Vernier callipers;
- Heater/oven (350°C max);
- Thermometer (accurate to 1.0°C);

Method

The test piece was prepared by removing 200-320g (depending on clay density) of the taphole clay from the pressed clods after manufacturing. The sample was then placed into the oven and heated to the desired test temperature which in this case was 35°C. After the sample reached the desired test temperature, the sample was placed into the cylindrical sample holder and placed into position under the impact device. The impact device was pressed down slowly until it contacted the test piece and compacted. The impact device was then lifted, and 10 blows were given to the sample in the cylinder. After the first 10 blows, the impact device was lifted, the cylinder

rotated, and the other side of the cylinder placed into the sand rammer. The impact device was lowered again until it contacted the sample and another 10 blows were given. After the second set of blows, the sample was extruded from the cylinder and the height of the sample was measured to the nearest 0.1mm (H_1). If the sample height was not 50 ± 1mm, the above procedure needed to be repeated and the appropriate bulk sample weight needed to be measured.

After the sample was extruded from the cylinder, the sample was then placed under the impact device and centred. The impact device was lowered quickly onto the sample until it made contact. After contact, another 3 blows were given, and the sample measured (H_2).

The workability index (W_i) was calculated using the following equation:

$$W_i = \frac{H_1 - H_2}{H_1} \, x \, 100 \qquad (3)$$

3.2. Marshall extrusion pressure

The extrusion pressure measured by the Marshall extruder is a method used whereby the plasticity of a taphole clay is determined. The maximum pressure is measured while a constant extrusion rate is maintained. The temperature and feed rate are also kept constant.

Apparatus

- MarshallTest automatic extruder with heating chamber
- ELE control system
- Water bath
- Balance
- Thermometer
- Extrusion moulds (piston, cylinder and extrusion die)
- Extrusion test rig
- Plastic bags
- Lubrication agent
- Oven (accurate 45±1°C)

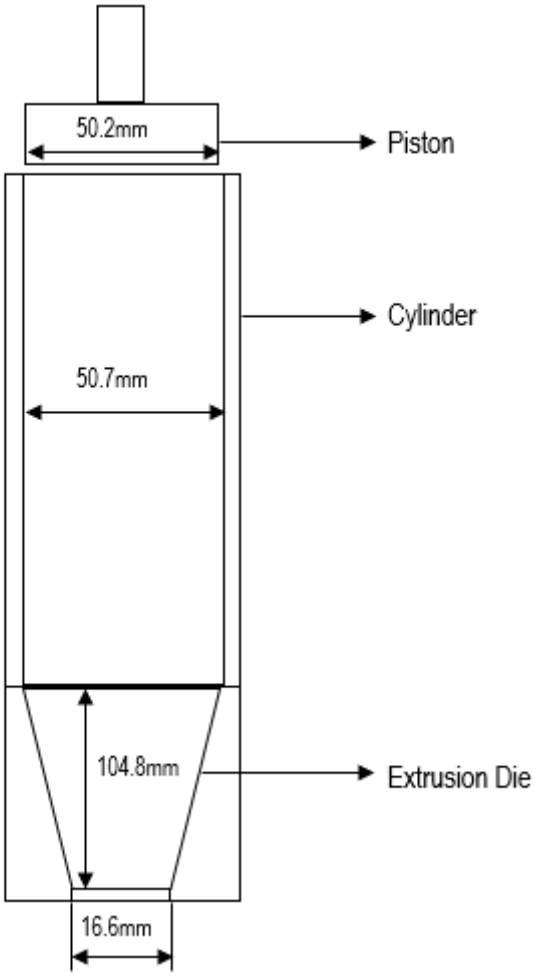

Figure 30: Schematic of the extrusion mould assembly

Method

The test was started by weighing 450g of clay to be tested and placing it in a plastic bag. The extrusion moulds were placed in a separate bag and both bags, i.e. clay and extrusion moulds, were placed inside a water bath to heat the clay and moulds to 45°C. The clay and moulds were left in the water bath for approximately 2 hours. After the clay sample and moulds have been heated, the clay was removed from the bag, moulded into a cylinder and the temperature of the clay measured to confirm its at 45°C. The extrusion mould and piston were sprayed with a lubricant and the clay mass placed inside of the mould. The piston was then applied on top of the sample into the cylinder and the whole extrusion mould assembly was placed onto the extrusion test rig. The load cell was lowered onto the piston to make contact just so that the ELE measures a pressure >0MP. The ELE was zeroed and the extruder turned on. After the clay mass was pushed through the bottom end of the extrusion die, the test was stopped. The force readings were recorded during the test, and the maximum force reading was used to calculate the extrusion pressure. The Marshall extrusion pressure (MEP) was calculated using the average of equation 4 and 5.

$$Maximum\ pressure\ at\ Piston = \frac{Maximum\ load}{curved\ surface\ area\ of\ piston}\ x\ 1.01972x10^4 \quad (4)$$

$$Maximum\ pressure\ at\ Die = \frac{Maximum\ load}{curved\ surface\ area\ of\ die}\ x\ 1.01972x10^4 \qquad (5)$$

The maximum pressure is measured in kg/cm^2 , the maximum load measured in kN and the curved surface area of the die or piston in cm^2.

3.3. Particle Size Distribution (PSD)

The PSD analysis of raw materials, as well as a composite material, reports the distribution of particles within certain size ranges. Two of the main test methods used include screening and Malvern analysis. During the screening, screens of sizes according to a Tyler series, are used and stacked on top of one another. The samples were vibrated through the screens after which the weight on the screens was used to calculate the PSD. The Malvern is an electronic test method in contrast to the manual vibrating screen analysis and can be used to determine the particle sizes of raw materials and composite materials by using a dispersing liquid and a very sensitive analyser to separate particles. The larger the particles that are analysed the greater the error will be, and for that reason, the Malvern was only used in this investigation on particles sizes of <1mm.

Apparatus

- Malvern Mastersizer with Hydro 2000G sample cell running Mastersizer software for analysis on the computer;
- Mastersizer dispersing liquid for powder samples (samples finer than 45µm use 0.5wt% Sodium Hexameta and for carbon (or silicon carbide) samples use 0.01wt% Flube PA120 organic dispersant);
- 50ml beaker;
- Magnetic stirrer;
- Ultrasonic bath;
- Pipette;

Method

The sample preparation started by placing 25ml of dispersing liquid (depending on sample nature) into a 50ml beaker and stirring with a magnetic stirrer for 2 minutes. After that, the appropriate quantity (1g) of powder to be analysed was placed in the dispersing liquid and stirred for an additional 2 minutes. After stirring, the beaker was placed in an ultrasonic bath for 2 minutes. After the sample was placed in the ultrasonic bath, a pipette was used to transfer 5-10ml of the slurry into the Hydro 2000G sample cell to analyse. Caution was taken to ensure that when analysing a slurry, that at least 10 measurements were taken to have an accurate result.

3.4. Wettability

In the wettability test, the surface contact angle of a particle suspended in a polar (water) or non-polar (hexane) medium, can be determined. There are multiple ways in which the wettability can be determined but the method explained is the easiest and gives satisfactory results. The method that was used, utilised an automatic tensiometer

to measure weight gain of a sample suspended in a test medium, i.e. water or hexane. The data obtained from this wettability test was used in Washburn's equation to determine the contact angle and wettability (Galet, et al., 2010).

Apparatus

- Attension Tensiometer with One Attension Sigma 700-701 software
- Sample vessel (cylindrical) – powder sample vessel obtained with Tensiometer
- 60mm petri dish
- Water
- Hexane

Method

This method explains the sample preparation as well as the process for determining the contact angle with the Washburn capillary rise method. The sample preparation started with placing a small paper filter in the bottom of the sample vessel (the part that comes in contact with the test liquid). A 3g sample of the raw material to be tested was weighed and placed in the sample vessel. Thereafter, the sample vessel was connected to the Tensiometer so that it is suspended. The petri dish, in which the sample vessel needed to be suspended into, was filled with the test liquid also ensuring that the sample vessel did not come into contact with the test liquid to wet the sample before testing. The sample parameters such as weight and density were entered into the program and the sample was suspended into the test liquid and the weight increase measured. The Sigma software reported a mass^2/time value for each sample. This value was the gradient of the mass/time graph given as a result. The gradient of the graph as well as some liquid parameters could be used to determine the contact angle of the sample tested. The same process was done for both water and hexane to see the change in contact angle for each sample.

The Washburn capillary rise method is used to determine the contact angle by obtaining a Mass^2/time value for both water and hexane scenarios on each raw material. Equation 6 is a refined version of the Washburn method and can be used to determine the contact angle:

$$\frac{M^2}{t} = C_w \frac{\rho_l^2 \gamma}{\mu} \cos\theta \qquad (6)$$

Where m^2/t is the gradient obtained from the wettability test, the C_w a constant, the ρ the density of the test liquid in kg/m^3, μ the viscosity of the test liquid in Pa.s, the γ being the surface tension of the test liquid and the θ the contact angle.

The process in determining the contact angle of the powder raw material in water starts by using equation 6 and the hexane liquid parameters for viscosity, surface tension and density to determine the constant C_w. For this calculation the Cosθ = 1 because it is assumed that the hexane is a perfect wetting fluid. The gradient value given for the raw material tested suspended in hexane is used in this calculation to determine C_w. After the constant, C_w, has been determined, the contact angle for the raw material surface in contact with water can be determined by

using the gradient value obtained from running the wettability test in water, along with the water liquid parameters and constant C_w.

3.5. Fourier-transform infrared spectroscopy (FTIR/ATR)

The FTIR is a test method used for identifying the molecular structure of organic, inorganic and polymeric materials. The analysis involves either solid or liquid as a sample. This method collects high-spectral-resolution information via an IR spectrum method. This analysis method was used to analyse a sample at 25°C after they have been exposed to higher test temperatures.

Apparatus

- PerkinElmer SPECTRUM 400 FT-IR using Perkin Elmer spectrum software for analysis;
- Methanol;
- Wiping towel;

Method

There is no sample preparation required for FTIR/ATR except that the sample needs to be either powder or liquid. There are a few important changes that need to be made to the software standard settings to be able to properly analyse the test sample. The analysis starts by implementing the following important changes in the software standard settings before starting analysis:

Advanced tab:
→ Resolution : 4 cm -1
→ Sample scan time: 24 scans
→ Background scan time: 24 scans
→ Save data from: 4000 to 400 cm-1
→ Results Spectrum: Absorbance
→ Data blocks to be saved: checkboxes for Absorbance, Single Channel and Background only

Acquisition:
→ Wanted high-frequency limit: 8000
→ Wanted low-frequency limit: 0
→ High Pass filter: On
→ Acquisition mode: Double Sided, Forward-Backward
→ Correlation mode: ON

FT:
→ Phase resolution: 32
→ Phase Correction mode: Mertz / No Peak Search

→Apodization function: Blackman-Harris 3-Term

→ Zerofilling factor: 2

After the Perkin Elmer software was changed to reflect above, the diamond cell needed to be cleaned with methanol to ensure there was no dust or residue from previous samples present on the cell. After the cell was cleaned, a background scan needed to be run on the Perkin Elmer to ensure background noise was cancelled as well as CO_2 and H_2O from the atmosphere. After the background scan was completed, the sample was placed onto the diamond cell and analysed.

3.6. X-Ray Fluorescence (XRF)

The use of X-Ray Fluorescence was to determine the chemical composition of a ceramic material. The analysis involved exciting a fused powder sample with an x-ray and the diffraction pattern from the sample was collected and measured against previously analysed standards to determine the composition of a material. The standard used for analysis for this specific method was retrieved from X-Ray Spectroscopy by John R Evans (Bennett, et al., 1992).

Apparatus

- Philips PW2400 X-ray spectrometer with SuperQ software;
- Platinum – 5% gold alloyed crucibles;
- Platinum – 5% gold alloyed casting dishes;
- Ceramic crucibles with maximum 1065°C temperature;
- X-Ray Flux – 66% Lithium Tetraborate + 34% Lithium Metaborate;
- Drying oven;
- Fusion furnace (minimum temperature 1250°C)
- Balance;
- Bunsen burner;
- Hot plate or another heat reservoir;

Method

The sample preparation started by milling the ceramic raw materials to a powder that is 100% -45µm. The powder samples were then placed into the ceramic crucibles and ignited to 1000-1050°C for at least 30 minutes before weighing. This step was done to remove moisture and calcine the hydrates present in the sample. Any samples that contained carbon, graphite, silicon carbide or metallics needed to be treated at 650°C in an oxidising atmosphere for minimum 48 hours. This step was done to prevent these raw materials from reacting with the platinum crucibles and casting dishes. The powder samples were then placed in the platinum crucibles and flux added accordingly:

- If the sample contained chrome/chromite then 0.25g of dried powder sample (accurately to 0.1mg) and 6g of flux (accurately to 0.1mg) were mixed;

- If the sample did not contain chrome/chromite then 0.6g (accurately to 0.1mg) of the powder sample and 6g of flux (accurately to 0.1mg) were mixed;

After the samples were weighed off, they were placed into a muffle furnace at 1220°C for 40 minutes. Once the samples melted, the melt was poured into casting dishes that were preheated on a Bunsen burner. Thereafter the samples in the casting dishes were placed on a hot plate to allow to slow cool and prevent cracking. Once the sample had cooled to the hot place temperature, the beads were removed from the casting dishes and submitted for XRF analysis.

In addition to the test, samples run on the XRF, standards needed to be run daily and checked for any deviations to ensure correct and accurate results.

3.7. X-Ray Diffraction (XRD)

The use of X-Ray diffraction was to determine the molecular structure of a crystal and with that, the possible phases present in a mineral. The samples used for analysis were refractory ceramic powder samples that had been analysed by XRF and SEM to supplement the XRD analysis and confirm the phase analysis. The samples were prepared in accordance with Panalytical backloading system (PANalytical, 2013). The samples were interpreted using a PANalytical X'Pert Pro powder diffractometer in Θ-Θ configuration with a XÇelerator detector and variable divergence-and fixed receiving slits with Fe-filtered Co-Kα radiation (λ=1.789Å) (Chatterjee, 2001).

Apparatus

- PANalytical X'Pert Pro powder diffractometer – PW3204 X'PERT;
- Milling facility if samples are particulate;
- Zero diffraction plate sample holder, 10mm diameter;
- Small compactor, cylindrical with a 15mm diameter;
- Microscope glass slide;

Method

The method described was for powder samples, i.e. 100% -45µm particle size. After milling of the samples had been completed, the powders were placed into the circular opening in the zero-diffraction plate sample holder and compacted with a compactor. Only after the material had been compacted, the excess of the material could be scraped off with a microscope slide ensuring the surface that was to be analysed was levelled properly. Sample holders were placed on a sample rack which was transferred to the diffractometer for analyses.

3.8. Scanning Electron Microscopy (SEM)

The use of the scanning electron microscopy was to evaluate the mineralogy and microscopy properties of a particle such as size and shape. The SEM-EDS (Energy Dispersive X-Ray Spectroscopy) was used to capture a backscattered image of the particles for analysis purpose where point and area atomic percentage analysis was done to confirm the phases that were identified with XRD. The SEM was also be used to identify impurities more

effectively if they were in small quantities or enclosed in the particles. The method of analysis was in accordance with the standard mentioned in Appendix A. Some carbon/graphite samples were prepared using Iodoform to distinguish between the carbon of the resin used for preparing samples and the actual carbon/graphite particles in the sample preparation for analysis (Ogunniyi, et al., 2009). The Iodoform dissolved into the resin distinguished, as analysis will show, the resin as Iodine and the carbon from the carbon/graphite particles as carbon.

Apparatus

- Jeol JSM IT300 microscope using Oxford XMax 50 software for EDS analysis;
- Conductive tape
- Gold coater;
- 15mm diameter plastic sample holders, height 10mm – one end of the sample holder needs to be closed;
- Liquid Epoxy resin;
- Hardener;
- Syringe;
- Mixing cups;
- Mixing sticks;
- Vacuum pump and vacuum chamber;
- Oven;
- Grinder + grinding pads (Grit sequence: 80, 100, 200, 400, 600, 1000, 1200, 1500);
- Polisher + polishing pads (9µm, 3µm, 1µm);
- Diamond polishing fluid (9µm, 3µm, 1µm);
- Lubricant;

Method

The sample preparation started by placing the powder or particle samples into an oven and drying the sample at 110°C for 24 hours. After the samples have been dried the preparation could start. The resin for mounting was weighed to be enough to fill the plastic sample holders with the sample included in the sample holder. The hardener was weighed to be added to the resin for hardening. The ratio for resin curing was single part hardener and three parts epoxy resin. Once the hardener was mixed into the resin the mounting started. The desired sample was placed on the closed end of the sample holder to cover the bottom part of the sample holder. Thereafter the epoxy resin mixture was added to fill the whole sample holder. The samples were each marked for traceability. After the epoxy resin was added to the sample holder with the sample suspended beneath, it was placed inside a vacuum chamber for 10 min (2 bar pressure) to allow air bubbles to be removed from the sample and allowing the resin to move into the pores of the particles or pores in powder samples.

After the vacuum was removed, the samples were placed into an oven at 65°C to assist with the curing of the epoxide for 24 hours. For carbon samples the same procedure was used but included was the addition of Iodoform

to the resin before pouring it into the sample chamber. The Iodoform (2% by mass of total resin weight) was mixed into the epoxide before the hardener was added to assist with distinguishing the carbon sample from the epoxide. The epoxide mixture was then added to the sample holder with the sample suspended and the same procedure as mentioned followed.

The mounted samples needed to be prepared for microscopy work by grinding and polishing the sample surface smooth. The grinding started by using a grit 80 and grinding the closed end of the plastic holder open to reveal the sample and the bottom of the holder. After the sample became visible, the grinding process continued whereby grinding with a grit starting from 100 up to 1500 and rotating the sample 90° with every new grinding grit used. The grinding needed to be done with running water on the grit to prevent the sample from overheating and altering or damaging the sample. The sample, after grinding was finished, was polished with a polisher and starting with a 9µm polishing cloth, 9µm polishing fluid and lubricant on the polishing cloth. Polishing commenced on the ground surface of the sample until no visible scratches could be seen.

The sample surface needed to be made conductive to prevent electron charging and ensure a clear surface image of the sample. This was done by coating the polished sample surface with gold in an argon atmosphere. After the sample surface was coated with gold, the sample could be analysed using SEM. The sample was placed into the sample holder and for the conductive sample surface to make contact with the conductive sample holder, the conductive tape was placed between the sample surface (side of the sample and not on the whole polished section) and the sample holder.

3.9. Coal Analysis

In this investigation, coal analysis included ash content, volatile matter, moisture and fixed carbon and sulphur content. The ash and moisture content was tested according to ASTM D3172-13 (2013) standard, volatile matter according to SANS 927:2013 (2013) standard, fixed carbon content according to ASTM D5373-16 (2016) standard and sulphur content according to ASTM D4239-18e1 (2018) standard (Appendix A).

3.10. Rheology

The rheometer was used to determine flow properties of the resin, pitch binder and combinations thereof. The rheometer was used to determine the fluid behaviour, i.e. Newtonian or non-Newtonian. Other additional tests such as temperature ramp experiments were conducted inside of the Peltier heating system. These analyses were used to determine flow decay and change in the flow properties after ageing and during curing.

Apparatus

- Anton Paar Physica MCR301 with Peltier heating system using Rheoplus as software package
- 50mm parallel plate spindle

Method

Before the test was conducted, the rheometer was calibrated and set up for the liquid that was to be analysed. After the setup process, a test liquid was placed onto the platform of the rheometer to cover the platform and the spindle lowered to maintain a 1 mm gap between the platform and the spindle where the liquid was. The excess liquid was removed from the side of the spindle and the test was conducted. Where temperature ramp experiments were conducted, the Peltier heating system was used.

3.11. Thermogravimetric analysis (TGA)

The TGA was used to determine the mass loss of the resin and pitch binder during heating. This test was conducted to see determine the temperature range in which the binder samples volatilise. The maximum heating temperature obtained from the TGA determined the temperature used in conducting the differential scanning calorimetry.

Apparatus

- TA Q600 SDT with thermal advantage as software package
- 30µL alumina crucibles

Method

The liquid samples were weighed in the alumina crucible to about maximum 20mg of the test liquid inside the crucible. The crucibles were placed onto the balance arm of the TGA and the tube furnace closed. The balance was tarred, and the heating program entered. The samples were heated in a nitrogen inert environment up to the desired temperature.

3.12. Differential scanning calorimetry (DSC)

The DSC was used to identify endothermic and exothermic reactions that occur in the resin, pitch binder and combinations thereof when heated. The endothermic and exothermic reactions, and temperatures at which they occurred, were used along with the rheology and FTIR to explain the behaviour of the binder mixtures.

Apparatus

- Perkin Elmer DSC 4000 with Pyris as software package
- 30µL aluminium pans and lids

Method

The liquid samples were placed inside of the aluminium pans ensuring that they are not filled more than half full of liquid. The liquid weight was recorded, and the aluminium lid placed on top of the pan. The assembly was placed in a press and the lid pressed into the pan to enclose the liquid in the pan. A small hole was made in the lid to allow for volatile release during heating. The DSC was calibrated using a reference pan and lid. Thereafter a background was run with the reference and the background programmed into the ramp setup. The weighed and prepared liquid sample enclosed in the pan, was placed in the heating chamber alongside the reference and closed. The ramp rate, maximum temperature as well as sample weight was entered into the program and allowed to run. The samples were heated in an inert (nitrogen) environment with heat flow rate measured.

Chapter IV – Results and discussion

This section reports on the results from the analyses performed and how these analyses can be used to explain the premature ageing of the taphole clay.

4.1. Workability

Workability decay curves of two clays, i.e. Clay A and Clay B with a specification on the workability for these specific designs are shown in Figure 31. The workability specification is a request from a client for a clay designed for a specific furnace and process. The two clay designs are the same as mentioned in Table 10 except that Clay B only contains 18% liquid pitch and no resin, while Clay A contains 17% liquid pitch and 1% resin. The results from Figure 31 show an initial decrease in workability for both clays but a plateau for Clay B. The workability decreases for Clay A down to 26% workability at day 21. The ageing is defined as the percentage decay from the start of clay production to 21 days for this investigation. Clay A has a 28% decrease in workability over 21 days as compared to Clay B with an 8% decrease over 21 days. This difference in workability between the two clays substantiates that removing the resin does reduce the ageing workability of the clay.

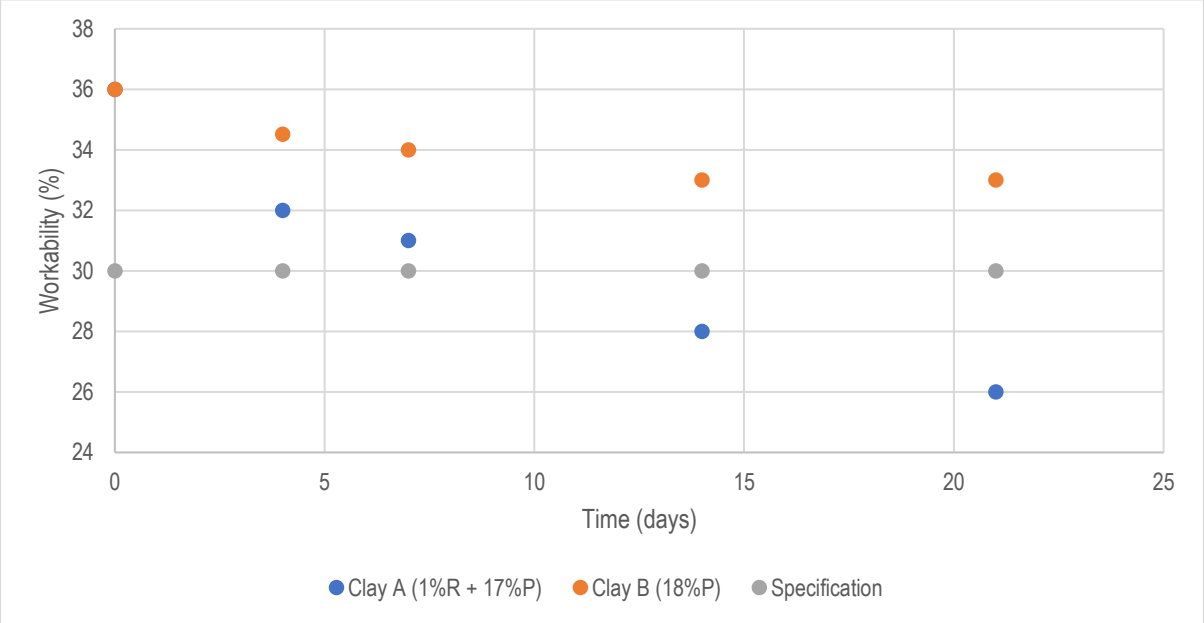

Figure 31: Workability ageing of two clays compared (P = Liquid pitch; R =Resole resin; Test temperature 35°C)

4.2. Marshall Extrusion Pressure (MEP)

The ageing of the clay has a great impact on the performance as well as plugging and drilling of the clay. The Marshall Extrusion Pressure measurement over 21 days is shown for both Clay A and Clay B in Figure 32. The MEP test indicates the pressure needed per square dimension to push the clay through an orifice with a constant exit diameter. This test simulates the conditions during plugging of the clay where it is required to push the clay through a mud gun into the tap hole. The increase in extrusion pressure of Clay A, over 21 days, is shown in

Figure 32. Clay B extrusion pressure increases, the same as with the workability, over 7 days but then reaches a plateau. This plateau is an indication that the clay has reached an equilibrium and is stable regarding liquid absorption and ageing. This continual increase in MEP of Clay A, will make the pushing of the clay very difficult and reduce taphole clay lengths which will have an adverse effect on the tap hole integrity.

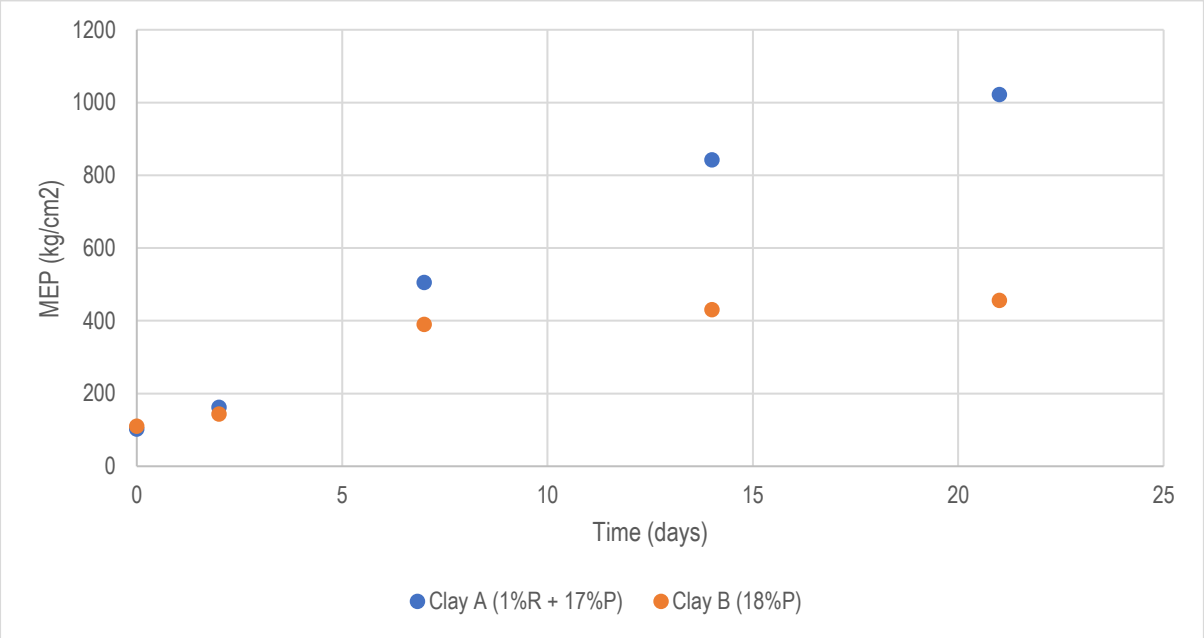

Figure 32: MEP of two clays comparing ageing (P = Liquid pitch; R = Resole resin; Test temperature 35°C)

4.3. Effect of binder viscosity on the workability of Clay A

The effect of the increase in binder viscosity on the workability of the Clay A is shown in Figure 33.

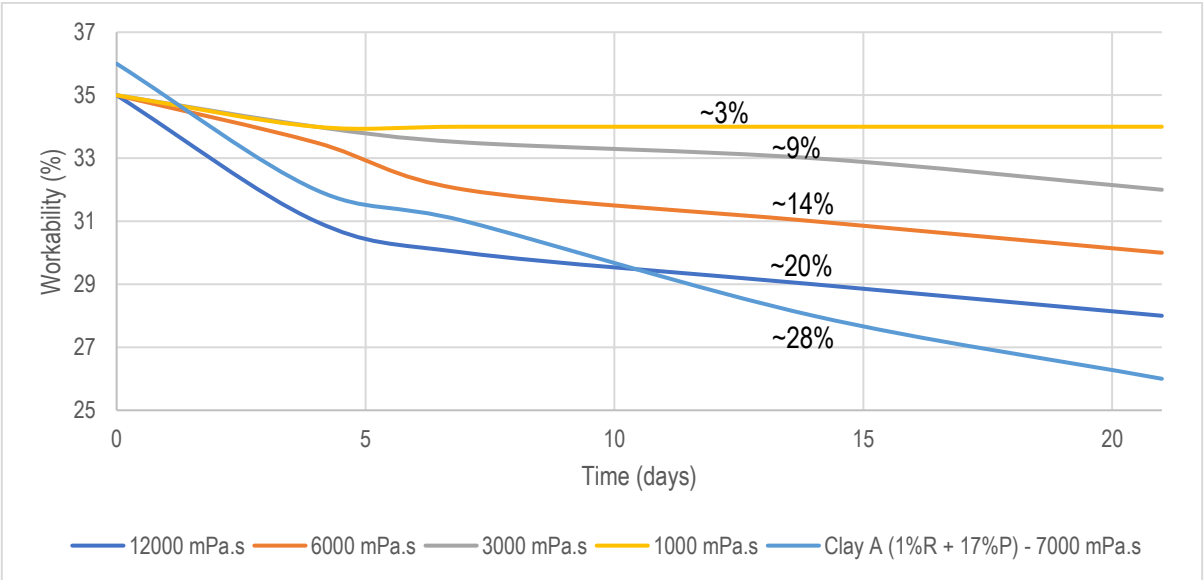

Figure 33: Workability ageing of Clay A at different binder viscosities, showing the effect of binder viscosity on the workability of Clay A. Percentage of workability decreases are present on the curves.

The workability decay results (Figure 33) show that as the binder viscosity increases the workability decay of the taphole clay increases. This is particularly important to evaluate when looking at polymerisation or cross-linking effects of the binder as these reactions increase the viscosity of the binder due to curing reactions of thermosetting resins. The sample that contains resin in Figure 33, has a higher initial workability. This is because of the 1% resin added which increases the clay workability. With the addition of the resin, some of the liquid pitch needed to be reduced when the experiment was conducted. The reduction in workability of Clay A in Figure 31 is representative of clay that contains a resole resin and liquid pitch mixture as a binder. The results of the effect of binder viscosity on clay workability (Figure 33) is of clay that contains only liquid pitch of which the viscosity was altered by using different quantities of the liquid pitch carrier liquid to attain the desired viscosity. The viscosities of the binder remained constant during the duration of the experiment. The reduction in workability for the first five days of the samples only containing liquid pitch, is due to internal porosity of the raw material aggregates in which the liquid needs to penetrate. This is a slow process of which the effect is seen in Figure 33 where all the samples that contain liquid pitch only have a modicum reduction in workability after the 5 days as compared to the clay sample that contains resin, which after five days continues to reduce in workability, significantly. This reduction might be as a result of interaction between the resole resin and liquid pitch as a binder in the clay.

4.4. Examination of factors and properties that can potentially influence the workability and ageing of Clay A

To understand the workability ageing of Clay A, all the possible contributing factors were evaluated, as mentioned in Figure 28. The properties mentioned, i.e. gradings, raw material polarities, raw material impurities, clay design, particle distribution and temperature (Figure 28) were characterised and evaluated to ensure no other parameters are influencing the workability and ageing of the clay. The viscosity being the independent variable was investigated in different scenarios and experimental setups shown in Figure 29. This was done to determine if the presence of the liquid pitch in the matrix of the resin, could cause polymerisation or cross-linking of the resin structure and if this polymerisation or cross-linking could increase the viscosity of the binder combination and reduce the workability of Clay A.

4.4.1. Taphole clay granulometry and raw material particle size distribution

The granulometry of a taphole clay is important in that it determines the flow characteristics and sinterability. It also influences parameters like liquid binder addition quantities when the clay is manufactured, ageing, strength development and volatile loss. The grading of the individual raw materials is important in that the grading of a specific raw material is used to construct the product grading of the clay. The particle size distribution of Clay A, as well as the individual raw materials, is shown in Figure 34 (See Appendix A for the enlarged graph).

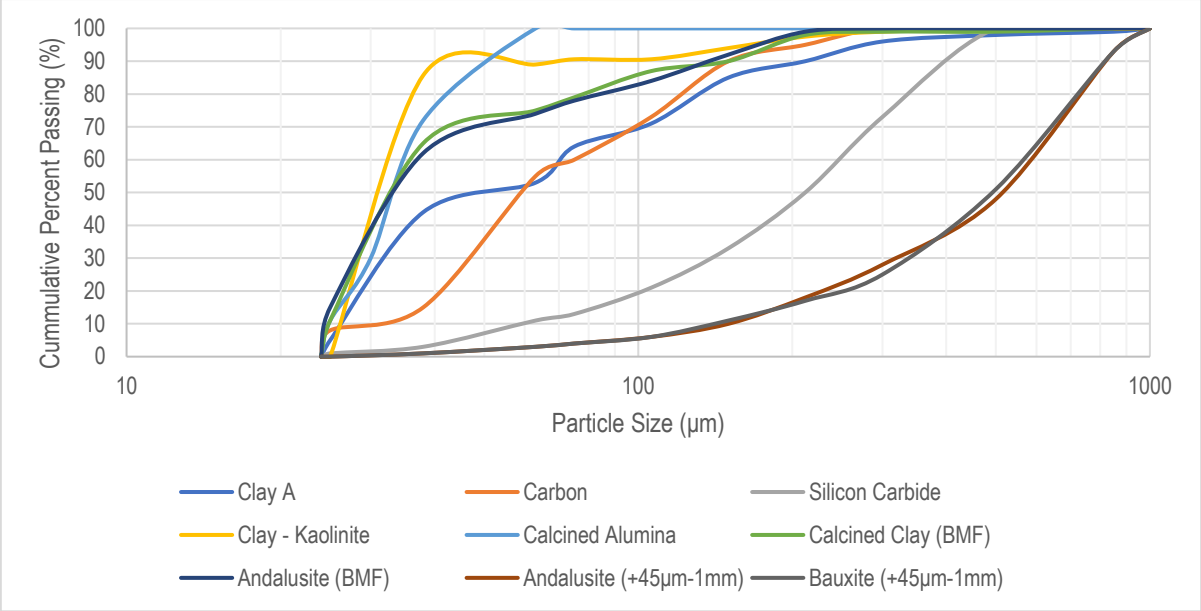

Figure 34: PSD of the individual raw materials as well as Clay A (BMF = ball mill fines)

The grading of bauxite +45µm-1mm and andalusite +45µm-1mm are similar because the classification of the raw material on size range is a function of largely the sizing practices, i.e. crushing and screening. The breakdown of the raw material does affect this to some extent, but processing would ensure that these raw materials are largely sized to a standard. The +45µm-1mm size range for these 2 raw materials should be 85-100% passing which is confirmed in Figure 34. If the clay contains an excess of fines (by mass%), the quantity of binder must be increased to achieve the same workability, and this not only alters the ageing of the clay but it also has a cost implication due to the cost of the binder. The use of 1mm as top fraction makes this a sinteractive clay since less of the 3-5mm or 1-3mm fractions are used which delay the sintering or reduce the intensity of sintering.

The grading of andalusite BMF and calcined clay BMF are also similar except for the slight decrease in particle size at 0.3mm. The desired distribution for the BMF would be that 60-70% is -45µm which is the case for both the andalusite and calcined clay. This is a specification that is implemented on this specific raw material and alterations to it can be made but BMF are generally considered 60-70% -45µm. The calcined alumina filler is a very fine raw material and nearly 85% of this material is -45µm which is shown in Figure 34. The kaolinite clay raw material shows an >90% at -45µm which is part of the filler material but coarser than the calcined alumina and finer than the +45µm-1mm size range raw materials. As for the silicon carbide and carbon, both these raw materials have size ranges between 45µm and 1mm. The Clay A results refer to the taphole clay granulometry and on closer examination, the split between +45µm-1mm and the fines (-45µm) is at 50%. The passing for -45µm is around 50%, but since there is no aggregate, i.e. 3-5mm and 0-1mm, the granulometry needs to be shifted so that the PSD is optimised for effective sintering but also not over sintering, i.e. the majority of particles in the -45 µm size range. The particle size distribution graph for Clay A is continuous, with no gap in the distribution that might affect the flow properties of the clay when extruded or pushed through a mud gun.

4.4.2. Aggregate and powder raw material wettability

The wettability was examined to confirm that there is no polarity mismatch between solid particles, i.e. fines and aggregate, and the binders, i.e. resin and liquid pitch. The match in polarity between the binders and particulates are important because of two reasons. The one is that the solubility of the resin and pitch is highly dependent on the polarity of the compounds it contains and the molecular mass distribution (Li, et al., 2000). Having a polarity incompatibility may cause problems in the solubility of the resin and pitch into each other and its interaction with the particulates in the clay (Lin, et al., 1993). The other reason is that if there is a polarity mismatch between one of the particulate raw materials and the rest of the oxides, carbides and the binders, the clay will start to separate due to repulsive forces inside the clay. This might cause the clay to separate after some time which may influence the workability of the clay. The main raw materials that might be of concern are the ones that contain organic carbon (clay kaolinite, silicon carbide) as well as the carbon added to the clay which if it is pure graphite, it might cause a problem due to its hydrophobic nature.

For this reason, the aggregate as well as the powdered filler materials were characterised as to the surface polarity of the particles. The wettability results for samples tested in both polar (water) and non-polar (hexane) mediums are shown in Figure 35. The phenolic resin is considered to be polar because of its functional groups but is dependent on the ratio of phenol-to-formaldehyde (Li, et al., 2000). The liquid pitch is also considered to be polar due to one of its major constituents being coal tar pitch. The coal tar pitch has hydroxyl and amino functional groups which constitute more polar behaviour of this liquid (Knicker, et al., 1996) (Sutrisna & Kabe, 2004).

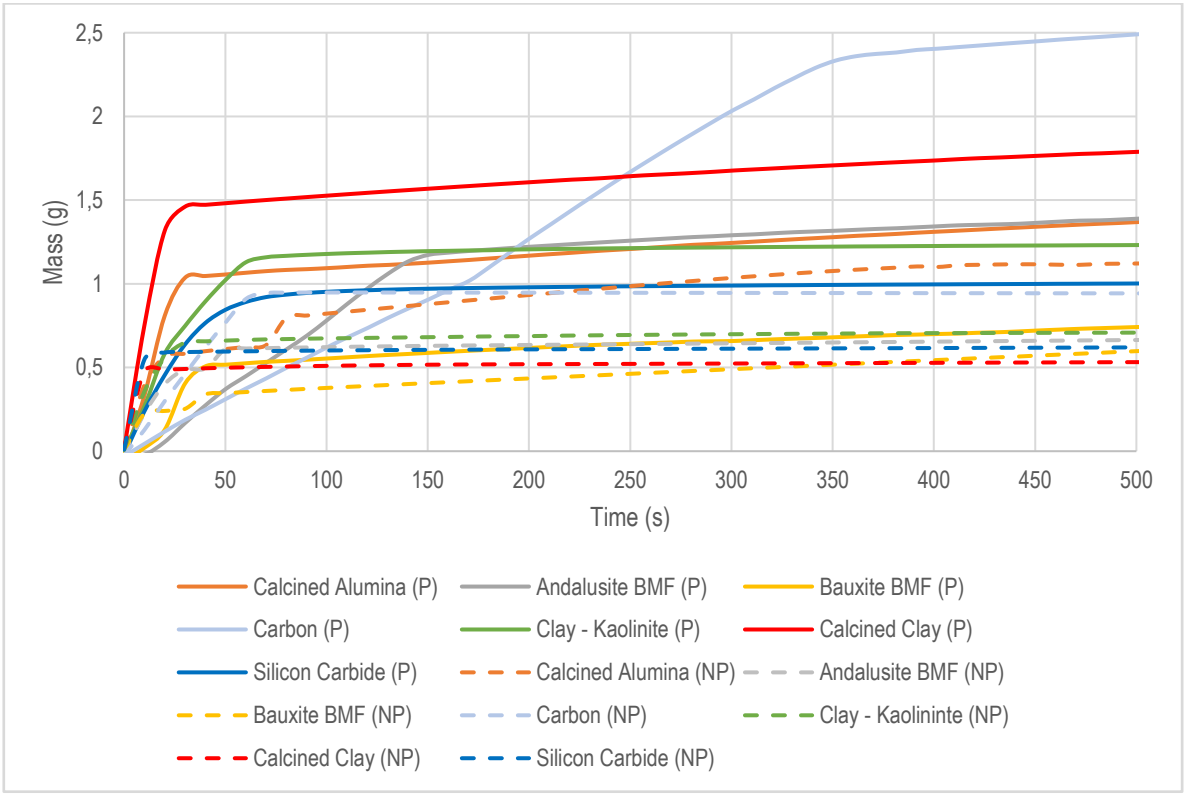

Figure 35: Graph showing wettability results for aggregate and matrix raw materials used in Clay A and Clay B (P = Polar medium, NP = Non-polar medium)

The wettability curves shown in Figure 35 can be used to determine the contact angle of the liquid onto the particle surface. As stated in Section 3, the software used for constructing the graphs and info shown also report a gradient of the graph as mass^2/time. This gradient along with the properties of the liquids can be used to determine the contact angle. The gradients from Figure 35 for both hexane and water as well as the calculated angles are given in Table 11 (calculations of contact angles in Appendix A). The calculated contact angles in Table 11 are all <90°, which indicates that all raw materials, i.e. aggregate and matrix material, are wettable by water and therefore considered polar surfaced minerals. The calcined alumina and calcined clay show the highest degree of wettability by water followed by the other raw materials. The calcined alumina and calcined clay surface properties are strong hydrophilic. The wettability of the carbon used in the Clay A shows that it is wettable (partially) by water. The polarity nature of all the raw materials used in Clay A will not lead to separate solid phases in the clay due to repulsive forces. The proceeding analyses can be assumed that the clay mass is a homogeneous mass.

Table 11: Wettability constants and data for calculating contact angle for water (polar) wettability

	Calcined Alumina	Andalusite	Bauxite	Carbon	Clay - Kaolin	Calcined Clay	Silicon Carbide
mass^2/time (Hexane)	0.00574	0.00743	0.00286	0.02149	0.02117	0.00529	0.02985
m^2/t (Water)	0.00553	0.00675	0.00120	0.01751	0.00549	0.00520	0.01209
C_w	1.26E-07	1.63E-07	6.27E-08	4.71E-07	4.64E-07	1.16E-07	6.54E-07
θ	15.54	24.76	65.22	35.43	74.98	11.47	66.10

4.4.3. Aggregate and powder raw material characterisation

The characterisation of the aggregate and powder raw materials are reported in this section. By characterising the raw materials, the effect of impurities on possible polymerisation or cross-linking of the resin or resin and pitch combination can be evaluated. The analysis methods that were utilised are XRF (chemical analysis), quantitative XRD (crystalline phase analysis) and SEM-EDS (to confirm both XRF and XRD results, as well as determine the phase composition of the raw materials). The combination of these analyses confirmed that none of these raw materials could cause polymerisation of the resin or resin-liquid pitch mixture. The possible impurity oxides or elemental compounds that can contribute to the polymerisation or cross-linking, that was investigated, are elemental sulphur, free lime (CaO) or small halide concentrations.

4.4.3.1. X-Ray Fluorescence

The elemental composition of each aggregate and matrix raw material that was used in Clay A and Clay B is reported in Table 12. The analysis of the carbon filler raw material that was used is reported in Table 13. The objective of the XRF analysis is to identify any impurities in the raw materials that can promote polymerisation or cross-linking of the binder system, such as free calcium oxide (CaO) or elemental sulphur (S).

Table 12: XRF analysis results of aggregate and powder raw materials fused in Clay A and Clay B

	Calcined alumina	Andalusite	Bauxite	Clay - Kaolinite	Calcined clay (BMF)	Silicon carbide
SiO_2	0.04	36.52	6.41	63.74	52.47	3.64
Al_2O_3	99.52	61.92	88.73	28.96	44.23	1.32
Fe_2O_3	0.02	0.54	0.80	1.27	0.74	0.70
Cr_2O_3	0.02	-	0.04	0.06	-	0.01
TiO_2	0.02	0.02	3.38	1.03	1.56	0.01
CaO	0.01	0.16	0.06	0.10	0.14	0.01
MgO	0.01	0.17	0.02	0.46	0.15	0.01
K_2O	0.01	0.38	0.24	3.12	0.50	-
Na_2O	0.14	0.10	0.01	0.68	0.10	-
P_2O_5	-	-	0.30	0.24	-	-
ZrO_2	-	-	-	0.02	-	-
C	-	-	-	-	-	1.85
SiC	-	-	-	-	-	92.4
Sum	99.79	99.81	99.99	99.69	99.89	99.95

The calcined alumina is rich in alumina (Al_2O_3) with negligible amounts of oxide impurities. The andalusite has a typical alumina to silica mass ratio of 3:2 that is distinctive of an andalusite raw material. The typical impurities in andalusite is iron oxide (expressed as Fe_2O_3) present in the iron oxide-containing chiastolite cross and in ilmenite ($FeTiO_3$). Some trace oxide impurities are also present namely K_2O and calcium oxide (CaO) contents. The bauxite has a high alumina content (88.7 mass%) and low silica (SiO_2) content (6.4 mass%). The typical impurities present in the bauxite is titanium oxide (TiO_2) as well as iron oxide. Some traces of P_2O_5, K_2O, CaO and MgO are also present in the bauxite. The kaolinite clay used as matrix material is high silica and low alumina material (63.7 mass% SiO_2, 29.0 mass% Al_2O_3) with some iron oxide, titanium oxide and potassium oxide as impurities. The impurities in the kaolinite clay do not include any elemental sulphur (S) or free calcium oxide (CaO) that might promote the polymerisation or cross-linking effect. The calcined clay BMF contains 52.5 mass% alumina and 44.2 mass% silica with iron oxide and titanium oxide as its major impurities. The silicon carbide has a purity of 92% silicon carbide. The remainder is made up of free carbon and some silica and alumina. Some metallic silicon might be present in the silicon carbide, but this could only be confirmed with XRD.

The analysis of the coal raw material shows a high fixed carbon content with a moderate amount of volatile matter, some ash and low moisture content (Table 13). The volatile matter of this raw material is sufficient to generate some volatiles in the taphole clay when pushed during plugging and in operation. The ash content is high (13.1 mass%) but considering the grade of carbon, the comparison of ash to carbon content makes this a sufficiently suitable carbon source for the taphole clay. There is some sulphur present in the sample, but it is not considered enough to be able to cause a noticeable polymerisation effect.

Table 13: Analysis of carbon raw material used in Clay A and Clay B

	Moisture (%)	Ash (%)	Volatile Matter (%)	Fixed Carbon (%)	Sulphur (%)
Carbon	3.80	13.09	12.52	70.60	0.20

4.4.3.2. X-Ray Diffraction

The crystalline phase analysis of each of the aggregate and powder raw materials that were used in Clay A and Clay B is reported in Table 14. This was done using quantitative XRD analysis.

Table 14: Quantitative XRD analysis of aggregate and powder raw materials used in Clay A and Clay B

Oxide phase	Calcined alumina	Andalusite	Bauxite	Carbon (Coal)	Clay - kaolinite	Calcined clay (BMF)	Silicon carbide
Andalusite[1]	-	98.4	-	-	-	-	-
β-alumina[2]	0.67	-	42.21	-	-	-	-
Calcite[3]	-	-	-	1.30	-	-	-
Corundum[4]	99.02	-	30.41	-	-	29.70	2.60
Graphite[5]	-	-	-	-	-	-	1.60
Kalsilite[6]	-	-	0.90	-	-	-	-
Kaolinite[7]	-	-	-	12.32	66.08	-	-
Leucite[8]	-	1.15	-	-	-	-	-
Moissanite 6H[9]	-	-	-	-	-	-	62.13
Moissanite 4H[10]	-	-	-	-	-	-	27.96
Mullite[11]	-	-	22.99	-	-	18.05	-
Muscovite[12]	-	-	-	-	15.46	3.80	-
Quartz[13]	0.31	0.45	-	1.67	18.16	-	4.76
Cristobalite [14]	-	-	-	-	-	48,05	-
Rutile[15]	-	-	3.48	-	-	0.40	0.96
Talc[16]	-	-	-	-	0.30		-
Organic Carbon[17]	-	-	-	84.71	-	-	-

[1] Al_2SiO_5
[2] $Al_{21.86}K_{2.59}O_{34}$
[3] $CaCO_3$
[4] Al_2O_3
[5] C
[6] $AlKSiO_4$
[7] $Al_2Si_2O_5(OH)_4$
[8] $KAlSi_2O_6$
[9] SiC
[10] SiC
[11] $Al_6Si_2O_{13}$
[12] $(KF)_2(Al_2O_3)_3(SiO_2)_6$
[13] SiO_2
[14] SiO_2
[15] TiO_2
[16] $Mg_3Si_4O_{10}(OH)_2$
[17] C

The calcined alumina raw material consists mainly of corundum with some trace quantities of β-alumina and quartz. The andalusite shows andalusite as majority phase and some leucite. The leucite is seen as a trace impurity. The phase analysis of andalusite correlates with the chemical composition analysed with XRF. The phase analysis of bauxite indicated a third split each between β-alumina, corundum and mullite. The mullite present in the bauxite must be due to quartz present in the bauxite, which reacts with alumina during calcination to form mullite. The kalsilite and rutile are in smaller quantities and are considered the impurities. The coal mainly consists of organic carbon with no graphite. The ash content of the coal raw material was confirmed through the presence of calcite, kaolinite and quartz. Two-thirds of the kaolinite clay raw material consists of the mineral kaolinite and a third of muscovite and quartz. Potassium oxide in this clay raw material is found in muscovite.

The last two raw materials are calcined clay and silicon carbide. The phase analysis of the calcined clay consists of corundum and almost two-thirds of mullite, and a third of cristobalite. The trace impurities are some rutile and muscovite. The presence of mullite in this analysis confirms that the clay has been calcined. The silicon carbide exists in two polymorphic forms, i.e. H4 and H6, of ~88 mass%. The remainder of the mineral consists of corundum, quartz, rutile and graphite. The phase analysis of the calcined clay and silicon carbide are supported by the XRF analysis. There are no evident impurities in the aggregate or powder raw materials that can indicate a problematic effect on polymerisation or cross-link of the resin or resin and liquid pitch binder combination.

4.4.3.3. Scanning Electron Microscopy

The electron backscatter images and elemental X-ray maps of the aggregate and powder raw materials used in Clay A and Clay B are shown in this section. The spectrums refer to the EDS identification of the phases. The EDS spectrums are given in Appendix A. The scanning back scatter images and elemental X-ray maps were used to characterise the phases present in each raw material, their orientation in the aggregate crystal as well as confirm the analyses of both XRF and XRD of no free calcium oxide (CaO), elemental sulphur (S) or any other impurities that can aid in the possible polymerisation and cross-linking of the binders. The characterisation of each of the raw materials will assist in identifying raw materials to use in future experimental work or to repeat the work done in this investigation, that will not be the cause of polymerisation or cross-linking of the binder system.

4.4.3.3.1. Calcined alumina

The EBS image of calcined alumina is shown in Figure 36 and the X-ray map in Figure 37. The X-ray map reveals that the calcined alumina consists of an aluminium-rich phase. EDS analysis confirmed a $Al_{2.02}O_{2.97}$ stoichiometry (Table 15). The major phase present in the calcined alumina as analysed with XRF, XRD and SEM-EDS is corundum. Minor phases are quartz and β-alumina.

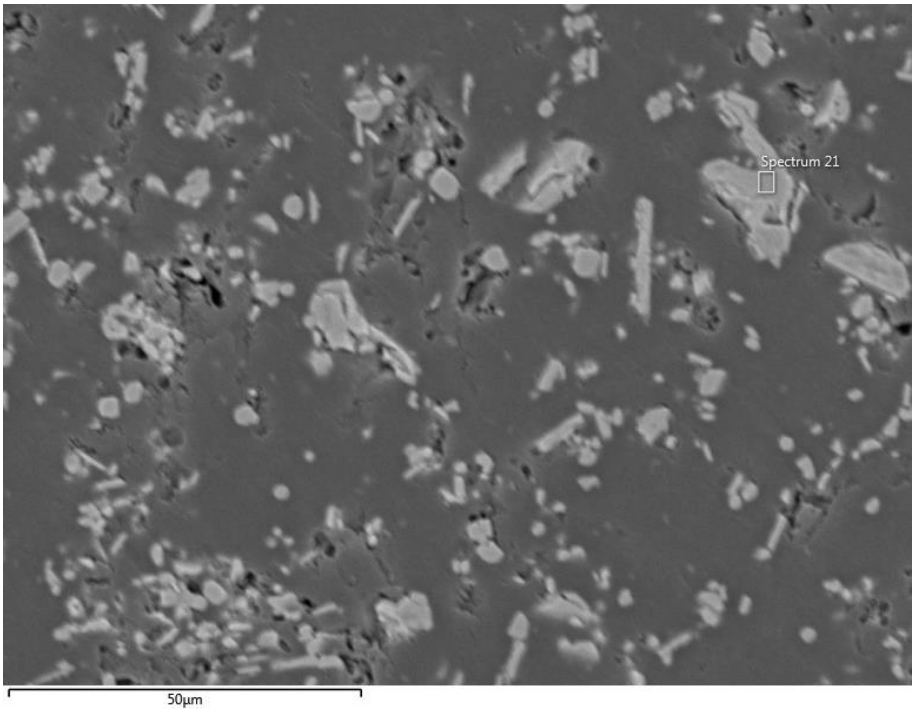

Figure 36: Electron backscatter image of calcined alumina (Spectrum 21: alumina (Al_2O_3))

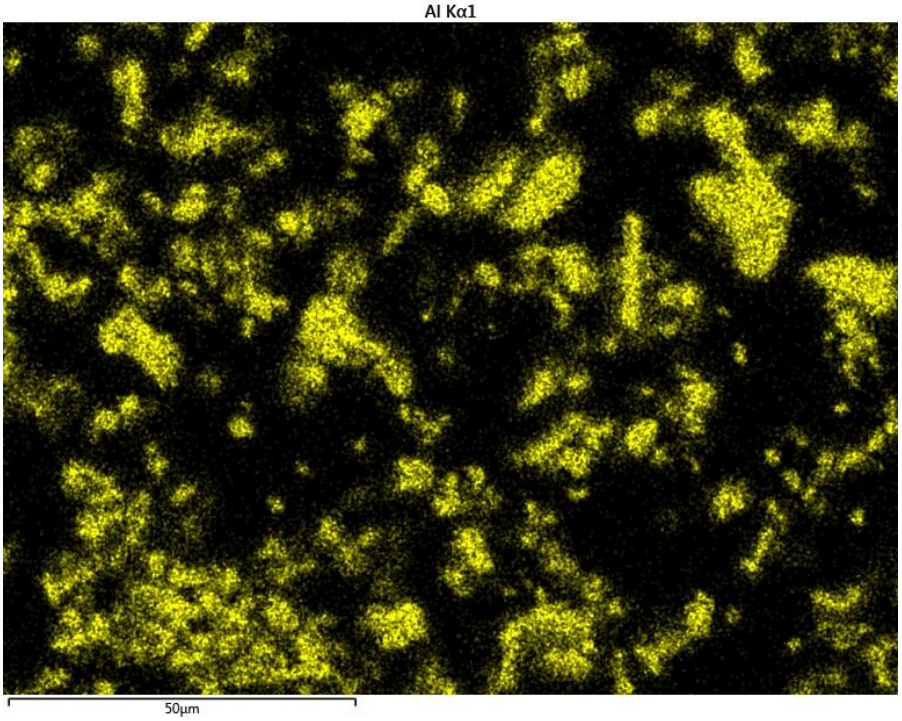

Figure 37: Aluminium X-ray map of calcined alumina confirming the dominance of aluminium in this raw material

Table 15: EDS analysis and calculated stoichiometry of phases in calcined alumina

Spectra	EDS Analysis – Calculated stoichiometry	EDS Analysis – phases
21	$Al_{2,02}O_{2,97}$	Alumina

4.4.3.3.2. Andalusite

The EBS image of andalusite is shown in Figure 38. The EDS analysis reveals that this raw material consists of andalusite, iron-and-magnesia bearing leucite (Washington, 1907) and silica. The phases and calculated stoichiometries from EDS analysis are given in Table 16. XRF, XRD and SEM-EDS confirmed that this raw material is unfired andalusite, which contains leucite and quartz as minor phases.

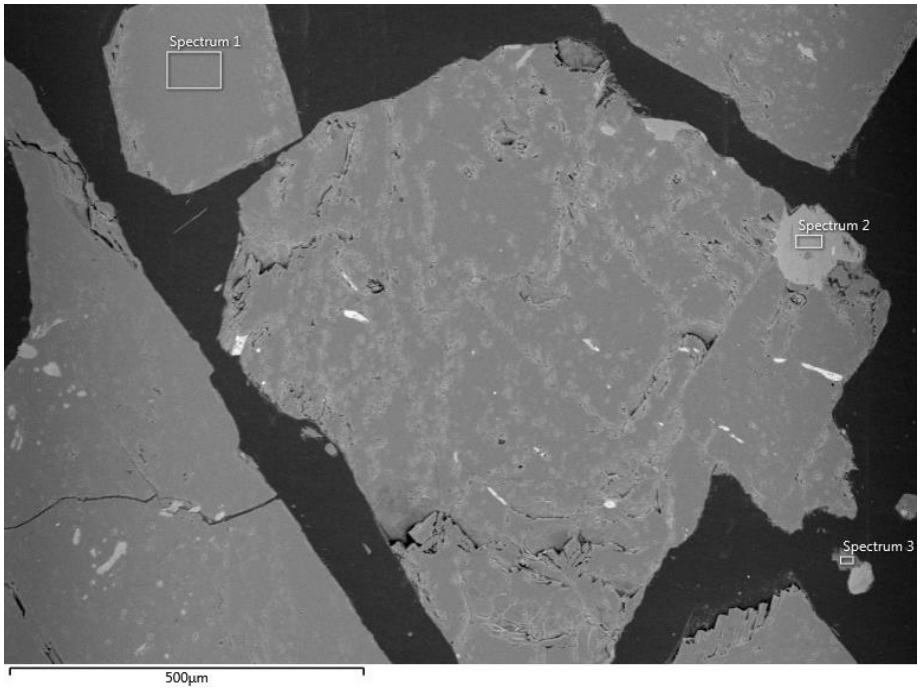

Figure 38: Electron backscatter image of andalusite (Spectrum 1: andalusite (Al_2SiO_5), Spectrum 2: iron-and-magnesia bearing leucite (Mg, Fe)$KAlSi_2O_6$, Spectrum 3: silica (SiO_2))

Table 16: EDS analysis and calculated stoichiometry of phases in andalusite

Spectra	EDS Analysis – Calculated stoichiometry	EDS Analysis – phases
1	$Al_{1,91}Si_1O_{4,06}$	Al_2SiO_5
2	(Mg, Fe)$K_{0,36}AlSi_{1,46}O_{6,25}$	(Mg, Fe)$KAlSi_2O_6$
3	$SiO_{1,70}$	SiO_2

4.4.3.3.3. Bauxite

The EBS images of bauxite are shown in Figures 39 and 40, with an X-ray map shown in Figure 41. The EDS analysis and X-ray map reveal that the bauxite consists of an alumina (Al_2O_3) rich phase, mullite, rutile and trace quantities of a potassium-rich phase. The phases and calculated stoichiometries from the EDS analysis are given in Table 17. The major phases as analysed with XRF, XRD and SEM-EDS present in the bauxite raw material are β-alumina, corundum and mullite. Minor phases are kalsilite and rutile.

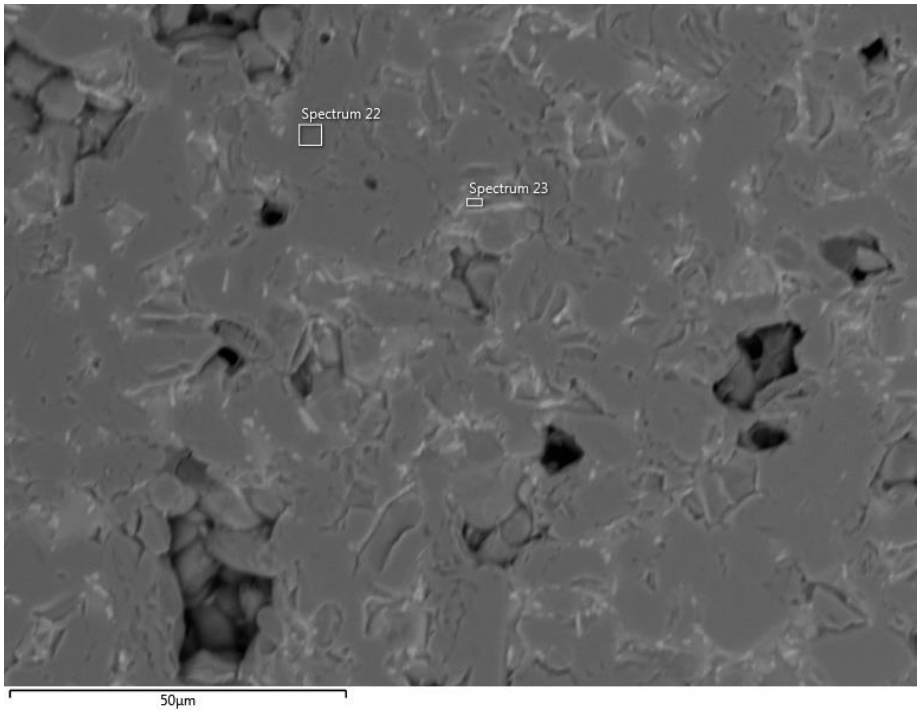

Figure 39: Electron backscatter image of bauxite (Spectrum 22: alumina (Al_2O_3), Spectrum 23: mullite ($3Al_2O_3.2SiO_2$))

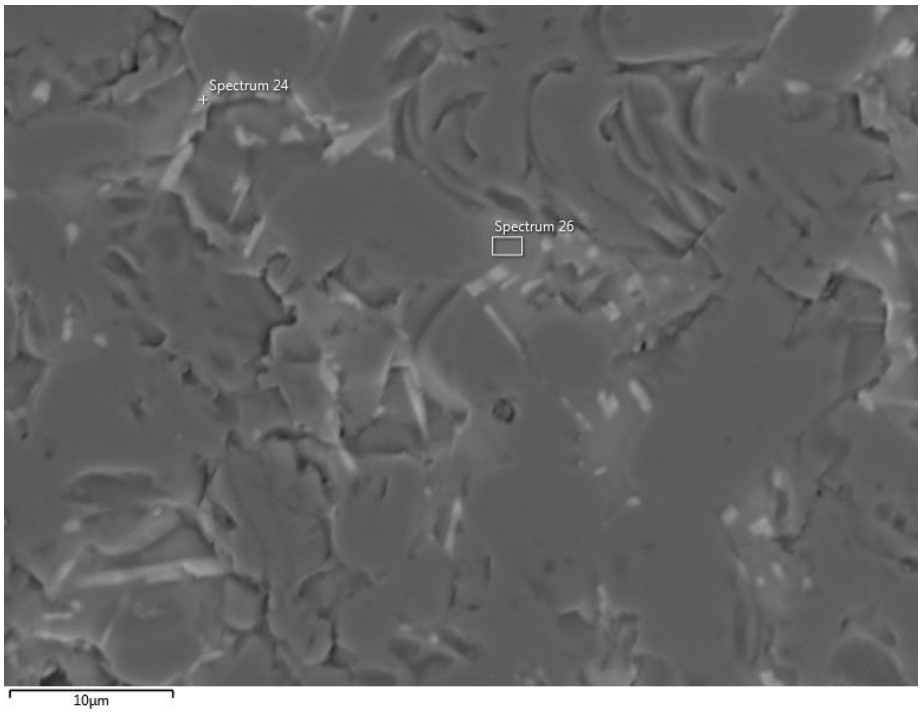

Figure 40: Electron backscatter image of bauxite (Spectrum 24: rutile (TiO_2), Spectrum 26: mullite ($3Al_2O_3.2SiO_2$))

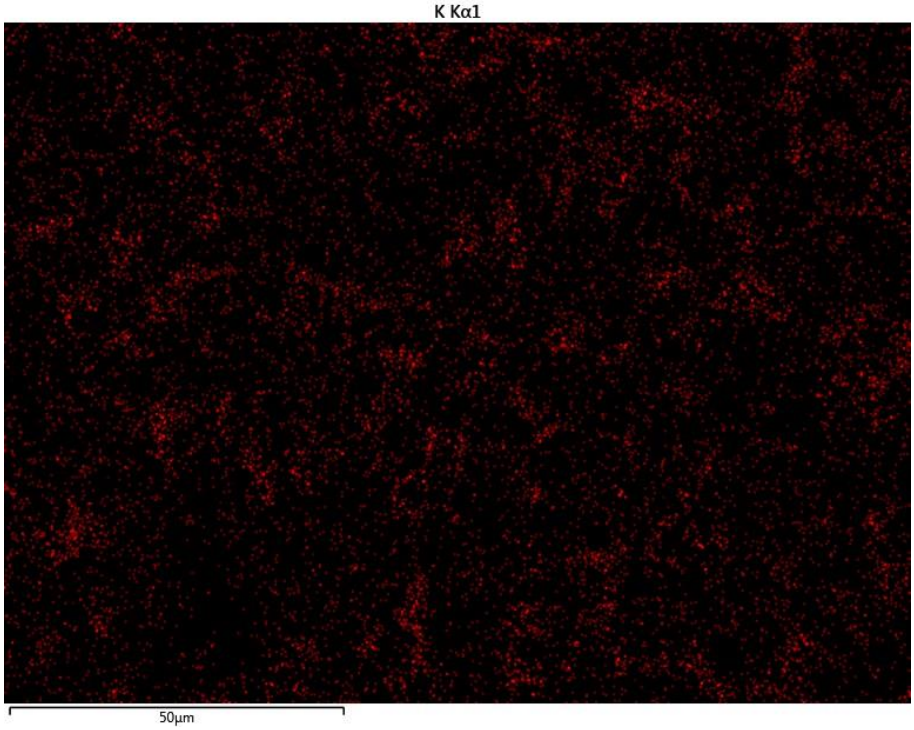

Figure 41: Potassium X-ray map of bauxite raw material

Table 17: EDS analysis and calculated stoichiometry of phases in bauxite

Spectra	EDS Analysis – calculated stoichiometry	EDS Analysis – phases
22	$Al_{2,04}O_{2,95}$	Al_2O_3
23 (26)	$Al_{5,82}S_{2,36}O_{10,92}$	$3Al_2O_3.2SiO_2$
24	$TiO_{2,74}$	TiO_2

4.4.3.3.4. Clay-Kaolinite

The EBS images of clay-kaolinite are shown in Figures 42 and 43. The EDS analysis reveals that the clay-kaolinite raw materials consist of kaolinite, silica and muscovite. The phases and calculated stoichiometries from the EDS analysis are given in Table 18. The major phases present in the clay-kaolinite as analysed with XRF, XRD and SEM-EDS are kaolinite, muscovite and quartz. The minor phase is talc.

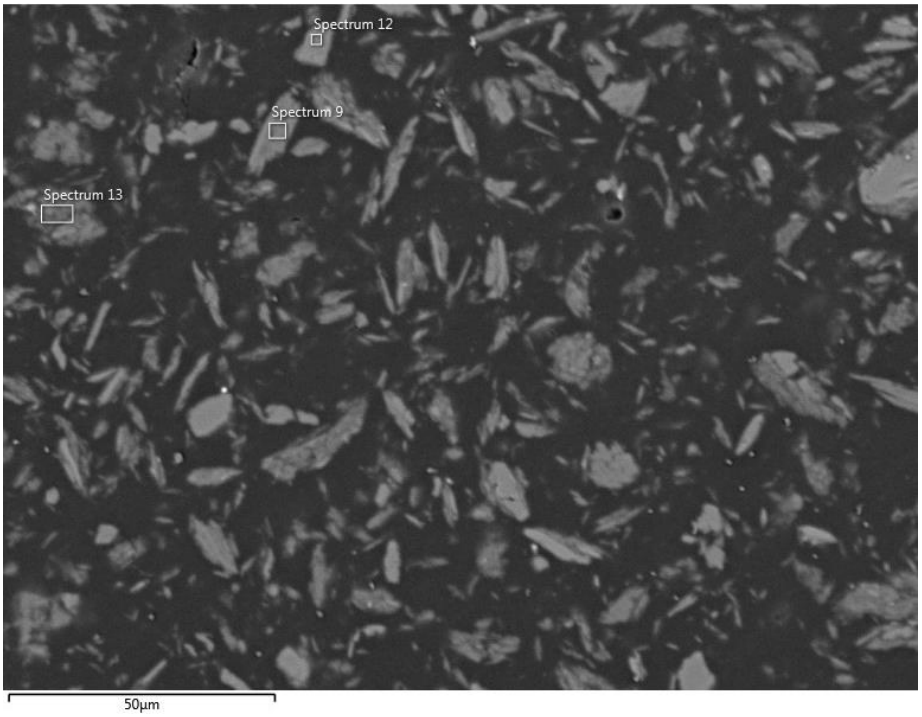

Figure 42: Electron backscatter image of clay-kaolinite (Spectrum 9: muscovite ($KAl_2(Si_3Al)O_{10}(OH)_2$), Spectrum 12: silica ($SiO_2$), Spectrum 13: kaolinite ($Al_2Si_2O_5(OH)_4$))

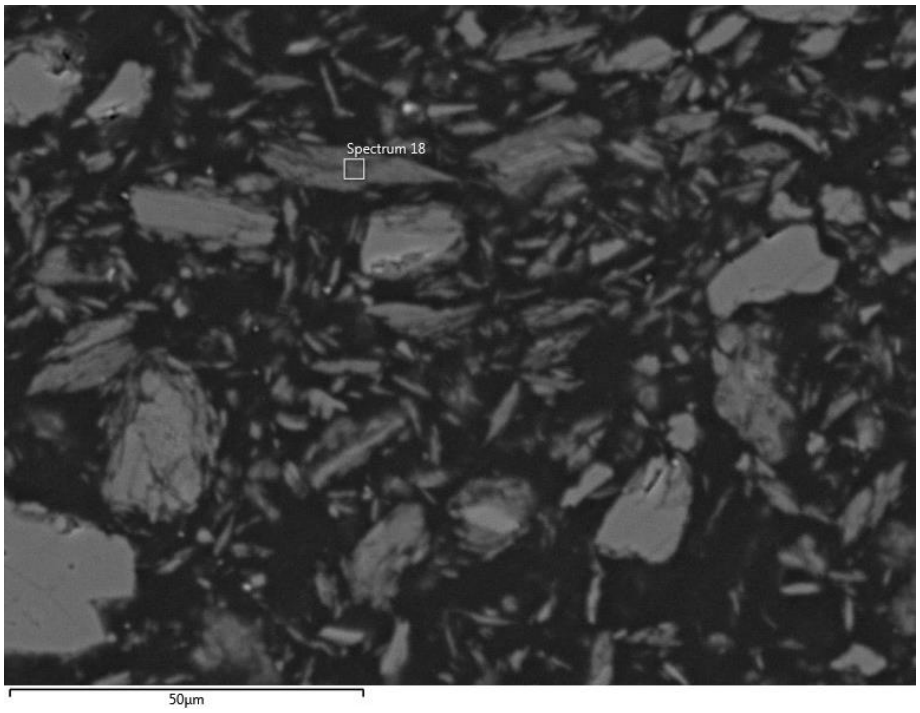

Figure 43: Electron backscatter image of clay-kaolinite (Spectrum 18: kaolinite ($Al_2Si_2O_5(OH)_4$))

Table 18: EDS analysis and calculated stoichiometry of phases in clay-kaolinite

Spectra	EDS Analysis – calculated stoichiometry	EDS Analysis – phases
9	$K_{0,5}Al_{3,21}Si_{3,52}O_{11,8}$	$KAl_2(Si_3Al)O_{10}(OH)_2$
12	$SiO_{1,81}$	SiO_2
13 (18)	$Al_{1,98}Si_{2,13}O_{6,94}$	$Al_2Si_2O_5(OH)_4$

4.4.3.3.5. Calcined clay

The EBS image of clay-kaolinite is shown in Figure 44. The EDS analysis reveals that the calcined clay consists of silica, rutile, mullite and alumina. The phases and calculated stoichiometries from the EDS analysis are given in Table 19. The major phases present in the calcined clay as analysed with XRF, XRD and SEM-EDS are corundum, mullite and cristobalite. Minor phases are muscovite and rutile.

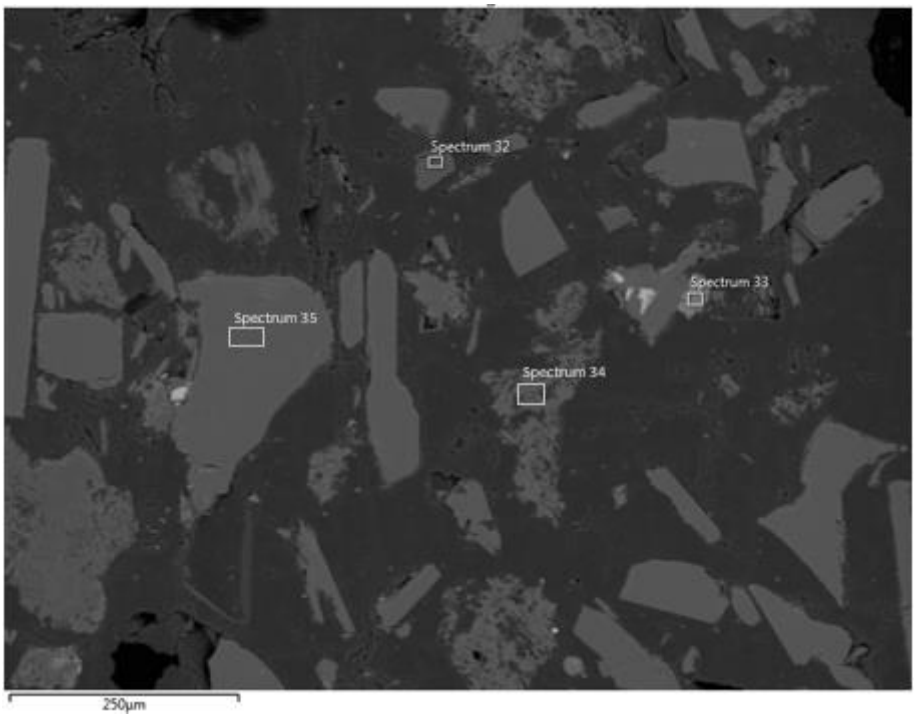

Figure 44: Electron backscatter image of calcined clay (+45µm-1mm) (Spectrum 32: silica (SiO_2), Spectrum 33: rutile (TiO_2), Spectrum 34: mullite ($3Al_2O_3.2SiO_2$), Spectrum 35: alumina (Al_2O_3))

Table 19: EDS analysis and calculated stoichiometry of phases in calcined clay

Spectra	EDS Analysis – calculated stoichiometry	EDS Analysis – phases
32	$SiO_{2,44}$	SiO_2
33	$TiO_{2,35}$	TiO_2
34	$Al_{5,48}S_{2,18}O_{11,64}$	$3Al_2O_3.2SiO_2$
35	$Al_{2,01}O_{2,93}$	Al_2O_3

4.4.3.3.6. Silicon carbide

The EBS image of silicon carbide is shown in Figure 45. The EDS analysis reveals that the silicon carbide raw materials consist of silica, alumina and a silicon phase. The phases and calculated stoichiometries from the EDS analysis are given in Table 20. The major phases present in the silicon carbide as analysed with XRF, XRD and SEM-EDS are moissanite 4H and moissanite 6H. Minor phases are corundum, quartz and rutile. The Si analysed with EDS was assumed to be SiC from the XRD results.

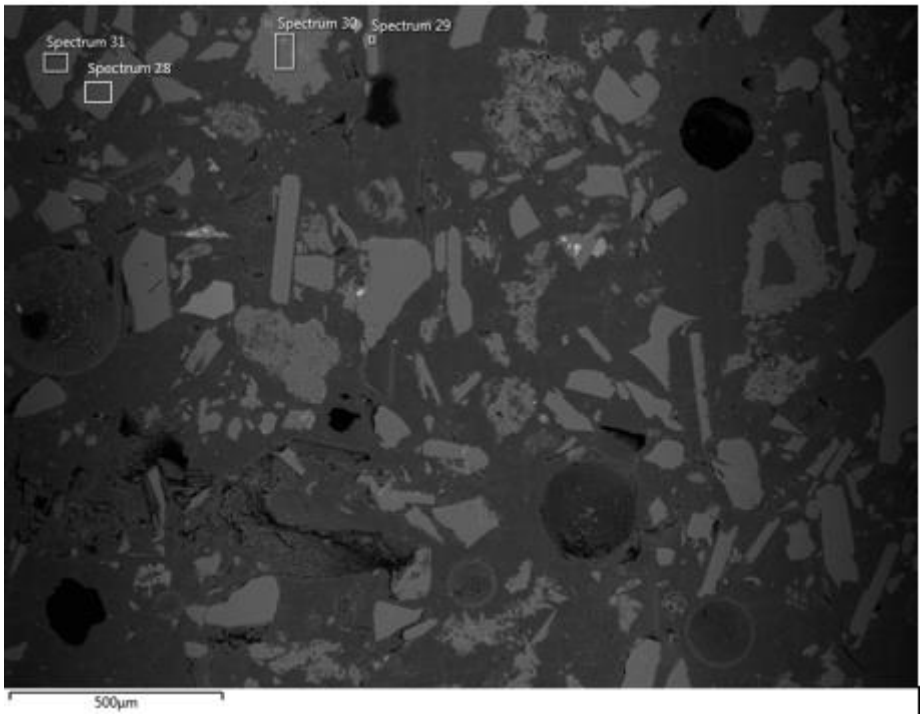

Figure 45: Electron backscatter image of silicon carbide (Spectrum 28: silica (SiO_2), Spectrum 29: alumina (Al_2O_3), Spectrum 30: moissanite (SiC))

Spectra	EDS Analysis – calculated stoichiometry	EDS Analysis – phases
28	$Si_{1,1}O_{2,2}$	SiO_2
29	$Al_{2,13}O_{2,86}$	Al_2O_3
30	Si	Si

The results from the XRF, XRD and SEM-EDS analyses confirmed that impurity elements such as free lime or sulphur are not present in any of the raw materials that can contribute to either polymerisation or cross-linking of the binder combination used in Clay A.

4.5. Characterisation of the resole resin, liquid pitch binder, as well as combinations thereof

In this section, the resin and liquid pitch binder used in Clay A were characterised and the possibility of polymerisation or cross-linking as the cause for increased ageing and reduction in workability of the clay was investigated. The resin and liquid pitch were characterised according to the functional groups they contain, using Fourier-transform infrared spectroscopy – FTIR. After the functional groups were identified, rheological properties of the resin and pitch were tested and any possible changes in viscosity and viscosity behaviour identified. The rheological work showed that there was an interaction between the resin and liquid pitch that both changed the viscosity of the resin and pitch mixture, but also altered the structure of the resin. These changes were investigated by using differential scanning calorimetry (DSC), thermogravimetric analysis (TGA) and further FTIR work.

4.5.1. Fourier-transform infrared spectroscopy (FTIR)

FTIR spectra of the liquid pitch, resin, as well as the combination of pitch and resin used in Clay A, are shown in Figure 46. The spectrum of Clay A in Figure 46 is that of a mixed sample before ageing. The Clay B binder was only the liquid pitch (no resin added) so the analysis would be that of the liquid pitch. The functional groups that were identified, are reported in Table 20. The part of the graph used for identification is between 1500 – 3000 cm^{-1}. The peaks in the region smaller than 1500 cm^{-1} are known as the fingerprint region and usually ignored. The identification of the functional groups for the resin and liquid pitch were however looked at in the fingerprint region as well because of some distinctive peaks associated with phenolic resins and confirming certain functional groups in the liquid pitch. The enlarged FTIR spectra are shown in Appendix A, for more detail.

Table 20: Interpretation of FTIR results for resole resin, liquid pitch binder and Clay A combination (Merck, 2015) (Poljanšek & Krajnc, 2005) (Yao, et al., 2018) (FTIR Raman, 2001-2020)

Observed wavelength (cm^{-1})	Wavelengths from literature (cm^{-1})	Functional groups
Liquid pitch binder		
~3050	3000 - 3150	SP2 C-H Stretch
~2900	2850 – 3000	SP3 C-H Stretch
~1605	1600	C=C stretch (aromatic)
~750 (fingerprint)	750	Benzene C-H Bending
~730 (fingerprint)	720	C-H Bending
Resole resin		
~3250	3200 – 3600	O-H Bonds (broad peak)
~3050	3000 – 3150	SP2 C-H Stretch (hybridised) – peak overlaps with O-H
~2920	2850 – 3000	SP3 C-H Stretch
~1590	1600 – 1650	C=C stretch (aromatic)

~1200 (fingerprint)	1000 – 1200 (multiple peaks)	C-O-C bonds
~1033 (fingerprint)	1000 – 1200	C-O-C bonds

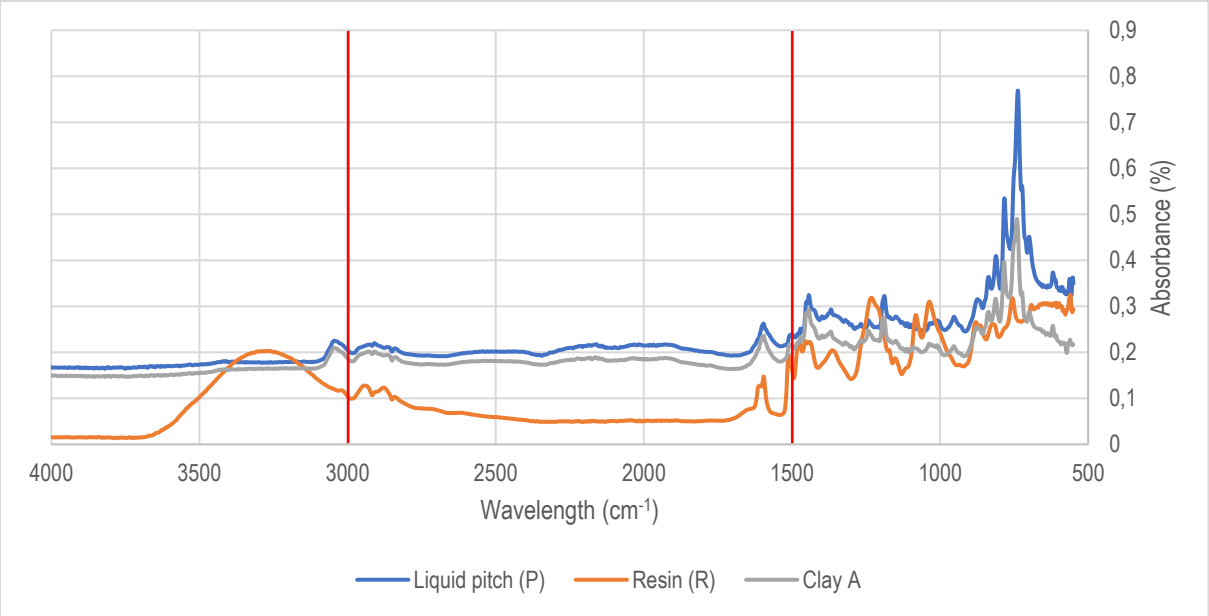

Figure 46: Identification of functional groups associated with the liquid pitch, resin and resin-pitch mixture used in Clay A using FTIR

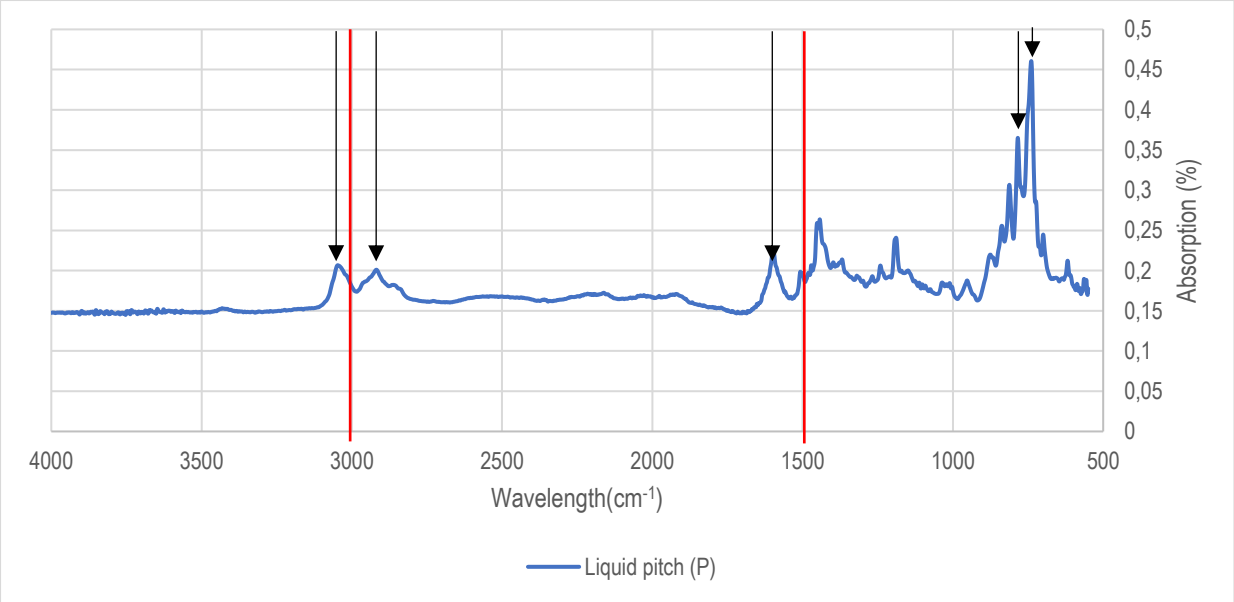

Figure 47: Identification of the functional groups associated with the liquid pitch binder

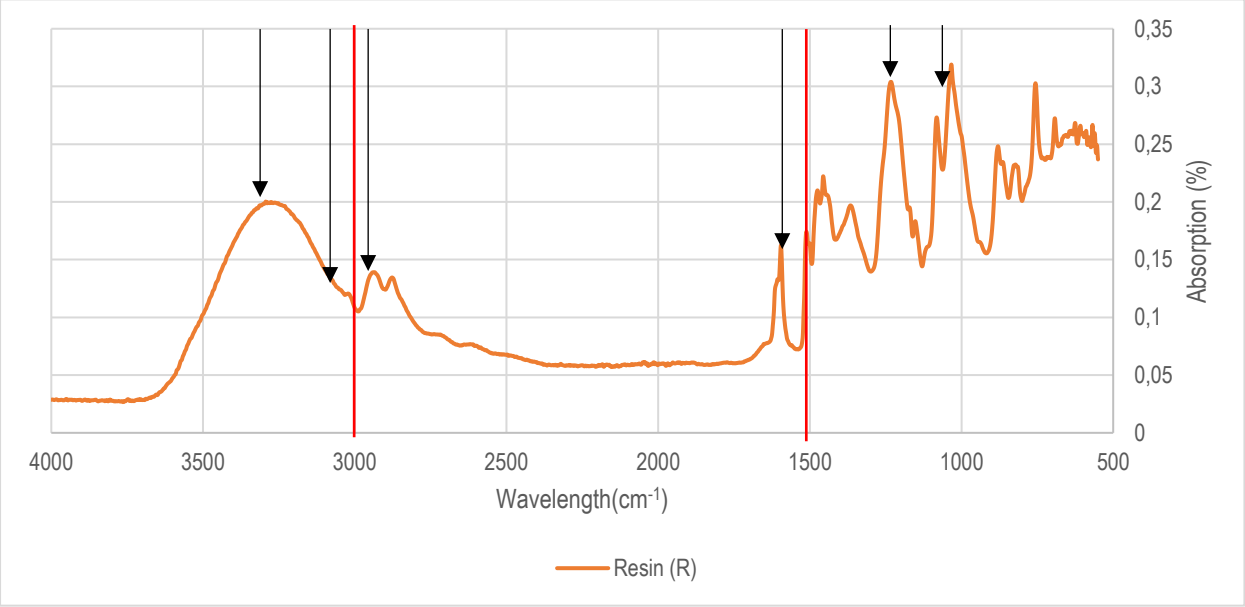

Figure 48: Identification of functional groups associated with the resole resin

The structure of the resole resin in Figure 48, is confirmed to be a phenol-formaldehyde structure. This is also confirmed by comparing the spectra of a phenol-formaldehyde resin in Figure 24 (before cure). The distinctive broad peak at 3250 cm^{-1} is indicative of O-H group as the carrier for the resin. There is some overlapping of the O-H peak at 3050 cm^{-1} on the SP2 C-H stretch. The peak at 1610 cm^{-1} confirms a cyclic aromatic structure of the phenolic resin and multiple strong peaks at 1000 – 1200 cm^{-1} is indicative of the C-O-C bonds between each of the polymer chains in the resin. The peaks at 1000 – 1200 cm^{-1} of the resole resin in Figure 24 are not as prominent due to overlap with a distinctive peak that originates at 1200 – 1300 cm^{-1}. The functional group results of the liquid pitch in Figure 47, showed some aromatics and SP C-H stretches. The structure of the liquid pitch is complex with some peak overlap from various compounds that are present in the liquid pitch. The spectrum for the Clay A binder combination shows no distinctive change in peaks. The spectrum looks like that of the liquid pitch with a very small change in the O-H region, which is contributed from the resole resin. There are also additional peaks in region 1000 – 1200 cm^{-1} due to the presence of the resole resin in the mixture.

4.5.2. Viscosity

The viscosity behaviour of the resole resin, liquid pitch and combinations thereof was studied. The resole resin and liquid pitch were tested as virgin raw materials. The combinations of resole resin and liquid pitch as mentioned in Figure 29, were also evaluated. The mixtures were evaluated after mixing and after the same mixtures were aged for two weeks at 45°C.

The influence of shear rate on dynamic viscosity, tested at 30°C, was determined for the resin, liquid pitch and combinations thereof (Figure 49). From the shear rate test, it is shown that both the resole resin and liquid pitch exhibit Newtonian behaviour since their viscosities remain constant with increasing shear rate. This behaviour was,

however, not seen in the resin-liquid pitch mixtures. When the resin and liquid pitch were mixed, there was an onset of shear thinning non-Newtonian behaviour. The extent of shear shinning increases as the mass ratio of resin to liquid pitch increases. The viscosities of the mixtures also increase with increasing resin content. This shear thinning could possibly be described by the linear bending rule or rings rule for three-dimensional liquids where the polymer chains can become distorted and polymer structure is broken up (Bartolo, 2020). The increase in viscosity between the aged mixed samples signifies the resistance to flow. The extent of shear thinning also becomes more prominent as the mixtures are aged. This observed shear thinning, indicates that there is a change in structure between the resin and liquid pitch which likely behaves as a complex emulsion and the shear thinning is a result of the deformation of the droplets in the bulk fluid. The 75 mass% resole resin - 25 mass% liquid pitch aged sample could not be evaluated because the sample was too viscous to be evaluated accurately. The 75 mass% resin - 25 mass% pitch sample already exhibited a higher viscosity than the virgin resin sample which was unexpected. The presence of the pitch of low viscosity was expected to lower the viscosity of the mixture, which was not observed.

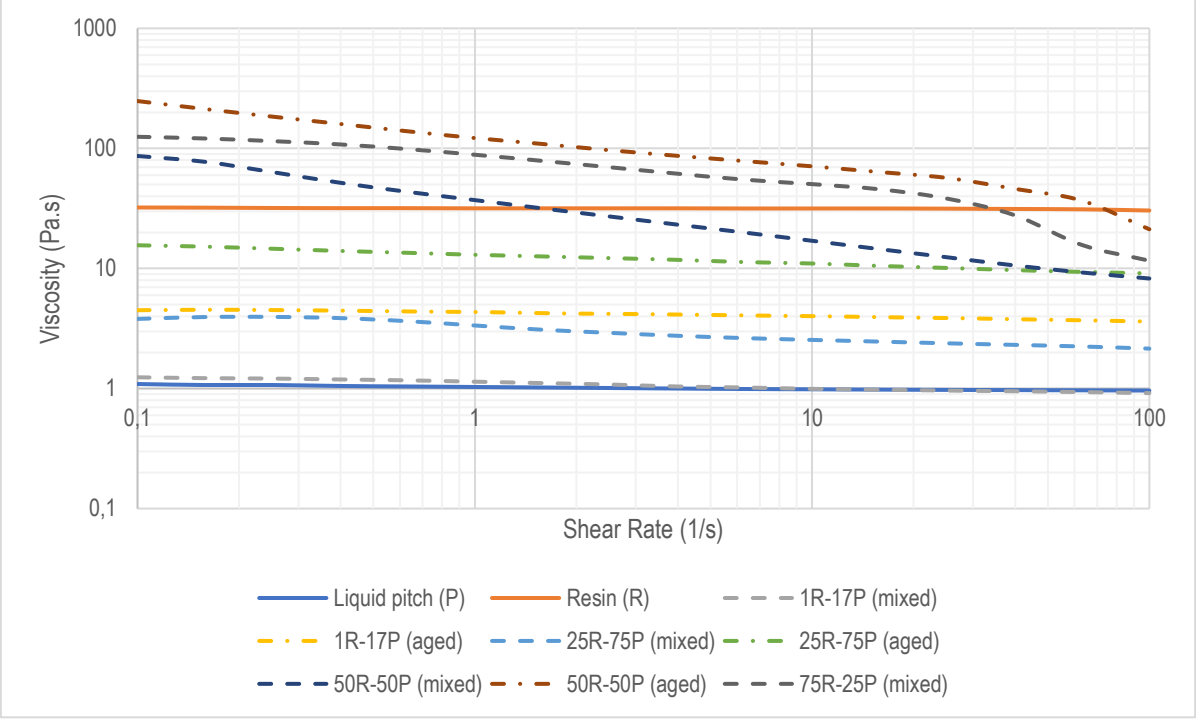

Figure 49: Shear rate vs. viscosity rheology test (after mixing and after ageing at 45°C for 2 weeks) of liquid pitch (P), virgin resole resin (R) and combinations thereof. Test conducted at 30°C

The second graph (Figure 50) reveals the change in viscosity with increasing temperature for the same samples, i.e. virgin resin, virgin pitch and resin-liquid pitch combinations. The start temperature was the same as for the shear rate test, i.e. 30°C, and the end temperature was chosen as 130°C as this is the specified curing temperature for this specific resole resin. The first discrepancy noticed is the difference between the viscosities in Figure 49 and Figure 50 at 30°C. This is due to a heating chamber not utilised during the viscosity test in Figure 50. The curing of the resin needed to be monitored thoroughly as to prevent the spindle of the rheometer being damaged

by resin curing onto it. The analyses are comparable due to the effective heating of the platform the materials are placed onto. The thin films (1 mm thick) of material between the heating pad and the spindle is heated and kept at temperature. The heat losses between the two experiments are negligibly. The heating chamber assists with rapid heating of the sample.

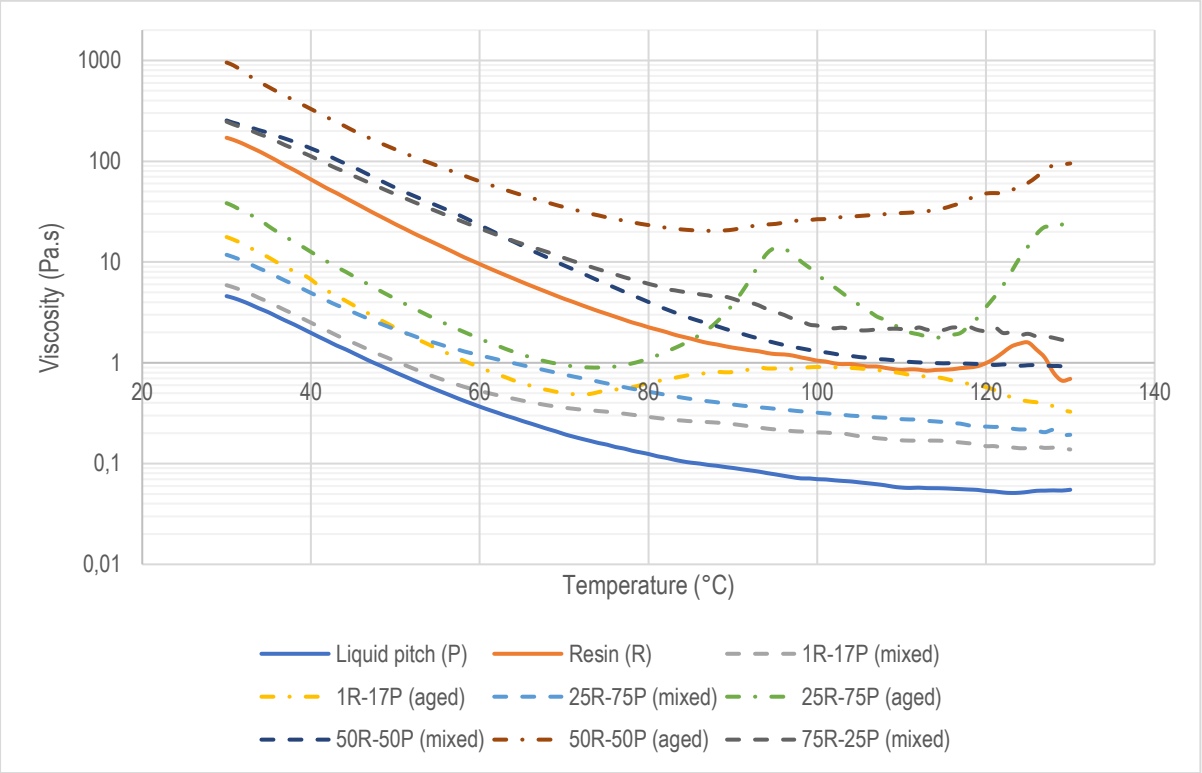

Figure 50: Temperature ramp vs. dynamic viscosity to identify changes in viscosity with an increase in temperature of resole resin, liquid pitch and combinations thereof (shear rate = 1 sec^{-1})

The viscosity of the virgin liquid pitch decreases with an increase in temperature up to 110°C where it starts to plateau (Figure 50). The viscosity of the virgin resin decreases with an increase in temperature up to 118°C, where it increases sharply between 121 - 126°C. This is known as the region in which the resole resin cures (Wilmer, 2014) (Gotro, 2014). This was accompanied by the formation of a semi-solid mass onto the spindle of the rheometer. The reduction on viscosity of the resole resin after 126°C is due to the breakdown of the solid material of the resin that started forming, i.e. cured material. As the resin content increases in the mixed samples, the viscosity increases. The difference in viscosity between the 25 mass% resole resin – 75 mass% liquid pitch and the 50 mass% resole resin – 50 mass% liquid pitch samples is an order of magnitude 10 times higher for the 50 mass% resole resin – 50 mass% liquid pitch. As the mixed samples are heated, there is not a distinctive increase in viscosity at any temperature between 30 - 130°C as seen with the virgin resole resin sample. This might indicate that the resin structure has been broken down from its original structure as the resin cannot start to curing as is characteristic for thermoset resins (Fan & Weclawski, 2017). This changes over time as the samples are allowed

to age where increases in viscosity peaks at certain temperatures show a possible new curing reaction in the resin structure emerging.

The viscosity behaviour of the aged samples is changed noticeably. The aged samples show an increase in viscosity in the temperature ranges 70 - 130°C. As the resin content is increased, the extent of increase in viscosity becomes more pronounced. The increases in viscosity are likely due to cross-linking starting at lower temperatures. This should be confirmed by DSC analysis as cross-linking is an exothermic reaction (Fan & Weclawski, 2017). The 25 mass% resole resin – 75 mass% liquid pitch aged sample shows multiple increases, one at 75 – 95°C and the other at 115 - 130°C. These might be attributed to multiple curing reactions (Strzelec, et al., 2012). The reduction in viscosity after the first peak (75 - 95°C) is likely due to small amounts of cross-linking occurring that form particulates which behaves like a suspension. Afterwards when the second peak (115 - 130°C) is reached, the bulk of the resin starts to cross-link. When the resin and liquid pitch are mixed and aged, the onset of curing occurs at lower temperatures. This reduction in curing temperature could be because of change in composition of the resin. This might be due to some volatilisation of the solution which creates an environment for the resin to separate out and react easier. As the resin content increases it causes multiple curing reactions to occur of which some move to temperatures higher than 130°C. The 50 mass% resole resin – 50 mass% liquid pitch aged sample steadily increases in viscosity at 85°C which proceeds past 130°C. This sample might reach maximum viscosity where curing occurs at temperatures higher than 130°C.

The viscosity test shows that the resin structure is broken down on mixing with the liquid pitch. As these mixtures are aged, early onset of cross-linking that drives the curing of the resin in the mixtures is moved to lower temperatures and that multiple curing reactions can occur as the resin content in the mixtures is increased. The viscosity of the mixtures increases significantly as they are aged which influences the workability of the taphole clay.

4.5.3. Thermogravimetric analysis (TGA)

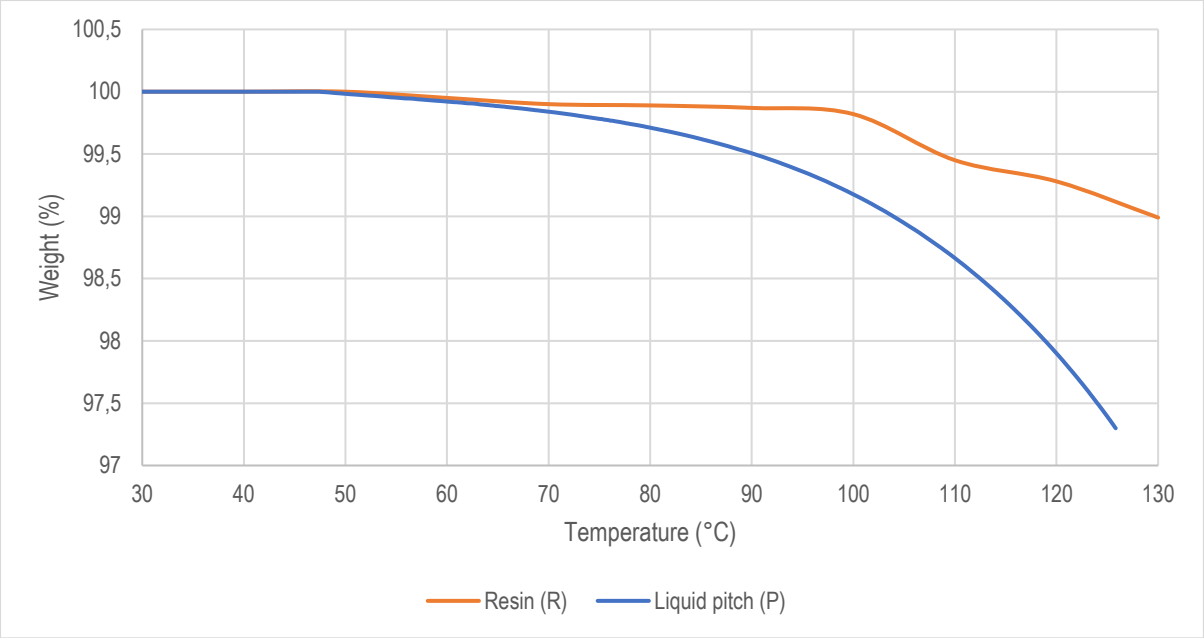

Figure 51: TGA analysis of virgin resole resin and liquid pitch binder (nitrogen atmosphere)

The observed rheology was supplemented with TGA, DSC and FTIR analyses. TGA was used to evaluate the mass loss of the virgin resin and liquid pitch samples between 30 - 130°C. The TGA curves (Figure 51) show that the mass of the resin and pitch remained constant up to ~50°C. The mass loss of the pitch increases exponentially with the temperature above 50°C, while the mass of the resin remains virtually constant up to 100°C. At temperatures between 100 - 110°C, there is a small reduction in mass and again at temperatures above 120°C, which is possibly due to the onset of gelation of the resin. The reduction in mass due to volatilisation above 100°C will influence the viscosity of the Clay A liquid mixture slightly causing it to increase. The DSC analysis (in the next section) was therefore used to identify possible exothermic and endothermic reactions between the resin and liquid pitch at temperatures below 130°C.

4.5.4. Differential scanning calorimetry (DSC)

The DSC analysis of the virgin resin, virgin liquid pitch, resin-pitch mixtures as well as aged mixtures is shown in Figure 52. These analyses were conducted from 20 to 130°C in air, to simulate the reactions that occur during manufacturing.

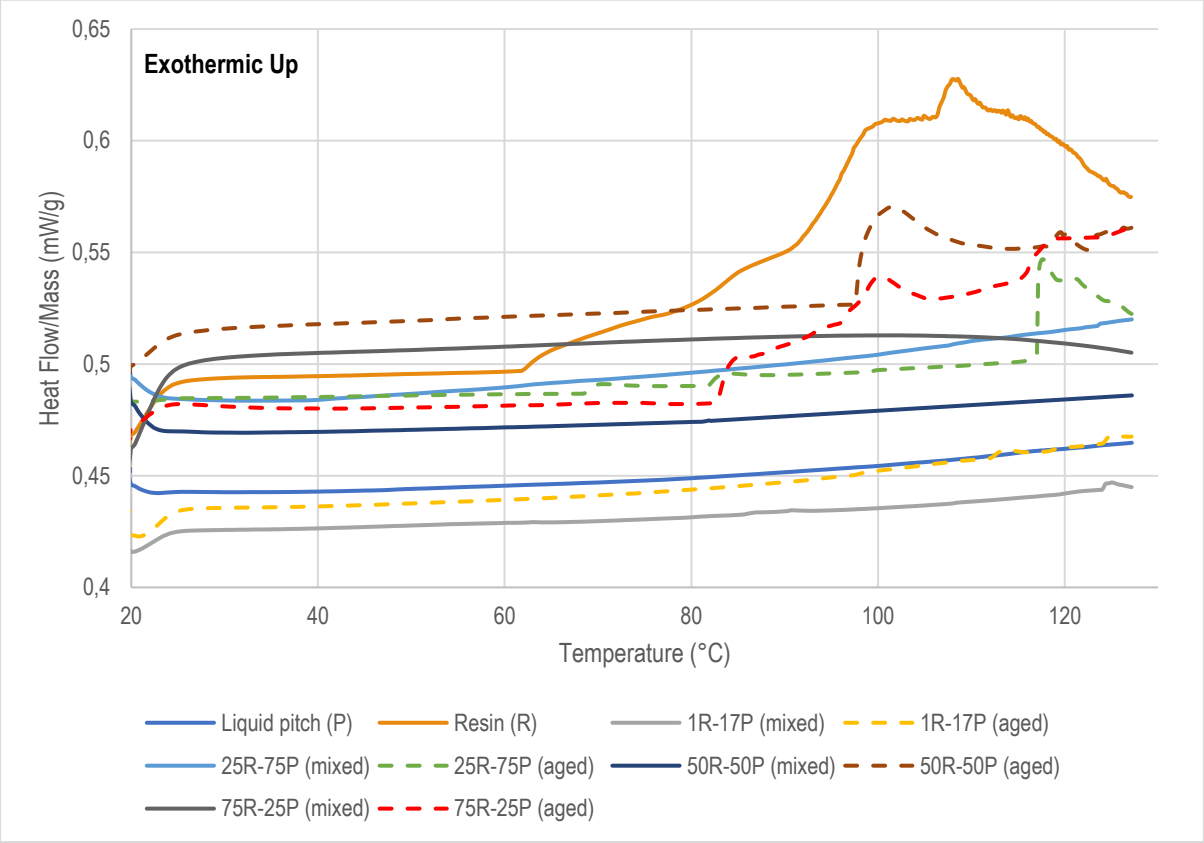

Figure 52: DSC results (during heating) for liquid pitch, virgin resin and resin-pitch combinations (mixed and aged in air)

The results from the DSC curves in Figure 52 show distinctive differences between the mixed samples themselves and between the mixed versus aged samples. The gradual increase in the energy for the virgin liquid pitch is indicative of the slow mass loss from the TGA which is due to volatilisation as the sample is heated. A broad exothermic peak could be distinguished in the DSC trace of the virgin resin, starting at ~62°C, reaching a maximum at ~106°C. This however is not a single exothermic reaction but rather looks like a convolution of several exothermic reactions. The 1 mass% resole resin - 17 mass% liquid pitch mixed and aged samples show small exothermic peaks, starting at ~124°C, with maxima at ~126°C. The aged sample has a second small exothermic peak with a maximum at ~114°C, which is not seen in the mixed sample. Exothermic peaks are observed at different temperatures as the mass% resin is increased, and the samples aged.

The peak at ~106°C for the virgin resole resin, corresponds to a mass loss at ~100°C on the TGA results (Figure 51). The curing reaction proceeds between 65 - 120°C where the only distinctive peak that is observed is shown as an exotherm (Haddadi, et al., 2017). The DSC curves of virgin liquid pitch and the mixed combinations between the resole resin and liquid pitch do not show any peaks as the samples are heated. This correlates to the viscosity results between the mixed samples themselves where there are no sudden changes in viscosity as the samples are heated. Both the DSC and viscosity results do not show any curing reactions taking place as the ratios between

resole resin and liquid pitch are changed between the mixed samples. At the highest mass% resin of all the mixtures, i.e. 75 mass% resole resin – 25 mass% liquid pitch, there is still no curing reaction observed. This is an indication that the structure of the resin has been altered after mixing of the resole resin and liquid pitch.

The aged mixtures show some distinctive exothermic peaks at various temperatures. These might correspond to a single curing reaction such as for the 50 mass% resole resin - 50 mass% liquid pitch aged sample or multiple curing reactions as seen for the 75 mass% resole resin - 25 mass% liquid pitch aged sample (Strzelec, et al., 2012). The trend that is noticed is that as the percentage of resole resin in the mixtures increases, the exothermic peaks move to lower temperatures. There might be more than one exothermic reaction in the 50 mass% resole resin - 50 mass% liquid pitch and 75 mass% resole resin - 25 mass% liquid pitch aged samples, but only at higher temperatures than 130°C (Strzelec, et al., 2012). By comparing the results from the DSC and viscosity analysis of the aged samples, curing of the resin-pitch mixtures is observed at lower temperatures than the virgin resole resin. The curing temperature lowers as the resole resin mass% is increased in the aged mixtures. This might be due to cross-linking interaction between the resole resin and liquid pitch which alters the resole resin structure when mixed and during ageing, the resole resin starts to cross-link prematurely. This was examined in detail in the next section by utilising FTIR.

4.5.5. Fourier-Transform Infrared Spectroscopy (FTIR) – ageing and curing tests

The second set of FTIR tests were conducted to identify functional group changes when the resin and pitch were mixed in the ratios mentioned in Figure 29. This highlighted certain structural changes in the mixtures, which were used together with the DSC and rheology results, to explain what happens in Clay A during ageing.

Since the resole resin is a temperature curing resin, its functional groups will change when gelation starts until it is completely cured. For the curing test, the resin was cured at 130°C for 2 hours until it formed a complete solid (Figure 53). The curing test was repeated for the liquid polymer (Figure 54) as well as the combinations of the resin and liquid pitch (Figures 55 to 58). FTIR curves of the mixed samples aged at 45°C for 2 weeks are also shown in Figures 55 to 58. The FTIR spectrum of the virgin liquid pitch sample is identical to that of the cured sample (Figure 54). It can therefore be concluded that no distinctive structural changes take place in this liquid pitch during curing at 130°C for 2 hours.

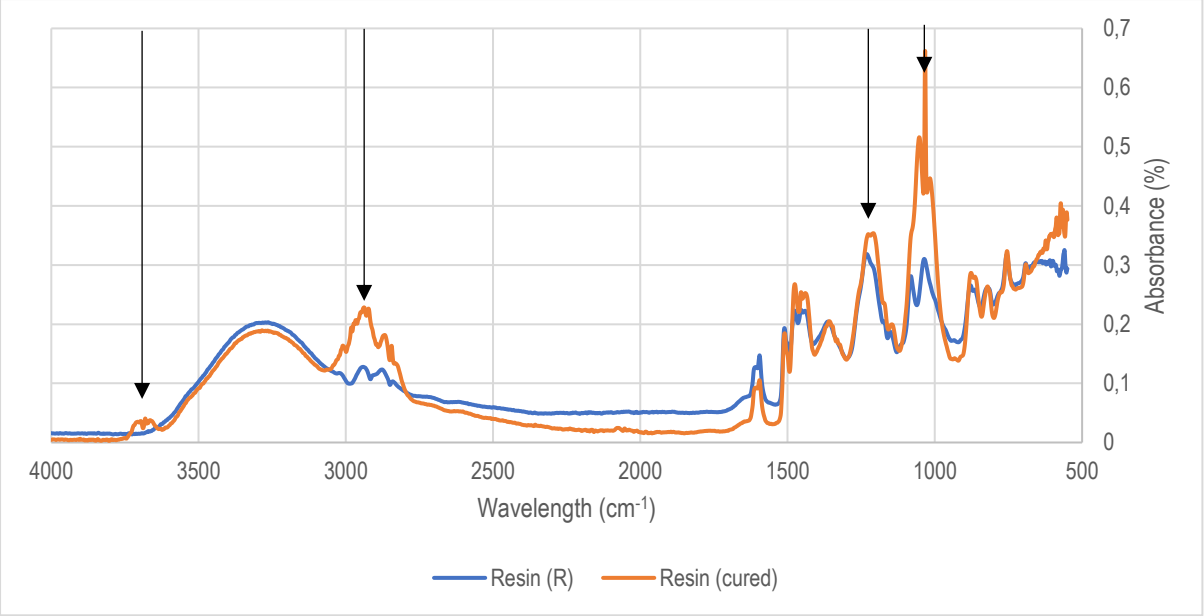

Figure 53: FTIR curve of virgin resole resin and the liquid pitch cured at 130°C

The resin curing test does show some changes in the functional groups (Figure 53). The SP3 C-H stretch at ~2920 cm^{-1} increases and the presence of some free O-H bonds at ~3680 cm^{-1} is shown. The C-O-C stretch at ~1020 cm^{-1} increases significantly which can be attributed to increased cross-linking density during the curing process (Zhou, et al., 2010).

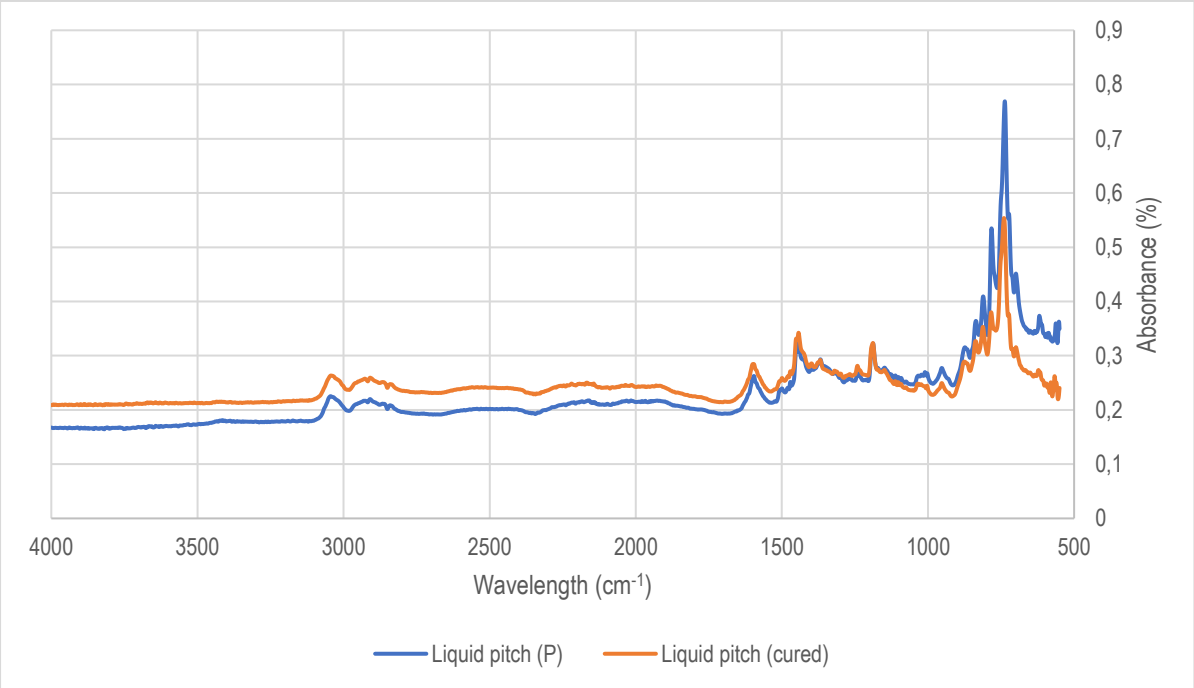

Figure 54: FTIR curve of virgin liquid pitch and the resin cured at 130°C

No changes could be observed in the FTIR spectra of the 1 mass% resole resin – 17 mass% liquid pitch mixed samples after ageing and curing (Figure 55). The structure does not seem to change since peak shifts and changes in peak heights could not be observed. The low quantity of the resin in this sample could be a reason that any

changes to its functional groups could not be detected. As the resin content increases, some distinctive changes are noticed in the FTIR spectra. The presence of O-H bonds at ~3680 cm^{-1} becomes more pronounced as the mass% of resin in the cured sample is increased (Figures 55 to 58), except for the 75 mass% resole resin – 25 mass% liquid pitch. The O-H bonds in this sample are not detected which translates to this functional group not being present in the sample. The SP3 C-H stretches at ~2920 cm^{-1} become more pronounced as well as the C-O-C stretch peaks at ~1020 cm^{-1}. The peak at ~1220 cm^{-1} increases for the aged samples as compared to the mixed samples with an increase in mass% resin. Functional group changes at ~1610 cm^{-1} and ~1220 cm^{-1} could be observed in the FTIR spectra of the 75 mass% resole resin – 25 mass% liquid pitch cured sample (Figure 58). This signifies that the functional groups have changed between being either mixed or aged and cured.

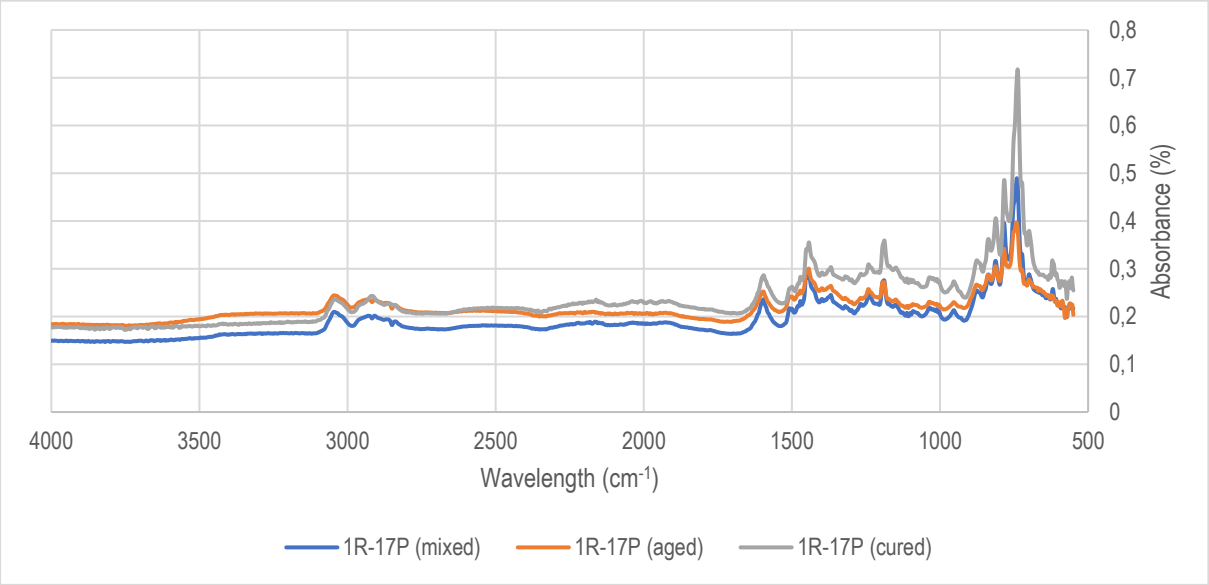

Figure 55: FTIR curves of 1 mass% resin-17 mass% pitch samples: mixed and aged at 45°C; cured at 130°C

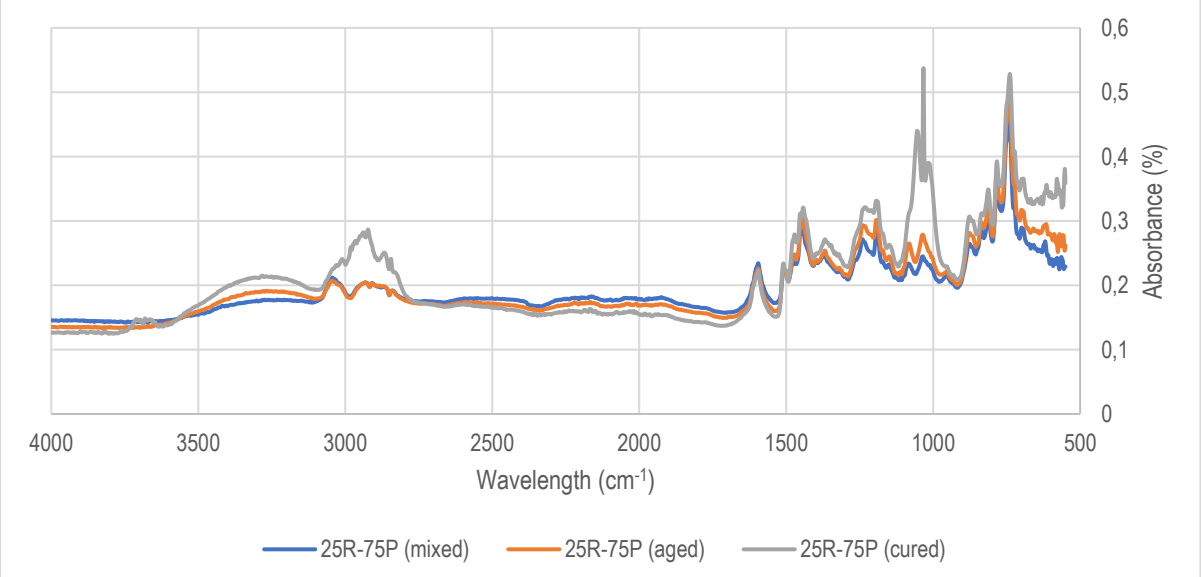

Figure 56: FTIR curves of 25 mass% resin-75 mass% pitch samples: mixed and aged at 45°C; cured at 130°C

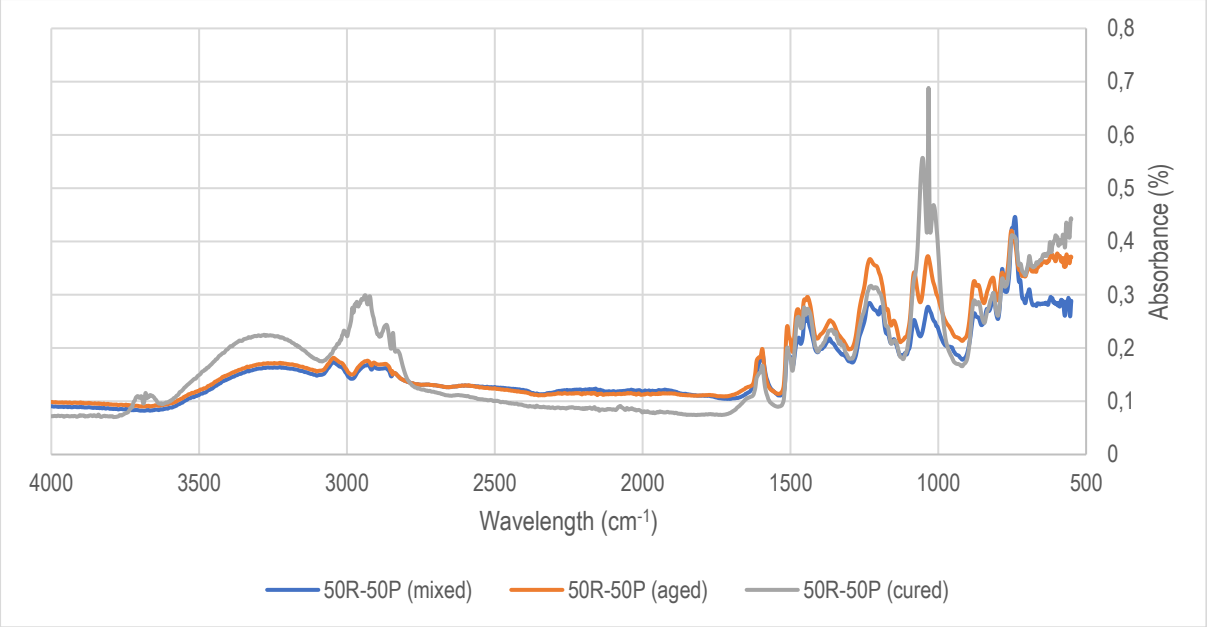

Figure 57: FTIR curves of 50 mass% resin-50 mass% pitch samples: mixed and aged at 45°C; cured at 130°C

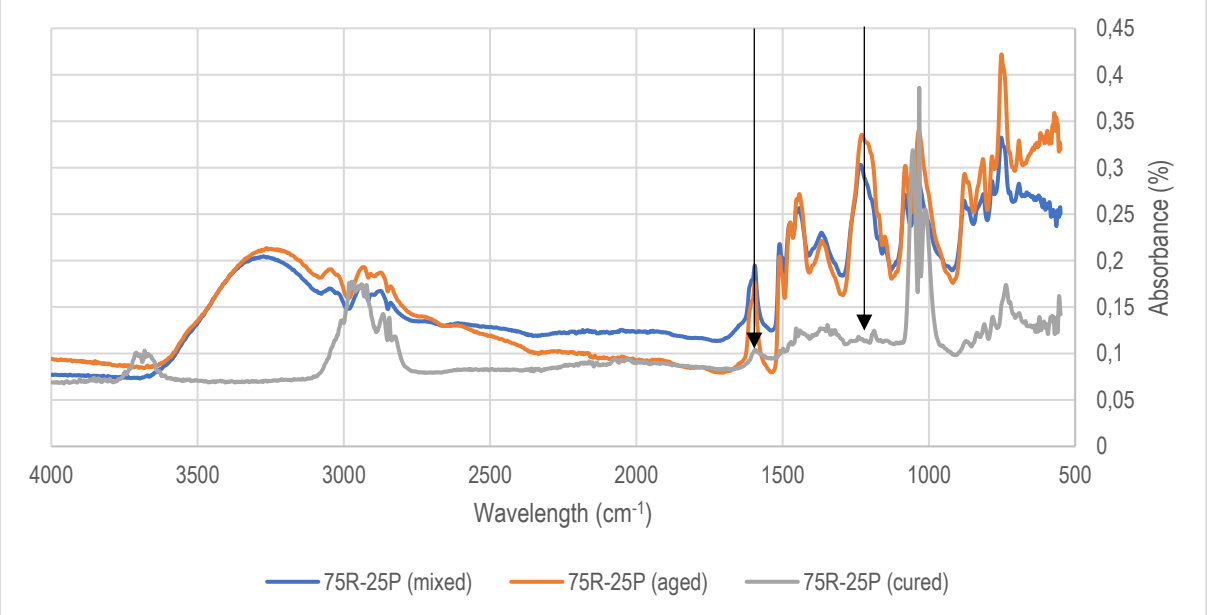

Figure 58: FTIR curves of 75 mass% resin-75 mass% pitch samples: mixed and aged at 45°C; cured at 130°C

4.5.5.1. Summary of FTIR results

The increase in peak intensity of the C-O-C stretch functional groups at ~1020 cm^{-1} of the 25R-75P, 50R-50P and 75R-25P aged samples compared to the mixed samples, is significant. As the mass% resin increases, these C-O-C stretch functional groups associated with the aged samples, also become more prominent. These increases in C-O-C functional groups between the mixed and aged samples is due to a cross-linking reaction between the resole resin and liquid pitch (Anis, et al., 2011) (Dole, 1979). There are no changes in the peak position but rather

the intensity of the C-O-C peaks. The FTIR results of the aged and cured samples show that as the mixtures were aged, the resin started to cross-link which increased the peak intensity of the C-O-C stretch functional group. These functional group increases are mostly due to acetal ring formation which results because of cross-linking reactions between the resole resin and the liquid pitch (Anis, et al., 2011). This is one of the three ways in which curing can be accelerated in thermosetting resins, i.e. temperature increase, pH changes in the solution and cross-linking (Banerjee, et al., n.d.). FTIR analysis confirmed that mixing of the resole resin and liquid pitch caused the resin to prematurely cross-link. This caused the onset of gelation and final curing to occur at lower temperatures than what is observed for the virgin resole resin. This premature cross-linking causes an increase in the viscosity of the mixtures which lowers the workability significantly and increases the ageing.

Chapter V – Summary of results

This report investigates the causes of reduced workability and increased ageing of a blast furnace taphole clay containing resole resin and liquid pitch as a binder. Techniques that were utilized during the investigation are workability tests, Marshall extrusion pressure tests to evaluate workability ageing and particle size distribution (PSD) to assess clay flow characteristics. Wettability tests were conducted to identify the polarity of the aggregate and matrix raw materials for compatibility with the binders. X-ray fluorescence (XRF), X-ray diffraction (XRD), scanning electron microscopy energy dispersive spectroscopy (SEM-EDS) were used to characterize the raw materials and presence of impurities that could interact with the resole resin. The Fourier-transform infrared spectroscopy (FTIR), viscosity testing at various shear rates and temperatures, thermogravimetric analysis (TGA) and differential scanning calorimetry (DSC) where used to characterize the individual binders as well as binder combinations.

The results from the workability tests conducted on Clay A (containing resole resin and liquid pitch) and Clay B (containing liquid pitch only) revealed that when the resole resin and liquid pitch are used together as binders in the taphole clay, the workability ageing of the clay increases significantly. After day 8 of ageing, the workability of Clay A had decreased to the minimum operation specification of 30% whereas the workability of Clay B was above the minimum operating specification at 33.5% workability. The workability of Clay B reduced to 33% after 14 days after which the workability reached a plateau. The workability of Clay A continuously reduced up to day 21 where workability of the clay was at 26% which is lower than the allowable operating workability for this taphole clay. The Marshall extrusion pressure ageing test revealed a similar trend where the MEP of Clay B increased with ~300 MPa during the first 7 days of ageing after which it reached a plateau. The MEP of Clay A increased with ~400MPa during the first 7 days of ageing after which it increased continuously to ~1000MPa after 21 days of ageing. The difference in MEP results between Clay A and Clay B at 21 days is ~580MPa. The effect of a change in binder viscosity on the workability and ageing of Clay A revealed that as the viscosity of the binder increased, the workability of Clay A, after ageing, also reduced and the ageing increased. After 5 days of ageing, the difference in workability between binder viscosities of 12000mPa.s and 1000mPa.s was 3.5% while after 21 days the difference in workability was 6%.

The PSD test revealed that Clay A is a sinteractive clay with a PSD split of 50% +45µm-1mm and 50% -45µm, with 90% -1mm. The +45µm-1mm andalusite and bauxite used in Clay A was according to a crushing and screening standard and was confirmed to both be >85% +45µm-1mm. The grading of the andalusite and calcined clay ball mill fines (BMF) was milled to a standard and was both confirmed to be 60-70% -45µm. The kaolinite clay filler was >80% -45µm which is slightly coarser than the andalusite and calcined clay BMF. The wettability test of all the aggregates and matrix raw materials revealed that the raw materials are polar and thus wettable by both the resole resin and liquid pitch used as the binder in Clay A (Li, et al., 2000).

The mineralogical analysis confirmed that the aggregate portion of the taphole clay consisted mainly of andalusite (62 mass% Al_2O_3), which contained trace amounts of iron-and magnesia-bearing leucite as well quartz. The

andalusite was not calcined. The clay aggregate was comprised of bauxite (89 mass% Al_2O_3) which consisted of mainly corundum and mullite, with trace amounts of kalsilite and rutile. The presence of corundum and mullite in the bauxite indicates that this raw material was calcined. The calcined clay (30 mass% Al_2O_3) consisted primarily of mullite and corundum, with trace amounts of muscovite and rutile. Pure alumina (99 mass%), fired kaolinite clay (64 mass% SiO_2), silicon carbide and coal constituted the matrix (filler) of the taphole clay. The kaolinite clay contained some muscovite and quartz. The silicon carbide (92 mass% moissanite) contained some trace amounts of corundum and quartz. The coal (70 mass% C) contained 13 mass% of volatile matter, 3 mass% moisture and 13 mass% ash content. The coal had a low sulphur content (0.2 mass%).

The functional group characterization of the binders, i.e. resole resin and liquid pitch, used in Clay A revealed that the resin had a phenol-formaldehyde structure. This was confirmed by the presence of a broad distinctive O-H bond peak (3250 cm^{-1}) as the carrier, SP2 C-H stretch peaks overlapping at 3050 cm^{-1}, a distinctive cyclic aromatic structure peak (1610 cm^{-1}) with some C-O bonds present between 1000-1200 cm^{-1}, and substantiated by looking at phenolic resole resins structures similar to the one used in Clay A. The liquid pitch used in Clay A had a complex structure with some SP C-H bonds which could be identified. The difficulty with identifying distinctive functional groups in this binder was due to various compound functional groups that overlap in the FTIR spectrum.

The viscosities of the binders were studied by examining the effect of shear rate and temperature on their dynamic viscosities. The shear rate tests showed that both the resin and liquid pitch exhibited Newtonian behaviour. The mixtures between the resole resin and liquid pitch exhibited shear thinning non-Newtonian behaviour. The extent of shear thinning increased with an increase in resin content. The shear thinning became more prominent between the mixed and aged samples. The viscosity of the aged samples increased significantly compared to the mixed samples of the same resin-liquid pitch ratios. Some of the aged mixtures (75 mass% resin-25 mass% liquid pitch) could not be evaluated due to their extreme viscous behaviour. The viscosity of the virgin liquid pitch decreased with an increase in temperature up to 110°C where it reached a plateau. The viscosity of the virgin resole resin decreased with an increase in temperature up to 118°C. Between 121-126°C, the resin cured completely which was noticed by a sudden increase in viscosity. The resin-liquid pitch mixtures did not show any distinctive increase in their viscosities, similar to that of the virgin resin, to signify curing of the mixtures. The viscosities of the mixtures decreased with temperature to a certain point and then plateaued. The behaviour of the mixed samples after ageing differ from the initial mixtures before ageing. The aged mixtures showed an increase in viscosity between 70-130°C with some mixtures exhibiting multiple increases as temperature increased (25 mass% resin-75 mass% liquid pitch peak 1 at 75-90°C and peak 2 at 115-130°C). The higher the resin content in the aged mixtures, the larger the increase in viscosity between 70-130°C.

The TGA results of the liquid pitch highlighted an exponential volatile release from 50°C up to 125°C whereas the results from the resole resin showed a reduction in mass at 50°C, a steady decline between 5-100°C with a sudden reduction in mass between 100-110°C and thereafter a steady decline in mass up to 130°C. The maximum temperature chosen for the DSC test was 130°C. The DSC results show a broad exothermic peak between 65-

106°C for the resole resin, with curing reaction(s) taking place between 65-120°C, which correspond to the temperature during which the resole resin experiences a sudden increase in viscosity. The exothermic maximum at 106°C corresponds to the mass loss experienced by the virgin resole resin starting at 100°C. The DSC curve for the liquid pitch did not show any exothermic or endothermic reactions between 30-130°C. The resin-liquid pitch mixtures also do not show any exothermic curing reactions or endothermic reactions which correlate to the viscosity trends of these samples. The aged mixtures do show distinctive exothermic peaks at various temperatures. The exothermic peaks might correspond to single curing reactions (50 mass% resin-50 mass% liquid pitch) or multiple curing reactions (75 mass% resin-25 mass% liquid pitch). The trend that was noticed was as the resin content increased, the exothermic peaks moved to lower temperatures, i.e. earlier onset of curing.

The curing test (130°C for 2 hours) results of the liquid pitch revealed that no functional group changes were observed. The resin exhibited some functional group changes where intensities of SP3 C-H stretch at 2920 cm^{-1} increased, presence of free O-H bonds at 3680 cm^{-1} and increased C-O-C peak intensities at 1020 cm^{-1}. These changes were compared to the mixed, aged and cured resin-pitch mixture results. The curing results of the resin-liquid pitch mixtures, except for 1 mass% resin-17 mass% liquid pitch, showed the presence of free O-H bonds (3580 cm^{-1}), increase in peak intensity of the SP3 C-H stretch bonds at 2920 cm^{-1} as well as an increase in peak intensities for C-O-C bonds at 1020 cm^{-1}. The effect was not noticed in the 1 mass% resin-17 mass% liquid pitch due to the low resin content in the sample. These peak intensity increases became more pronounced as the resin content of the mixtures were increased except for 75 mass% resin-25 mass% liquid pitch, where peaks at 1610 cm^{-1} and 1220 cm^{-1} were not present. The FTIR results of the mixed and aged samples highlighted that only the C-O-C bond peaks intensities at 1000-1200 cm^{-1} increased of which the effect became more pronounced as the resin content increased.

The workability reduction, the increased ageing and the increase in MEP of Clay A are not attributed to any of the aggregate or matrix raw materials. A correlation between the workability and MEP was observed in both Clay A and Clay B, where a lowering in workability resulted in an increased MEP. Both the workability and MEP of Clay B reached a plateau after ageing whereas with Clay A the workability continued to reduce, and the MEP continued to increase with time. The raw materials did not contain any impurity elements such as sulphur or free lime that could contribute to polymerization or cross-linking of the resin in the binder mixture as stated by (Young & Lovell, 1991). The particle size distribution of Clay A was continuous with no size range gaps or excess of fine material that could influence flow properties and workability of the taphole clay. All raw materials were crushed and screened according to and comply with standards associated with the specific raw materials. The polar nature of the aggregate and matrix (filler) raw materials is compatible with both resin and liquid pitch. The possibility of separation of the binder from the aggregate and matrix inside the clay due to a repelling action is highly unlikely.

The difference between workability ageing of Clay A compared to Clay B was due to the presence of the resole resin together with the liquid pitch. An increase in binder viscosity, during ageing, resulted in reduced workability and increased ageing of Clay A. The reduction in workability also resulted in an increase in MEP which was

problematic due to its continuous increase. This conforms to the work done by Wells (2002), highlighting the effect of binder changes to continuous MEP values with ageing. The increased binder viscosity between mixing and ageing was because of a reaction between the resole resin and liquid pitch confirmed by both viscosity testing, i.e. shear rate and temperature effect, DSC and FTIR. The reaction between the resole resin and liquid pitch resulted in the breakdown of the resole resin structure to smaller aggregate polymer chains, shown by shear thinning behaviour after mixing. The binder mixture, after ageing, had formed a new cross-linked structure which resulted in curing reaction(s) in the resin-liquid pitch mixtures to occur at lower temperatures. The types of functional groups in the resin-pitch mixtures and aged mixtures did not change, only certain peak intensities changed which signify an increase in the concentration of that specific functional group. The functional group changes observed during the curing tests in this investigation are similar to what was reported by Zhou et al. (2010). The C-O-C bond peak intensities increased between the mixed and aged samples noticeably, which was a result of cross-linking similar to what was noticed by (Anis, et al., 2011). The lowering in curing temperature due to cross-linking resulted in an early onset of curing by an increase in viscosity at temperatures as low as 60°C. The temperature effect observed in the viscosity test as well as DSC results of aged mixtures confirms the cross-linking with curing exotherms moving to lower temperatures. The effect of an increase in viscosity due to cross-linking became more prominent as the resin content was increased.

Chapter VI - Conclusions

This investigation examined the contributing factors and reasons for reduced workability and increased ageing of blast furnace taphole clay. The following conclusions were drawn from the investigation:

- The workability of the investigated taphole clay decreased with time when resole resin and liquid pitch were used as binders, as compared to only using liquid pitch.
- The workability of the investigated taphole clay decreased with an increase in binder viscosity.
- The MEP of the investigated taphole clay increased with time when the resole resin and liquid pitch was used as binders as compared to only using liquid pitch.
- The particle size distribution of the investigated clay was continuous with all aggregate and matrix raw materials crushed and screened according to specification. The taphole clay is highly sinterable due to the >90% -1mm. The matrix raw materials were not excessively fine that could cause a reduction in workability with time. The reduction in workability was not due to the particle size distribution of the aggregates and the clay.
- The surface chemistry of the aggregate and matrix raw materials is polar and compatible with that of the resole resin and liquid pitch that were used as binders. The reduction in workability was not due to separation inside the clay due to repelling actions between the binder, aggregates and matrix.
- There were no impurities, such as sulphur or free lime, present in any of the aggregate or matrix raw materials that could have contributed to polymerisation or cross-linking of the resin in the binder.
- The structure of the resole resin used in the binder was confirmed to be phenol-formaldehyde and the liquid pitch a complex structure of which only certain functional groups were identified. The curing temperature range for this resin is 121-126°C.
- The shear thinning behaviour of the resin-liquid pitch binder mixtures was due to interaction between the resin and liquid pitch when mixed, which resulted in the breakdown of the resin structure. The shear thinning behaviour continued with the ageing of the mixtures.
- The increased viscosity with time (ageing) was due to premature cross-linking of the resin structure. The C-O-C bonds between polymer chains became more prominent with time and as the resin content increased. This resulted in an increase in viscosity of the binder with time. The premature cross-linking of the resin, in the presence of the liquid pitch, resulted in the lowering of curing temperatures of the resin-pitch mixtures. Some mixtures exhibited multiple curing reactions starting at temperatures as low as 60°C.
- The observed reduction in workability of the taphole clay was due to an increase in binder viscosity during ageing of the taphole clay. The increase in binder viscosity was due to a reaction between the resin and liquid pitch that resulted in the resin cross-linking prematurely. The premature cross-linking resulted in curing temperatures of the resin-pitch mixtures to be lowered.

Chapter VII – Recommendations for future work

To broaden the understanding of the topic investigated, some future work can be done to better understand the structural changes which the resin and liquid pitch mixtures undergo. Future work should make use of mass spectroscopy, H-NMR, C-NHM, DEPT, 2D techniques and more detailed DSC and FTIR work to try and better understand the exact changes in the structure between the resin and pitch and fully characterize the structures of the virgin binders and mixtures thereof. The molecular structure of the liquid pitch should be studied in more detail to identify the compounds it is comprised of. Dynamic mechanical analysis (DMA) should be used to study mechanical as well as elastic behavioural changes in the mixtures of the binders, to better describe the rheology. The shear thinning behaviour exhibited by the resin and liquid pitch mixtures needs to be further investigated to understand if the structure breakdown is a two-phase structure, a one phase mixture or a semi emulsion that does not mix properly. There should also be some work done on the solubility of the liquid pitch into the resin and vise verse to aid in understanding the rheological behaviours in this binder mixture.

To improve the ageing resistance of the clay and develop a toxic-free binder, alternative binders, other than liquid pitch, should be identified and evaluated. The use of the resole resin in the clay is to assist with green strength formation when the clay is placed in the tap hole, hence it cannot be removed. Alternatives would be to look at different natural oils or organic substances with low volatile release and similar viscosity behaviour to that of the current liquid pitch but toxin-free. The binder also needs to be compatible with the resin so that cross-linking or polymerization does not occur when mixed.

Chapter VIII - References

Adeyinka, O., Samiei, S., Xu, Z. & Masliyah, J., 2009. *Effect of Particle Size on the Rheology of Athabasca Clay Suspensions,* Canada: Department of Chemical and Materials Engineering, University of Alberta.

Anis, A., Al-Zahrani, S., Banthia, A. & Bandyopadhyay, S., 2011. Fabrication and characterization of novel crosslinked composite membranes for direct methanol fuel cell application. *International journal of electrochemical science,* Volume 6, pp. 2561-2487.

ASTM, 2013. Standard Practice for Proximate Analysis of Coal and Coke. In: *American Society for Testing and Materials Handbook.* s.l.:s.n., pp. 1-2.

ASTM, 2016. Standard Guide for Examination of Hardened Concrete Using Scanning Electron Microscopy. In: *American Society for Testing and Materials Handbook.* s.l.:s.n., pp. 1-9.

ASTM, 2017. Standard Test Method for Metal Powder Specific Surface Area by Physical Adsorption. In: *American Society for Testing and Materials Handbook.* s.l.:s.n., pp. 1-4.

ASTM, 2018. Standard Practice for Pressing and Drying Refractory Plastic and Ramming Mix Specimens. In: *American Society for Testing and Materials Handbook.* s.l.:s.n., pp. 1-4.

ASTM, 2018. Standard Test Method for Workability Index of Fireclay and High-Alumina Refractory Plastics. In: *American Society for Testing and Materials Handbook.* s.l.:s.n., pp. 1-3.

ASTM, 2019. Standard Test Method for Molecular Weight Averages and Molecular Weight Distribution of Polystyrene by High Performance Size-Exclusion Chromatography. In: *American Society for Testing and Materials Handbook.* s.l.:s.n., pp. 1-13.

Australian Standard, 2017. *Method 34: Guide to determining the extrusion pressure and curing time of taphole clays,* Sydney: s.n.

Authier-Martin, M., Forté, G., Ostap, S. & See, J., 2001. The mineralogy of Bauxite for producing Smelter-Grade Alumina. *JOM,* pp. 1-2.

Banerjee, R., Khilar, K. & Ghosh, B., n.d. *Studies on phenol formaldehyde gel formation at high temperatures and at different pH.* [Online]
Available at: http://folk.ntnu.no/skoge/prost/proceedings/aiche-2005/non-topical/Non%20topical/papers/283a.pdf
[Accessed 19 August 2020].

Bartolo, D., 2020. Rings rule three-dimentional active matter. *Science,* 367(6482), pp. 1075-1076.

Baunn, J., Frare, J. & Hircnov, R., 1963. Natural Alpha Silicon Carbide. *The American Mineralogist,* Volume 48, pp. 1-4.

Bennett, H., Oliver, G. & Evans, J., 1992. *XRF Analysis of Ceramics, Minerals and Allied Materials.* Chicester: John Wiley and Sons, Ltd.

Brannbacka, J., Torrkulla, J. & Saxen, H., 2000. A study on liquid flow in the blast furnace hearth. *Future trends in Automation in Mineral and Metal Processing,* pp. 256-258.

British Petroleum, 2019. *List of Countries by Coal Reserve.* [Online]
Available at: https://en.wikipedia.org/wiki/List_of_countries_by_coal_reserves
[Accessed 7 January 2020].

Campbell, A. & Pericleous, K., 2002. Modelling of freeze layers and refractory wear in direct smelting processes. *Iron and Steelmaker,* 29(9), pp. 41-45.

Chatterjee, A., 2001. X-Ray Diffraction. In: *Handbook of Analytical Techniques in Concrete Science and Technology.* s.l.:Andrew William Applied Science Publishers, pp. 275-332.

Ciullo, P., 1996. The industrial minerals. In: *Industrial Minerals and Their Uses - A Handbook and Formulary.* s.l.:William Andrew Publishing/Noyes, p. 42.

Deer, H. Z., 1992. Corundum. In: P. E. Limited, ed. *The rock-forming minerals.* Tottenham: s.n., pp. 536-537.

Dick & John, S., 2009. Tackifying, Curing, and Reinforcing resins. In: *Rubber Technology - Compounding and Testing for Performance.* s.l.:Hanser Publishers, pp. 438-440.

Dole, M., 1979. Corss-Unking and crystallinity in irradiated polyethylene. *Polymer-plastics technology and Engineering,* 13(1), pp. 41-64.

Fan, M. & Weclawski, B., 2017. 6 - Long natural fibre composites. In: *Advanced high strength natural fibre composites in construction.* s.l.:Woodhead Publishing, pp. 141-177.

Fink, J., 2017. Phenol-formaldehyde resins. In: W. Andrew, ed. *Reactive Polymers: Fundamentals and Applications.* s.l.:s.n., pp. 155-165.

FTIR Raman, 2001-2020. *Spectral libraries.* [Online]
Available at: http://www.ftirsearch.com/Features/lib_list.asp
[Accessed 28 January 2020].

Galet, L., Patry, S. & Dodds, P. J., 2010. Determination of the wettability of powders by the Washburn capillary rise method with bed preparation by centrifugal packing technique. *Journal of Colloid and Interface Science, Elsevier,* pp. 470-475.

Geyers, P. & Halifa, Z., 2014. Blast furnace tapping practice at ArcelorMittal South-Africa, Vanderbijlpark Works. *The Southern African Institute of Mining and Metallurgy - Furnace tapping conference*, pp. 4-9.

Glikson, M. & Mastalerz, M., 2000. Minerals in Coal. In: *Organic Matter and Mineralisation.* s.l.:Kluwer academic publishers, pp. 314-326.

Goodman, S. & Ibeh, C., 1998. Phenol-formaldehyde resin. In: *Handbook of Thermoset plastics.* s.l.:William Andrew Publishing, pp. 28-30.

Gotro, J., 2014. *Rheology of Thermosets Part 5: Non-isothermal Curing.* [Online]
Available at: https://polymerinnovationblog.com/rheology-thermosets-part-5-non-isothermal-curing/
[Accessed 29 September 2020].

Gotro, J., 2018. *Polymers in Electronic Packaging: Rheological Measurements, Part 4.* [Online]
Available at: https://polymerinnovationblog.com/polymers-in-electronic-packaging-rheological-measurements-part-4/
[Accessed 29 September 2020].

Haddadi, S., Kardar, P. & Abbasi, F., 2017. Effects of nano-silica and boron carbide on the curing kinetics of resole resin. *Journal of Thermal Analysis and Calorimetry,* 128(2), p. 1219.

INSACO, 2006. *Machining Of Silicon Carbide - Process, Applications and Types.* [Online]
Available at: https://www.azom.com/article.aspx?ArticleID=3271
[Accessed 7 January 2020].

Inside Metal Additive Manufacturing, 2018. *Particle characteristics impact on powders.* [Online]
Available at: https://www.insidemetaladditivemanufacturing.com/blog/particles-characteristics-impact-on-granular-media-behaviour-in-powder-bed-fusion-am
[Accessed 13 July 2020].

ISO, 1998. Hard coal and coke — Determination of volatile matter. In: *International Organisation for Standardisation.* s.l.:s.n., pp. 1-7.

Kandola, K. & Horrocks, A., 2001. 5. Composites. In: D. Price, ed. *Fire retardant materials.* America: Woodhead Publishing Limited.

Kennedy, B., 1990. Kaolin, Ball Clay, Halloysite, and Refractory Clay. In: *Surface Mining.* s.l.:Society for Mining, Metallurgy, and Exploration, pp. 140-144.

Klein, C. & Dutrow, B., 2008. Clay Minerals. In: *Mineral Science.* Courtney Neslson ed. s.l.:Jay O'Callaghan, pp. 521-522.

Klein, C. & Dutrow, B., 2008. *Mineral Science.* Courtney Nelson ed. s.l.:Jay O'Callaghan.

Knicker, H., Hatcher, P. & Scaroni, A., 1996. A solid-state 15N NMR spectroscopic investigation of the origin of nitrogen structures in coal. *International journal of coal geology,* 32(1-4), pp. 255-278.

Kogel, et al., 2006. Kyanite, Andalusite, Sillimanite and Mullite. In: *Industrial Minerals and Rocks - Commodities, Markets, and Uses.* s.l.:Society for Mining, Metallurgy and Exploration, pp. 553, 554, 555, 557-558.

Kongoli, F. R. R. G., 2006. Advances in understanding phenomena in the blast furnace hearth. *Sohn International Symposium - Advanced processing of metals and materials*, pp. 139-141.

Laza, J., Vilas, J., Rodriguez, M. & Garay, M., 2001. *Analysis of the Crosslinking Process of a Phenolic Resin by Thermal Scanning Rheometry,* Spain: s.n.

Li, C. et al., 2018. *Effects of viscosity modifying admixture (VMA) on workability and compressive strength of structural EPS concrete,* China: Construction and building materials.

Lin, C., Yeh, T., Reiser, A. & Honda, K., 1993. *Mechanism of dissolution inhibition in phenolic resins.* San Jose, United States of America, Advances in Resist Technology and Processing.

Li, P., Coleman, D., Spaulding, K. & McClennen, W., 2000. *Separation and Characterization of Phenolic Resin by Using HPLC and GPC Combined with UV, RI, MS and Light Scattering Detection,* s.l.: s.n.

Mark, J., Erman, B. & Roland, C., 2013. Chapter 7 - Vulcanisation. In: *The science and technology of rubber.* Gulf of Mexico: Academic Press, pp. 337-381.

Mehl, M. J. et al., 2017. *Library of Crystallographic Prototypes.* [Online]
Available at: http://aflowlib.org/CrystalDatabase/AB_hP8_186_ab_ab.html
[Accessed 7 January 2020].

Merck, 2015. *IR Spectrum Table and Chart - Sigma Aldrich.* [Online]
Available at: https://www.sigmaaldrich.com/technical-documents/articles/biology/ir-spectrum-table.html
[Accessed 28 January 2020].

Miller & Bruce, 2005. Introduction to Coal. In: *Coal energy systems.* s.l.:Elsevier, pp. 1-15.

Moritz, H., 1989. Increase in viscosity and its influence on polymerization processes. *Chemical engineering & technology,* 12(1), pp. 71-87.

Nelson, L., 2014. The tap-hole - key to furnace performance. *Journal of the Southern Africa Institute of Mining and Metallurgy,* Volume 116, p. 482.

Njobuenwu, D., E.O, O. & Gumus, R., 2013. *Determination of Contact Angle from Contact Area of Liquid Droplet Spreading on Solid Substrate.* [Online]
Available at: http://lejpt.academicdirect.org/A10/029_038.htm
[Accessed 23 January 2020].

Ogunniyi, O., Vermaak, M. & Groot, D., 2009. Chemical composition and liberation characterization of printed circuit board comminution fines for beneficiation investigations. *Elsevier,* Volume 29, p. 2142.

PANalytical, 2013. *2a introduction to sample preparation.* [Online]
Available at: http://jiam.utk.edu/facilities/diffraction/Introduction%20to%20Sample%20Preparation.pdf
[Accessed 17 January 2020].

Parnahaj, P., Karickova, A., Misanekova, V. & Chudikova, D., 2012. Ecological taphole clay. *Intercerm Refractories,* 1(1), p. 24.

Pierro, P., Gnos, E., Grobety, B. & Armbruster, T., 2003. Rock-forming moissanite (natural alpha silicon carbide). *American Mineralogist,* Volume 88, pp. 1817-1821.

Pilarska, A., Wysokwski, M., Markiewicz, E. & T, J., 2013. Synthesis of magnesium hydroxide and its calcinates by a precipitation method with the use of magnesium sulfate and poly(ethylene glycols). *Powder Technology - Elsevier,* pp. 148-157.

Poljanšek, I. & Krajnc, M., 2005. Characterising of Phenol-formaldehyde prepolymer resin by in-line FT-IR spectroscopy. *Acta Chim. Slov,* Volume 52, p. 240.

Polymer Properties Database, 2020. *Properties of phenoplasts.* [Online]
Available at: https://polymerdatabase.com/polymer%20classes/Phenolic%20type.html
[Accessed 13 August 2020].

Renaud, A. et al., 2019. Sealing porous layers on AA2024-T3 with a low viscosity Benzoxazine resin for corrosion protection in aeronautical applications. *RSC Advances,* Issue 29, pp. 1-4.

Routschka, Wuthnow, G. & Hartmut, 2012. Unshaped Refractory Materials (Monolithics). In: *Handbook of Refractory Materials - Design – Properties – Testing.* s.l.:Vulkan Verlag, p. 142.

R, V. L., E, V. S. C. & M, G., 2003. Blast furnace hearth management for safe and long campaigns. *ISSTech 2003 Conference Proceeding,* pp. 1079-1090.

Saeki, Y. & Tanaka, K., 1980. *Method for accelerating cure of resole type phenolic resins.* Japan, Patent No. 53-58430.

SANS, 2013. Precast concrete kerbs, edgings and channels. In: *South-African National Standards.* s.l.:s.n.

Satyendra, 2015. *IspatGuru.* [Online]
Available at: https://www.ispatguru.com/blast-furnace-tap-hole-mass/
[Accessed 17 September 2020].

Siva Kumar, R., Raffi, M. & Srinivasa, R., 2017. Experimental study on environmental friendly taphole clay for blast furnace. *ICRAMMCE,* pp. 1-4.

Strzelec, K. et al., 2012. Synthesis and characterization of novel polythiourethane hardeners for epoxy resin. *Comptes Rendus Chimie,* 11(1), p. 1070.

Sutrisna, P. & Kabe, Y., 2004. 3- Pyrolysis. In: A. Basile & G. Centi, eds. *Studies in Surface Science and Catalysis.* s.l.:Elsevier, pp. 127-180.

Tec-Science, 2018/12/06. *Blast Furnace Process - Tec-Science.* [Online]
Available at: https://www.tec-science.com/material-science/steel-making/blast-furnace-process/
[Accessed 1 January 2020].

Tupkary, R. H. T. V. R., 2018. Construction of a blast furnace and it's accessories. In: *Modern Iron Making Handbook.* s.l.:Mercury learning and information, p. 248.

Washington, S., 1907. Formation of leucite in igneous rocks. *the journal of Geology,* 15(3), pp. 257-279.

Wells, L., 2002. *The rheology of a composite polymer ceramic plastic refractory,* Sydney: University of Wollogong.

Wilmer, R., 2014. *Thermoset materials MFG ppt video.* [Online]
Available at: https://slideplayer.com/slide/1554873/
[Accessed 29 September 2020].

Xuefei, L. et al., 2011. Mineralogical characteristics of the superlarge Quaternary bauxite deposits in Jingxi and Debao counties, western Guangxi, China. *Elsevier,* pp. 1-4.

Yang, Y., Raipala, K. & Holappa, L., 2014. Ironmaking. In: R. I. o. T. -. Stockholm, ed. *Treatise on Process Metallurgy. Volume 3.* Netherlands: Elsevier, pp. 2-12.

Yao, P. et al., 2018. A study on the preparation of pitch-based high strength columnar activated carbon and mechanism of phenol adsorption from aqueous solution. *Royal Society of Chemistry,* Volume 8, p. 17564.

Young, R. & Lovell, P., 1991. Synthesis. In: *Introduction to Polymers.* HongKong: Chapman & Hall, pp. 15-22.

Zhou, D., Du, S., Yu, L. & Liu, Z., 2010. *Nonisothermal curing of a solid resole phenolic resin,* China: Biochemistry and Chemical engineering department, Jiaxing College.

A. Appendix A

Table A. 1: Standards for each test method used for evaluation or testing

Test method	Standards used for testing
Workability	Sample preparation: ASTM C1054-18 (ASTM, 2018) Testing: ASTM C181-11 (2018) (ASTM, 2018)
Scanning electron microscopy	ASTM E1508-12a (2019) (ASTM, 2019)
Coal	Ash: ASTM D3172 – 13 (ASTM, 2013) Volatile Matter: SANS 927:2013 (SANS, 2013), ISO 562:1998 (ISO, 1998) Moisture: ASTM D3172-13 (ASTM, 2013) Fixed carbon: ASTM D5373-16 (ASTM, 2016) Sulphur content: ASTM D4239-18e1 (ASTM, 2018)

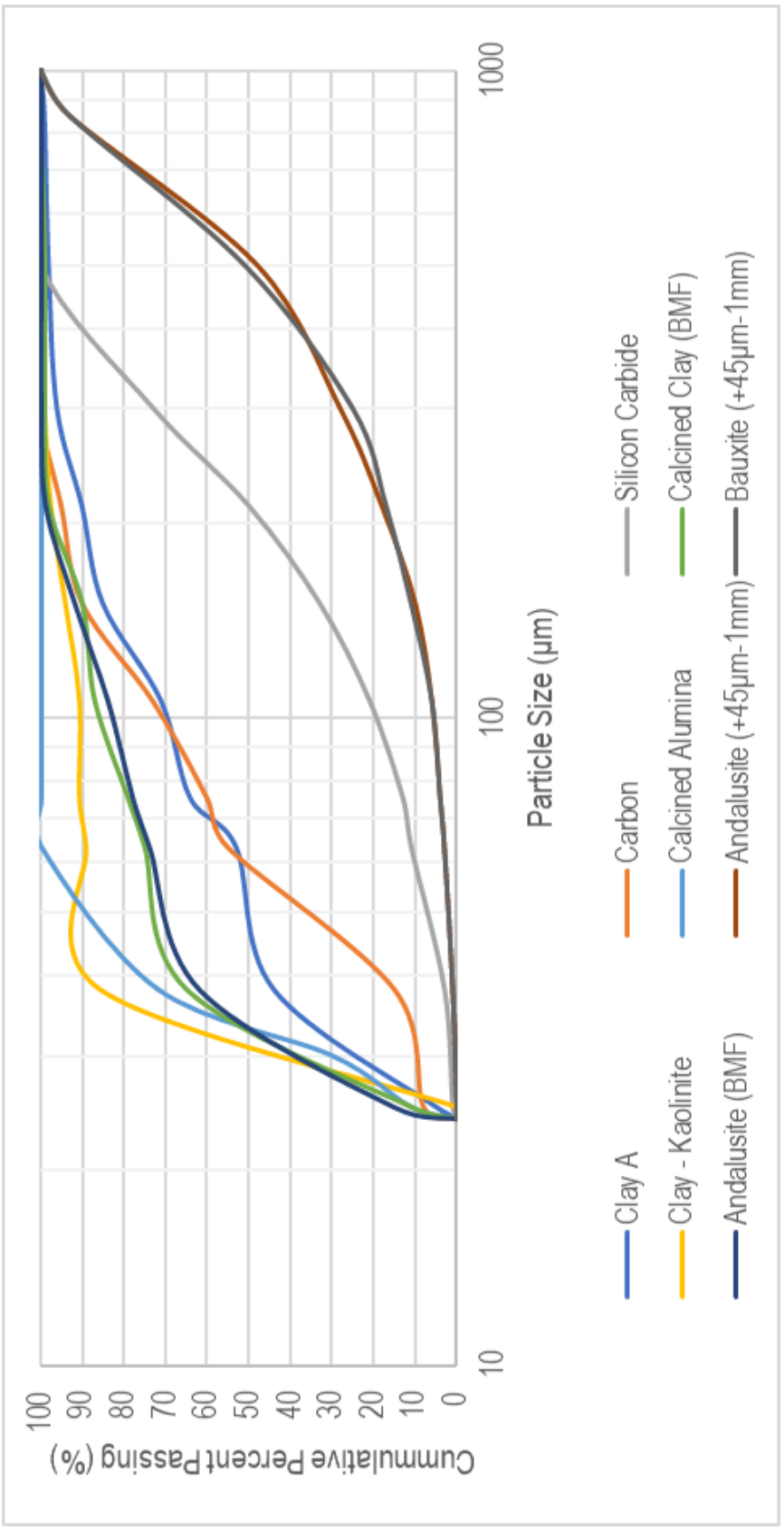

Figure A. 1: Particle size distribution graph of aggregate and powder raw materials used for Clay A and Clay B

Table A. 2: XRD analysis oxide phase formulas

Oxide phase	Oxide formula
Andalusite	$Al_2(SiO_4)$
β-alumina	$Al_{21.86}K_{2.59}O_{34}$
Calcite	$CaCO_3$
Corundum	Al_2O_3
Ferdisilicite	$FeSi_2$
Graphite	C
Hematite	Fe_2O_3
Kalsilite	$AlKSiO_4$
Kaolinite	$Al_2Si_2O_5(OH)_4$
Leucite	$KAlSi_2O_6$
Moissanite 6H	SiC
Moissanite 4H	SiC
Mullite	$Al_6Si_2O_{13}$
Muscovite	$(KF)_2(Al_2O_3)_3(SiO_2)_6$
Quartz	SiO_2
Rutile	TiO_2
Talc	$Mg_3Si_4O_{10}(OH)_2$
Organic Carbon	C(s)

Table A. 3: Wettability calculations for oxide and carbide raw materials used in Clay A and Clay B

	Calcined Alumina	Andalusite	Bauxite	Carbon	Clay - Kaolin	Calcined Clay	SiC
Cos(T)	1	1	1	1	1	1	1
Cw	1,25718E-07	1,62809E-07	6,26854E-08	4,70991E-07	4,63958E-07	1,15815E-07	6,54075E-07
Liq K	45636	45636	45636	45636	45636	45636	45636
Slope Hep	0,005737277	0,00742996	0,00286071	0,021494145	0,021173169	0,005285336	0,029849369
Slope Water	0,005527466	0,006747605	0,001198753	0,017513642	0,005493515	0,005195153	0,01208958
Con Ang	0,963430114	0,90816161	0,419040476	0,8148099	0,259456428	0,982937269	0,405019638
Theta	15,54	24,76	65,22	35,43	74,98	11,47	66,1
	Wettable	Wettable	Wettable	Wettable	Wettable	Wettable	Wettable

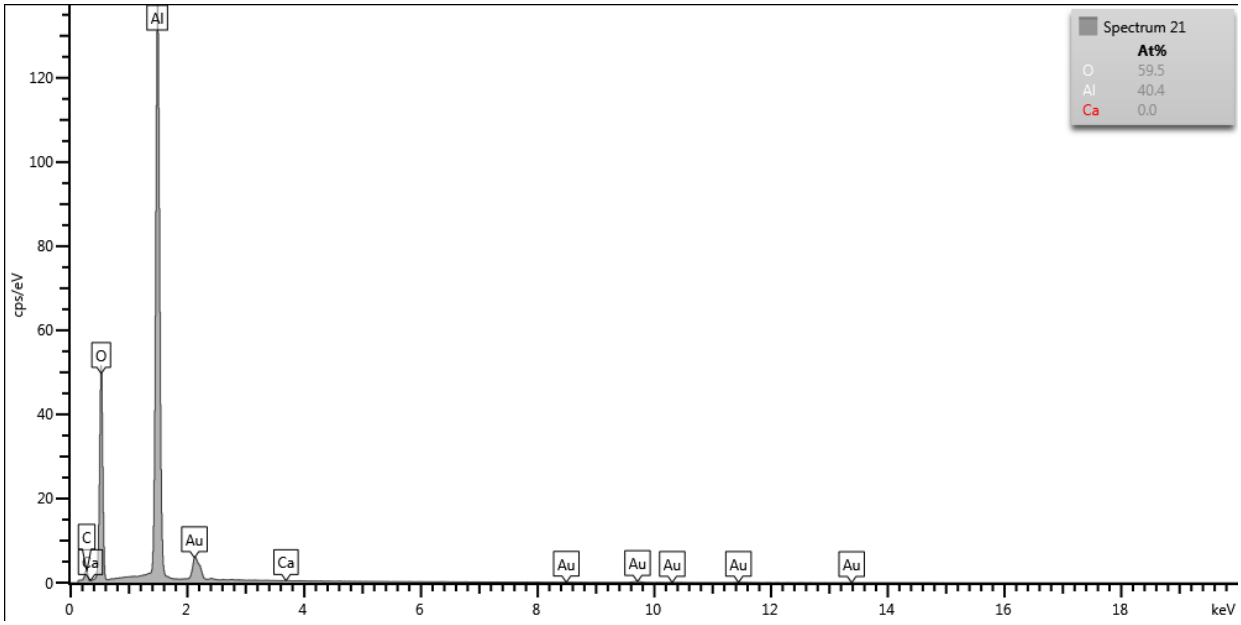

Figure A. 2: SEM-EDS spectrum 21 of calcined alumina

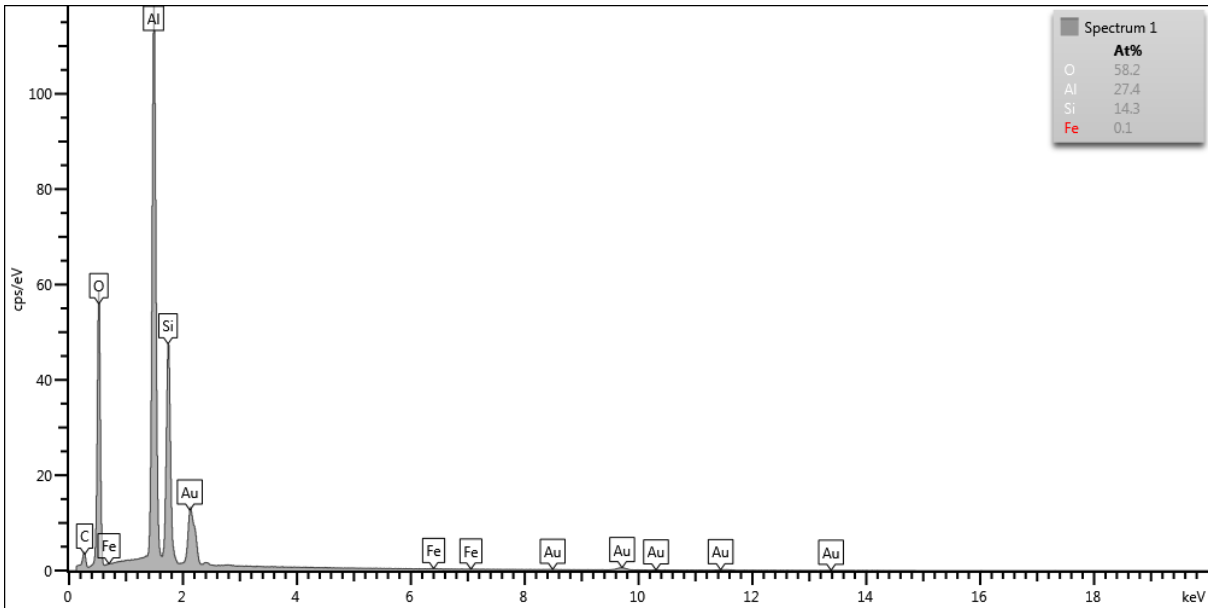

Figure A. 3: SEM-EDS spectrum 1 of andalusite

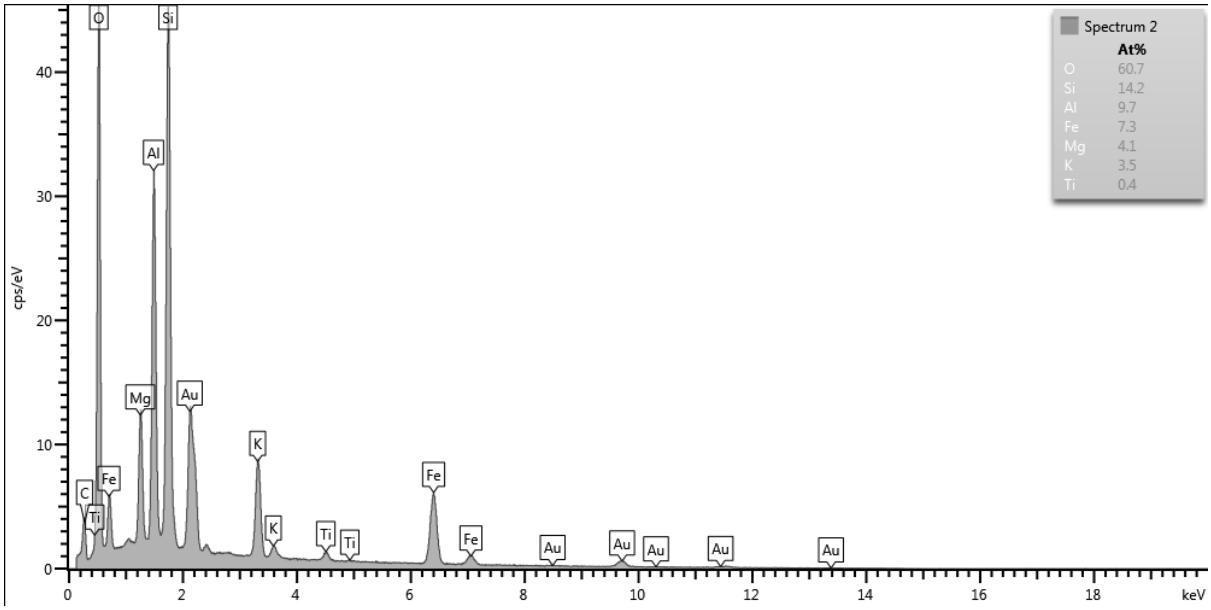

Figure A. 4: SEM-EDS spectrum 2 of andalusite

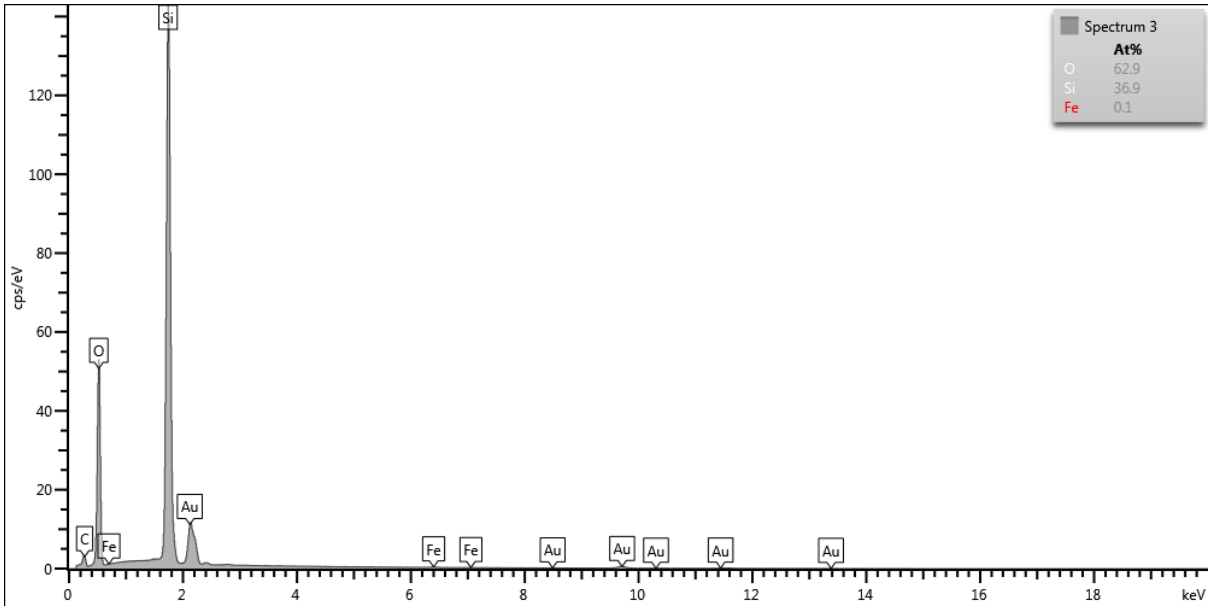

Figure A. 5: SEM-EDS spectrum 3 of andalusite

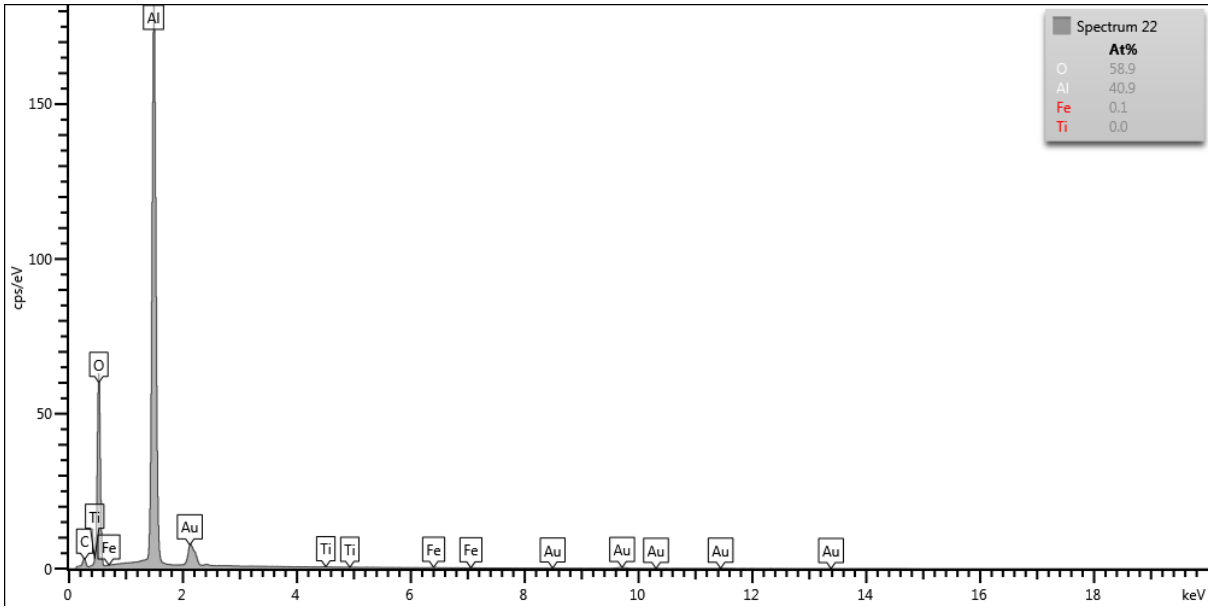

Figure A. 6: SEM-EDS spectrum 22 of bauxite

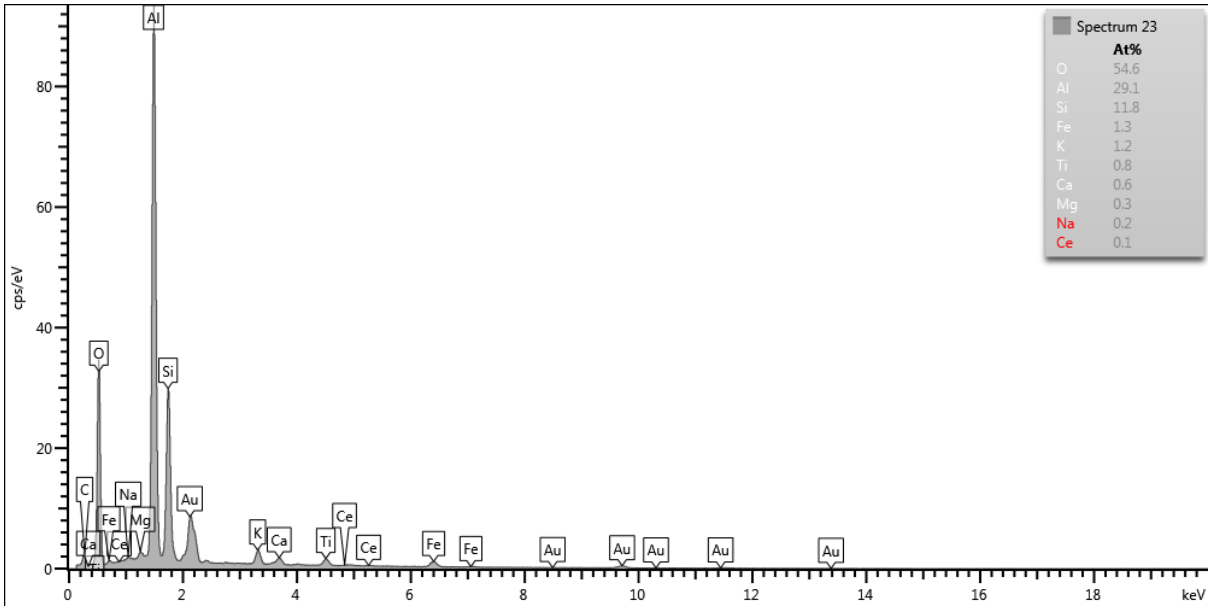

Figure A. 7: SEM-EDS spectrum 23 of bauxite

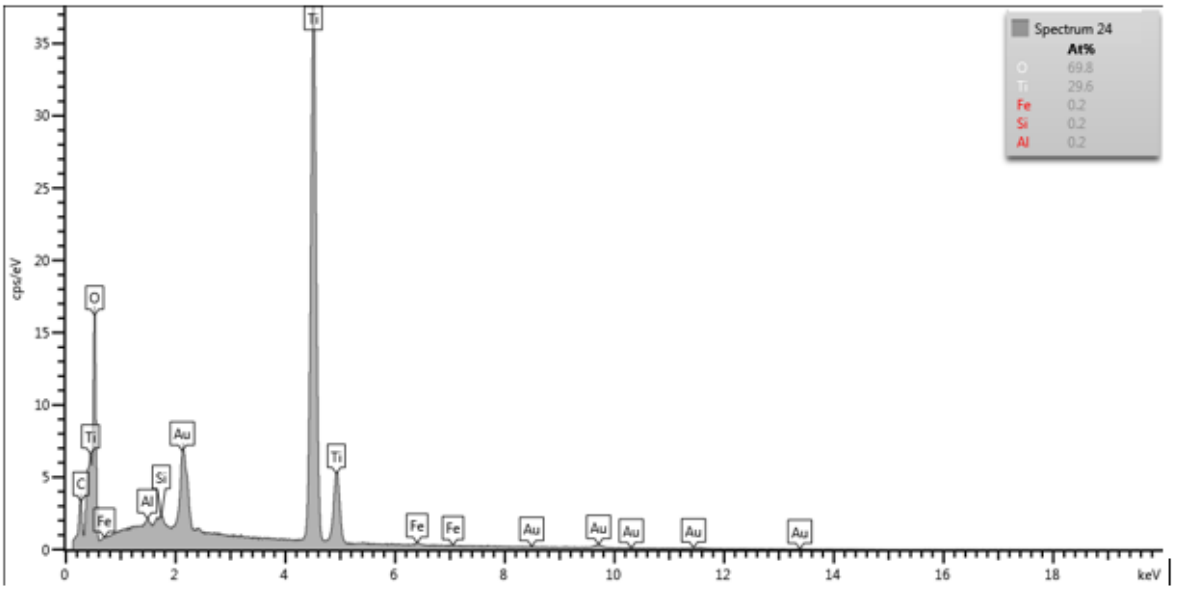

Figure A. 8: SEM-EDS spectrum 24 of bauxite

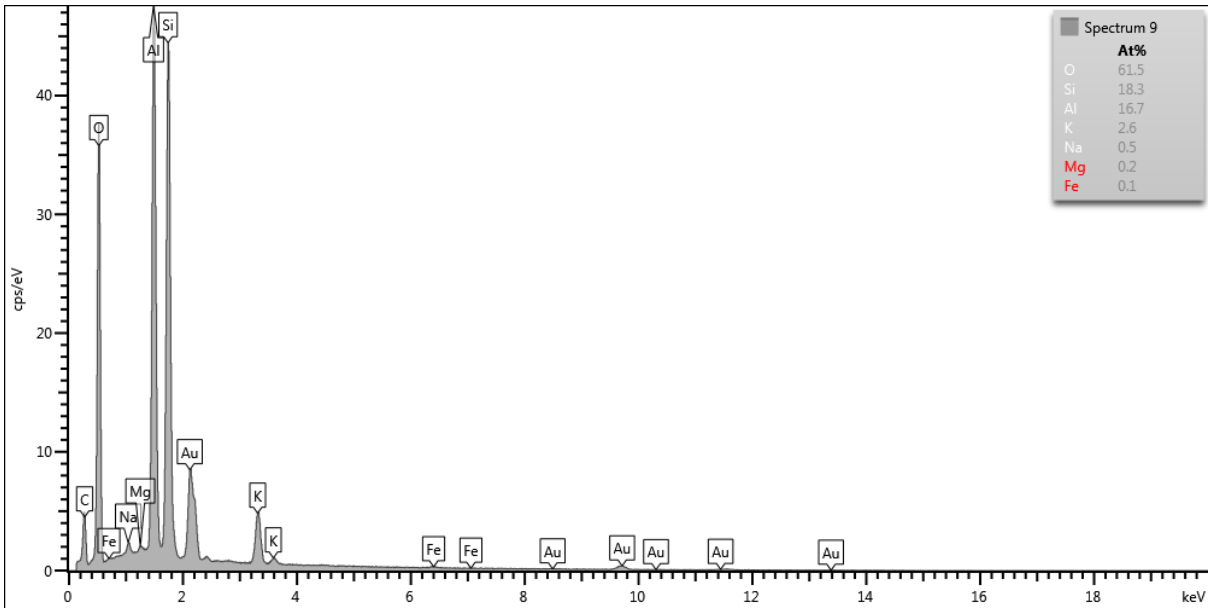

Figure A. 9: SEM-EDS spectrum 9 of clay - kaolinite

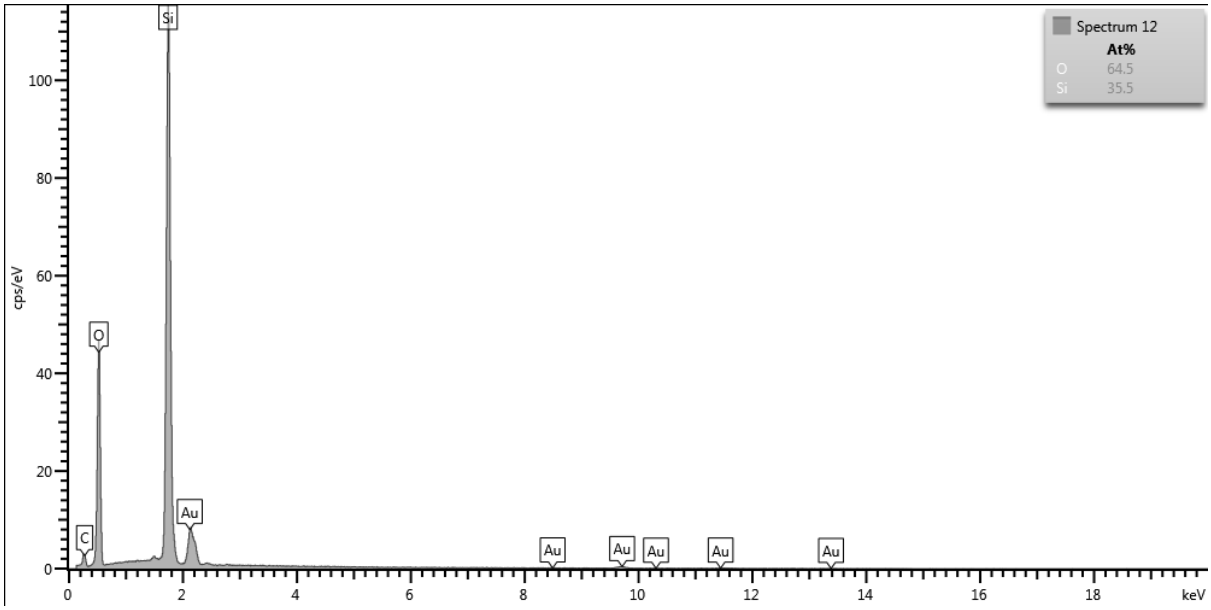

Figure A. 10: SEM-EDS spectrum 12 of clay – kaolinite

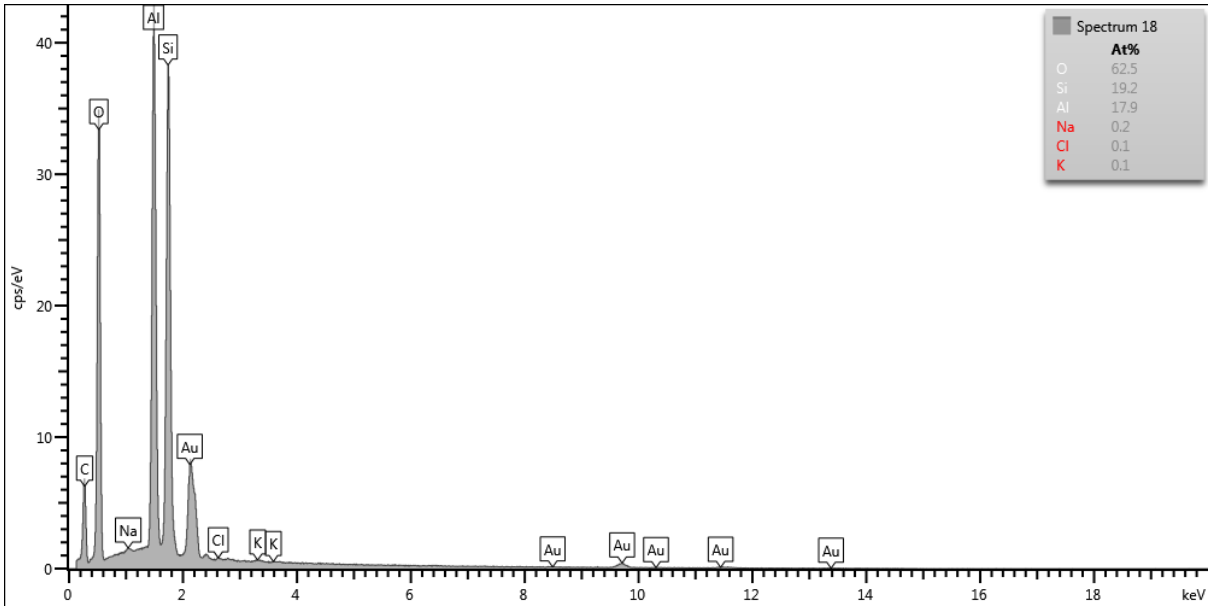

Figure A. 11: SEM-EDS spectrum 18 of clay – kaolinite

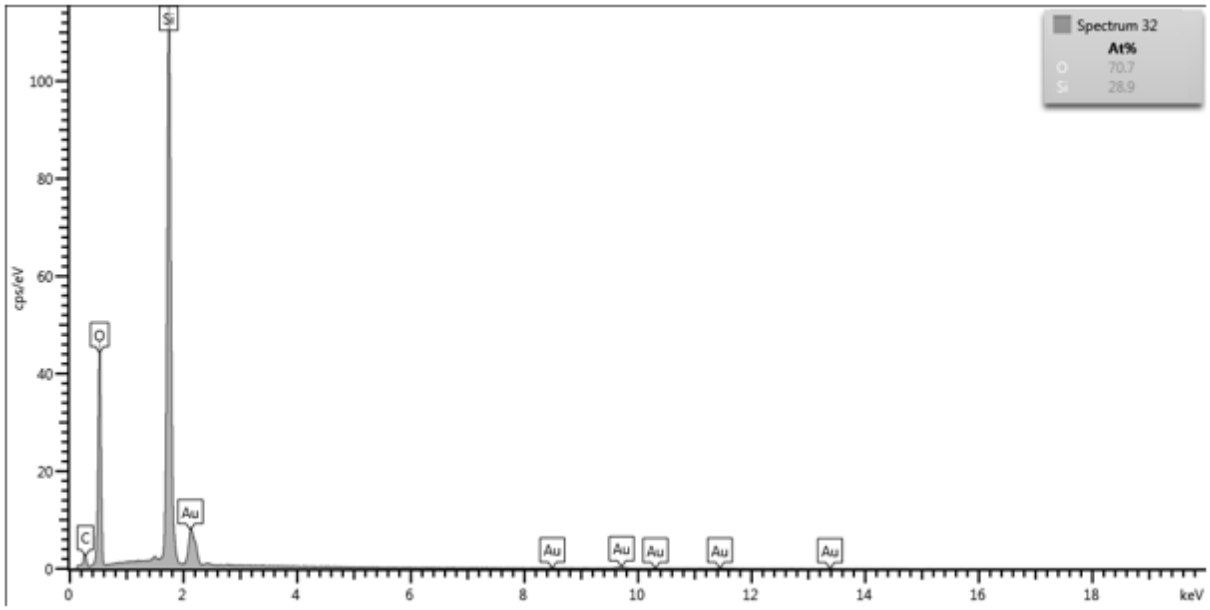

Figure A. 12: SEM-EDS spectrum 32 of calcined clay

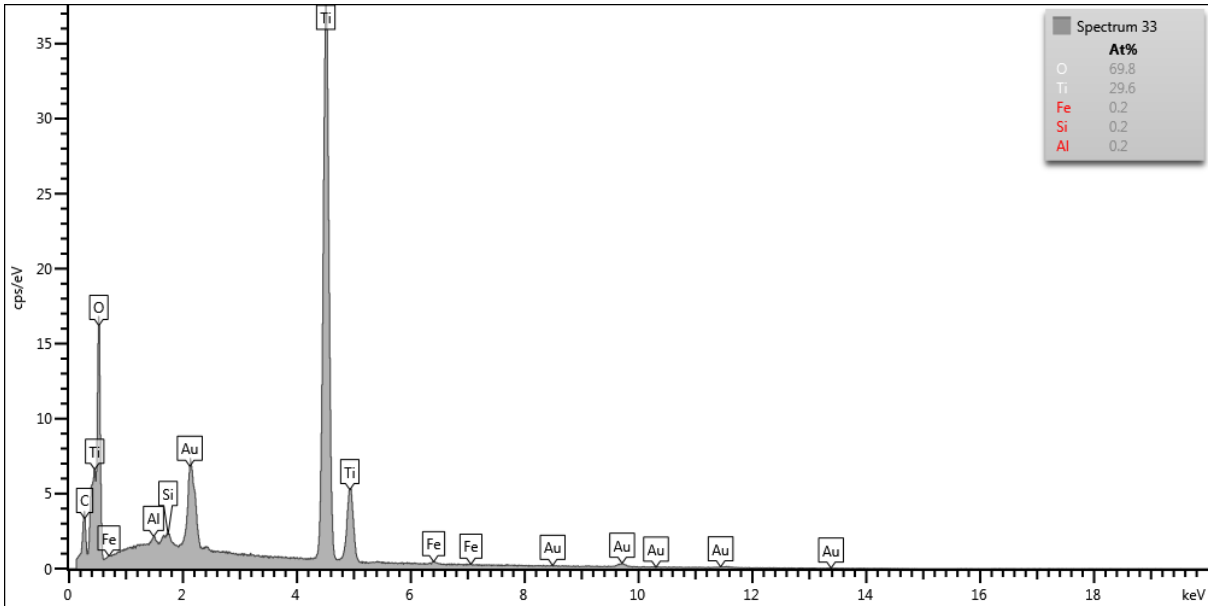

Figure A. 13: SEM-EDS spectrum 33 of calcined clay

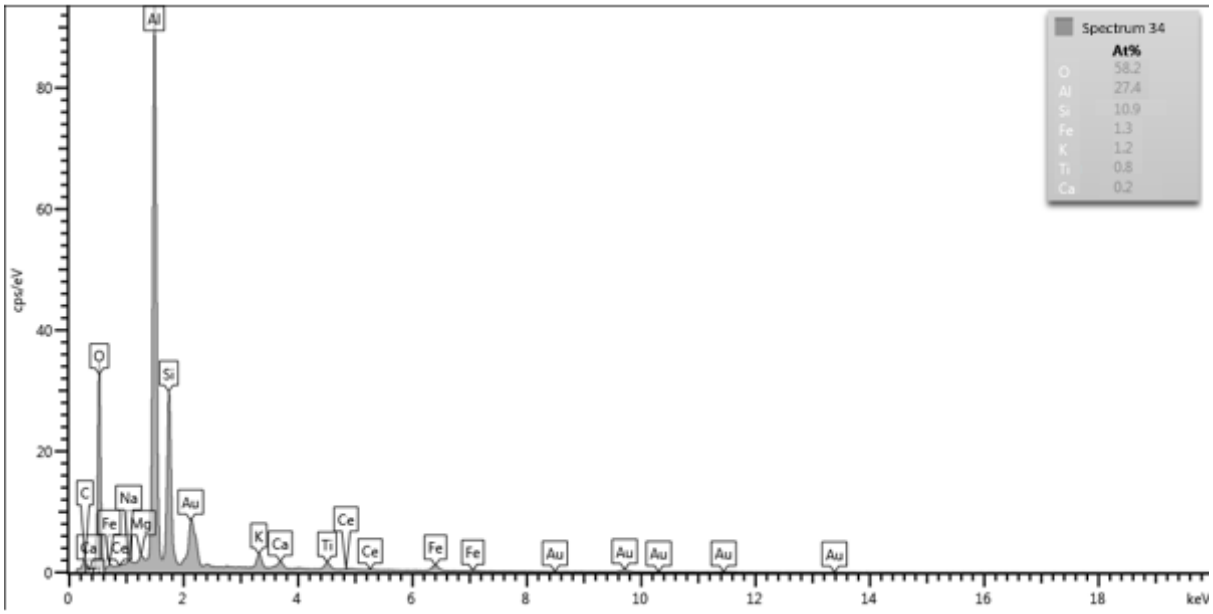

Figure A. 14: SEM-EDS spectrum 34 of calcined clay

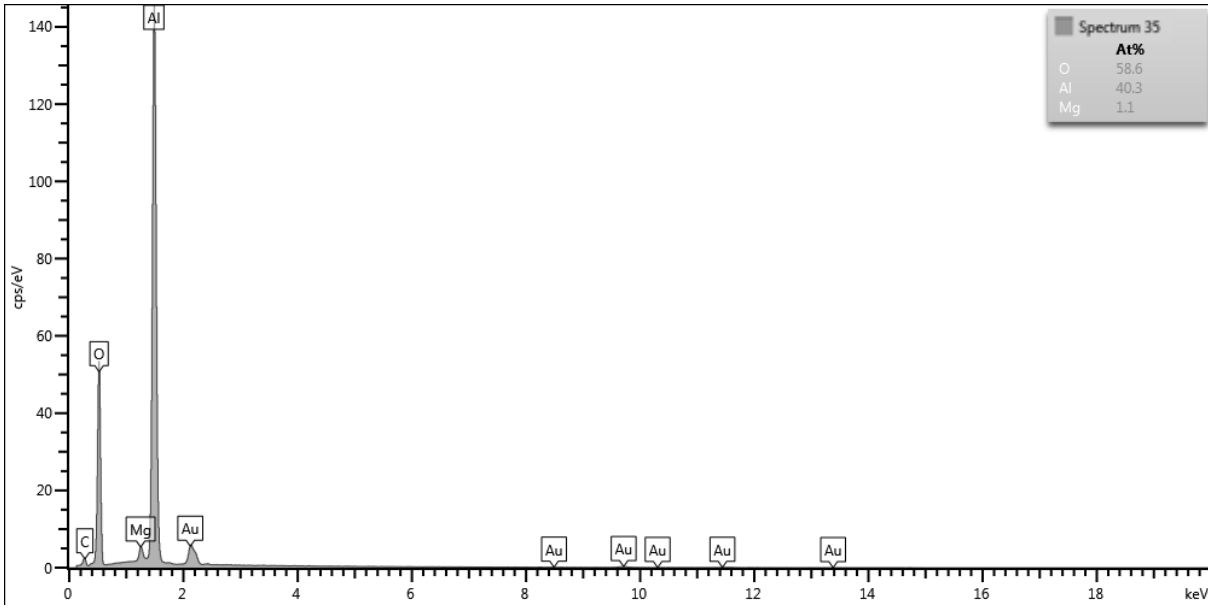

Figure A. 15: SEM-EDS spectrum 35 of calcined clay

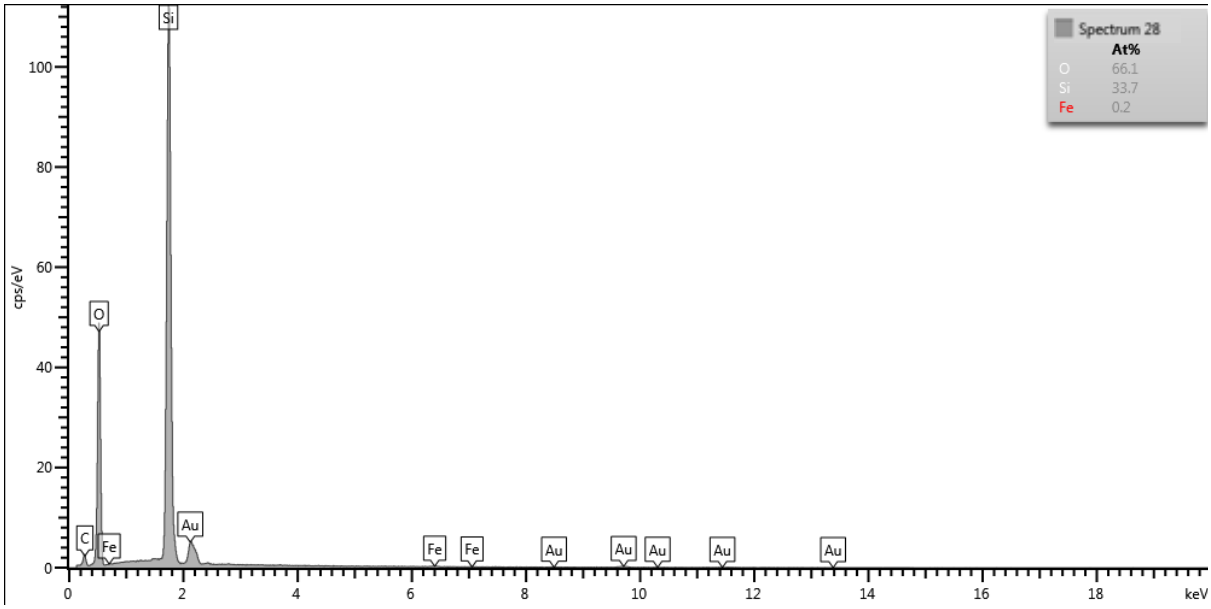

Figure A. 16: SEM-EDS spectrum 28 of silicon carbide

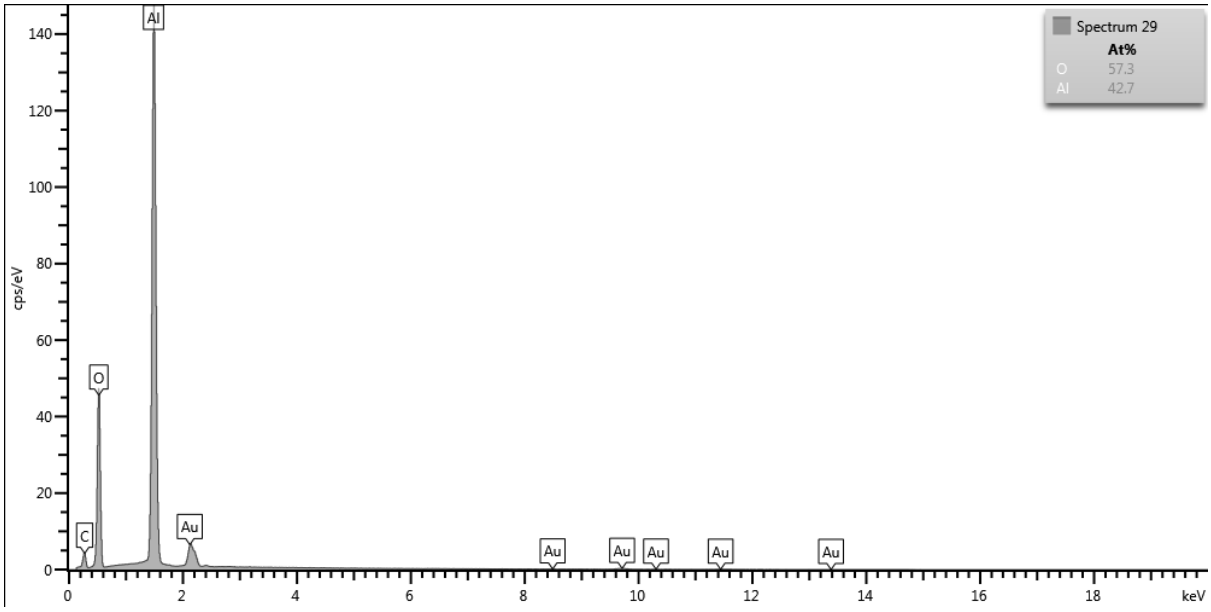

Figure A. 17: SEM-EDS spectrum 29 of silicon carbide

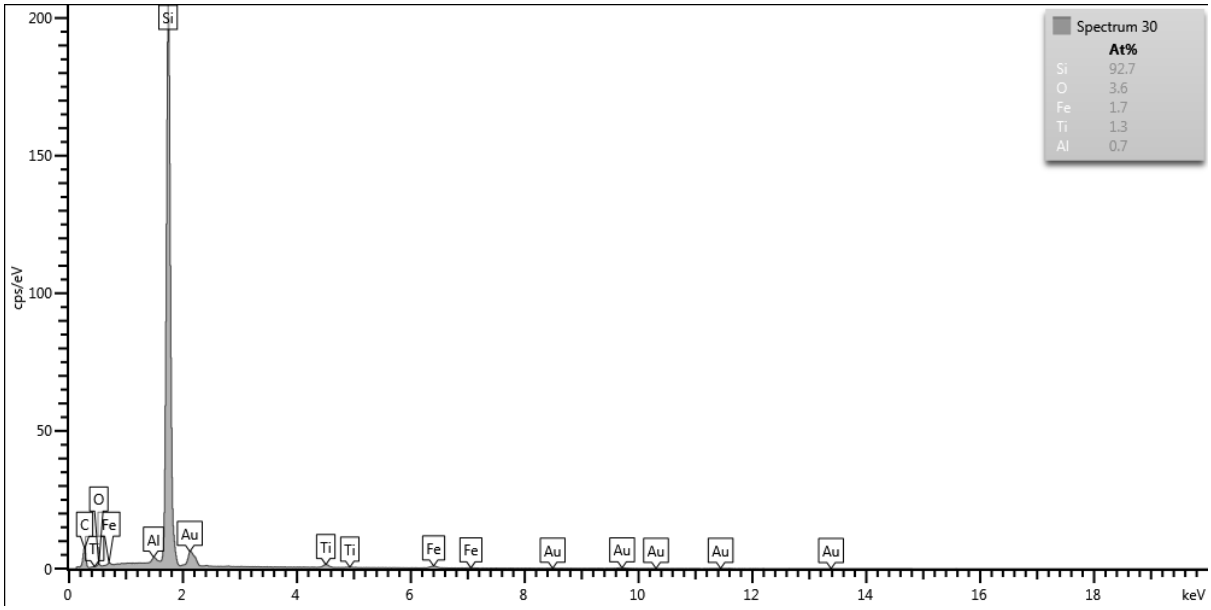

Figure A. 18: SEM-EDS spectrum 30 of silicon carbide

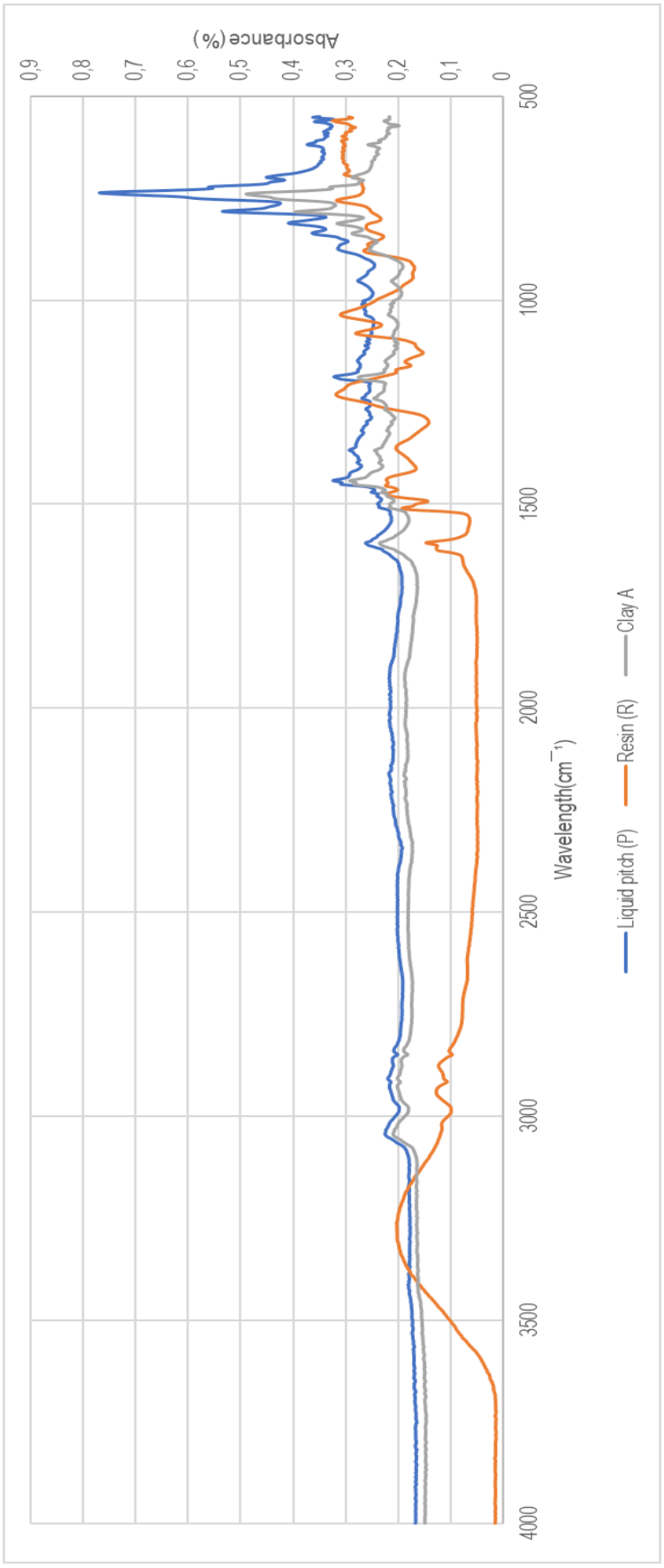

Figure A. 19: Enlarge FTIR graph to identify functional groups of resin, liquid pitch and mixture combination used in Clay A